ICES Cooperative Research Report
Rapport des Recherches Collectives

No. 326
May 2015

Calibration of acoustic instruments

Calibration of acoustic instruments

DAVID A. DEMER • LAURENT BERGER • MATTEO BERNASCONI • ECKHARD BETHKE •
KEVIN BOSWELL • DEZHANG CHU • REKA DOMOKOS • ADAM DUNFORD • SASCHA
FÄSSLER • STÉPHANE GAUTHIER • LAWRENCE T. HUFNAGLE • J. MICHAEL JECH •
NAIGLE BOUFFANT • ANNE LEBOURGES-DHAUSSY • XAVIER LURTON • GAVIN J.
MACAULAY • YANNICK PERROT • TIM RYAN • SANDRA PARKER-STETTER •
SARAH STIENESSEN • THOMAS WEBER • NEAL WILLIAMSON

Contents

Foreword

Acoustic instrument calibration is fundamental to the quantitative use of its data for estimating aquatic resource abundance. Regular calibrations also allow instrument performance to be monitored to detect changes due to the environment or component dynamics, degradation, or failure.

This is the second *ICES Cooperative Research Report* (CRR) focussed on calibrations of acoustic instruments. The first, CRR No. 144 (Foote *et al.*, 1987), was published during the era of analogue electronics more than a quarter of a century ago. Since then, not only has the acoustic equipment improved vastly with digital electronics and signal processing, but the techniques for applying them to studies of marine organisms have both advanced and diversified. Motivating, facilitating, and expediting these developments is the work of the Fisheries Acoustics, Science and Technology Working Group (WGFAST) of the International Council for the Exploration of the Sea (ICES).

CRR No. 144 guided the fisheries acoustics community to uniformly apply the sphere method to calibrate survey equipment, generally single-frequency, split-beam echosounders. Today, surveys of fishery resources are conducted using a large variety of acoustic instruments including, but not limited to, single-frequency, multifrequency, single-beam, split-beam, broad bandwidth, and multibeam echosounders; side-scan and scanning sonars; acoustic Doppler current profilers; and acoustic cameras. These instruments differ in the ways in which they function, are utilized, and the types of measurements they provide. In most cases, they also require different calibration techniques for optimizing the accuracy and characterizing the precision of the measurements.

With technological innovation proceeding at an ever faster pace, the challenge to create a comprehensive and practical guide to calibrating acoustic instruments is formidable. Obviously, not all acoustic instrumentation and methods are addressed here. The ones that are addressed are in various states of maturity. Therefore, the practical aims of this CRR are to document (i) acoustic instruments currently used in fisheries research and surveys, (ii) theoretical principles of calibrating these instruments, and (iii) methods currently being practiced for a selection of commonly used instruments.

To meet these goals, the WGFAST formed the Study Group on Calibration of Acoustic Instruments (SGCal) at its meeting in April 2009. The SGCal first met in San Diego, CA, USA in April 2010 to outline the document. Some chapters were drafted intersessionally. The SGCal met for the second time in Reykjavik, Iceland in May 2011 to collectively review some draft chapters. The drafts were refined intersessionally and merged. The draft CRR was collectively reviewed at meetings of the SGCal, in Pasaia, Spain in April 2013 and in New Bedford, MA, USA in May 2014. Multiple independent reviewers provided input, and the final editing was completed in 2014. The authors hope that this CRR will be a valuable reference to both novice and experienced users of fishery acoustic instruments, but recognize that it is a provisional guide that requires refinement and update as the field continues to progress.

David A. Demer
Chair, SGCal

Terms, symbols, and units

The names, symbols, and units of physical quantities must be precisely defined to assure effective scientific communication. However, different fields of study, e.g. physics, electrical engineering, radar, and sonar, often use different terms and symbols, and the same symbols may be used for different things, even within the same field. Furthermore, people generally have preferences for specific terms and symbols. Because universal consistency is not achievable, the aim for terms and symbols in this document is to define them uniquely and use them consistently.

The following terminology, based mostly on MacLennan *et al.* (2002), follows the Le Système International d'Unités (SI system). Symbols should uniquely represent a term. All symbols for variables should be italicized. Any symbol for a variable (x) that is not logarithmically transformed should be lower case. Any symbol for a logarithmically transformed variable, e.g. $X = 10\log_{10}(x/x_{ref})$, with units of decibels referred to x_{ref} (dB re x_{ref}), should be capitalized. Deviations from these rules should be noted.

Term	Symbol	Unit	Description
Environmental			
Water temperature	t_w	Degree Celsius (°C)	Heat, or average kinetic energy of particles in water.
Water salinity	s_w	Practical salinity unit (psu)	The total amount of dissolved material in water.
Water depth	d_w	Metre (m)	The vertical distance below the water surface.
Water pressure	p_w	Pascal (Pa) (= 10^{-4} dbar)	The force per unit area in water.
Water density	ρ_w	Kilogramme per cubic metre (kg m^{-3})	The mass density of water.
Electrical			
Voltage	u_e	Volt (V)	The square root of the mean of the squares (rms) of time-varying electric potential.
Current	i_e	Ampere (A)	The rms electric current.
Electrical impedance	z_e	Ohm (Ω)	The ability of a material to oppose the passage of an alternating electric current.
Electrical power	p_e	Watt (W) or VA or V^{2}Ω^{-1} or A^{2}Ω	The rms electrical energy per unit time.
Acoustic			
Water sound speed	c_w	Metre per second (m s^{-1})	The distance sound travels per unit time in water.
Water acoustic impedance	z_{aw}	kg m^{-2} s^{-1}	The product of ρ_w and c_w.
Acoustic frequency	f	Hertz (Hz) = cycles s^{-1}	The number of complete cycles of a periodic wave per unit time.

Acoustic frequency bandwidth	b_f	Hz	The difference between the highest and lowest f in a signal or device.
Acoustic wavelength	λ	m	The distance spanned by one cycle of a periodic pressure wave.
Acoustic wavenumber	k	m^{-1}	The number of periodic wavelengths per 2π-unit distance.
Pulse duration	τ	s	The duration of a signal pulse.
Effective pulse duration	τ_{eff}	s	The duration of a square shaped pulse that has the same energy as the echosounder-pulse shape after reception processing.
Range	r	m	The direct-path distance between objects, e.g. the transducer and the target.
Reference range	r_0	m	The r from an acoustic source or target to which measurements are referred, conventionally 1 m.
Acoustic pressure	p	Pa $(= N\ m^{-2} = kg\ m^{-1}\ s^{-2})$	The rms deviation of local pressure from the ambient.
Reference acoustic pressure	p_{ref}	Pa	The reference p, conventionally 1 µPa for underwater sound.
Acoustic power	p_a	W	The rms acoustic energy per unit time.
Acoustic intensity	i	$W\ m^{-2}$	The rms p_a per unit area.
Acoustic intensity at r_0	i_0	$W\ m^{-2}$	The rms i at r_0.
Reference acoustic intensity	i_{ref}	$W\ m^{-2}$	The i of a plane wave with rms $p = p_{ref}$.
Spherical spreading loss	No symbol	m^{-2}	The reduction in i with r resulting from spherical expansion of the wavefront.
Absorption loss	No symbol	m^{-1}	The reduction in i with r resulting from conversion to heat.
Absorption coefficient	α_a	dB m^{-1}	A metric of absorption loss.
Transduction			
Transmit voltage	u_{et}	V	The rms u_e input to a transducer.
Transmit current	i_{et}	A	The rms i_e input to a transducer.
Transducer electrical impedance	z_{et}	Ω	The ability of a transducer to oppose the passage of an alternating electric current.
Receiver electrical impedance	z_{er}	Ω	The ability of an echosounder receiver to oppose the passage of an alternating electric current.

Transmit electric power	p_{et}	W	The electrical power input to a transducer.
Transmit acoustic power	p_{at}	W	The acoustic energy per unit time output from a transducer.
Transducer efficiency	η	Dimensionless	The proportion of p_{et} converted to p_{at}.
Transmit pressure	p_t	Pa	The p output from a transducer.
Directional angles	α, β	Degree (°)	The angle coordinates in orthogonal planes, typically alongships and athwartships or aligned with the major and minor transducer axes, respectively.
Gain	$g(\alpha,\beta)$ or $G(\alpha,\beta)$	Dimensionless or Decibel referred to 1 (dB re 1)	The ratio of i values, observed at a distant point, resulting from transmissions, with constant p_{et}, of a real transducer, and an idealized lossless omnidirectional transducer. Gain accounts for losses referred to a point on the electrical side of the transducer.
On-axis gain	g_0 or G_0	Dimensionless or dB re 1	The $g(\alpha,\beta)$ on the transducer beam axis ($\alpha = \beta = 0$).
Transducer directivity	$d(\alpha,\beta)$ or $D(\alpha,\beta)$	Dimensionless or dB re 1	The one-way directional gain of a real transducer, omitting losses.
Transducer directivity pattern	$b(\alpha,\beta)$ or $B(\alpha,\beta)$	Dimensionless or dB re 1	The ratio of $d(\alpha,\beta)$ and its maximum value.
Transducer beamwidth	$\theta_{-3\ dB}$ or $\alpha_{-3\ dB}$ or $\beta_{-3\ dB}$	°	The angle from the transducer beam axis to the point of half-power, in the θ, α, or β planes.
Transducer beamwidth offset	α_o or β_o	°	The angular displacement of the transducer maximum-response axis beam from the axis of zero split-beam phase, in the α or β planes.
Transducer angle sensitivity	Λ_α or Λ_β	Electrical°/geometric°	A factor to convert split-beam electrical angles to target bearing angles in the α or β planes.
Source intensity or Source level	i_s or SL	W m^{-2} or dB re 1 μPa at r_0	The i_0 in the direction (α,β) of the target.
Transmit intensity	i_t	W m^{-2}	The intensity of a plane wave transmitted from a real transducer.

Omni-directional transmit acoustic intensity	$i_{t\,omni}$	$W\,m^{-2}$	The i_t for an idealized lossless omni-directional transducer.
Equivalent two-way beam angle	ψ or Ψ	steradian (sr) or dB re 1 sr	The solid angle subtended by an ideal conical beam that would produce the same volume integral as the square of the normalized transducer directivity.
Effective receiving area	$a_r(\alpha,\beta)$	m^2	The area of a real transducer available to receive acoustic power and transfer it to a matched load (i.e. $z_{er}=z_{et}$), referred to the same point on the electrical side of the transducer as g_0.
Received electric power	p_{er}	W or dB re 1 W	The p_e output from a transducer, referred to the same point as g_0 and a_r. .
On-axis received power	p_{er0} or P_{er0}	W or dB re 1 W	The p_{er} in the direction (α,β) of the maximum $b(\alpha,\beta)$.
Transmit voltage sensitivity	s_u or S_u	$\mu Pa\,V^{-1}$ or dB re 1 $\mu Pa\,V^{-1}$	The SL resulting from a 1-V rms sinusoidal signal applied to the transducer terminals.
Transmit current sensitivity	s_i or S_i	$\mu Pa\,A^{-1}$ or dB re 1 $\mu Pa\,A^{-1}$	The SL resulting from a 1-A rms sinusoidal signal applied to the transducer terminals.
Receive voltage sensitivity	m_u or M_u	$V\,\mu Pa^{-1}$ or dB re 1 $V\,\mu Pa^{-1}$	The unloaded u_e at a point on the electrical side of the transducer resulting from i_{ref} applied to the transducer surface.
Reciprocity parameter	j	dimensionless	The ratio of the response of a linear, passive, reversible electroacoustic transducer acting as a receiver, m_u, to its response as a transmitter, s_i.
Sphere			
Sphere density	ρ_s	$kg\,m^{-3}$	Mass density of an elastic sphere.
Sphere compressional wave sound sphere	c_c	$m\,s^{-1}$	The compressional (or longitudinal) wave sound speed of an elastic sphere.
Sphere shear wave sound speed	c_s	$m\,s^{-1}$	The shear (or transverse) wave sound speed of an elastic sphere.
Metrics			
Signal-to-noise ratio	r_{sn}	Dimensionless	The quotient of signal and noise power.
Spherical scattering cross-section	σ_{sp}	m^2	The area of an acoustic target effectively scattering acoustic power.

Backscatter- ing cross- section or Target strength	σ_{bs} or TS	m^2 or dB re 1 m^2	The area of an acoustic target effec- tively backscattering acoustic power, $\sigma_{bs} = \sigma_{sp}/4\pi$, at r_0.
Sampled area	a	m^2	The area contributing to a received sig- nal.
Surface backscatter- ing coeffi- cient or Surface backscatter- ing strength	s_s or S_s	$m^2\,m^{-2}$ or dB re 1 $m^2\,m^{-2}$	The backscattering cross-section per unit of surface area, assuming the area is the intersection of ψ and a sphere with radius r centred on the transducer.
Sampled volume	v	m^3	The volume contributing to a received signal.
Volume backscatter- ing coeffi- cient or Volume backscatter- ing strength	s_v or S_v	$m^2\,m^{-3}$ or dB re 1 $m^2\,m^{-3}$	The sum of σ_{bs} per unit of water vol- ume.
Survey area	a_s	m^2	The area of the survey region.
Area backscatter- ing coeffi- cient or Nautical- area backscatter- ing coeffi- cient	s_a or s_A	$m^2\,m^{-2}$ or m^2 nautical mile^{-2}	The integral of s_v over a range of depths; or s_a multiplied by a scaling factor ($4\pi(1852)^2$ nautical mile^2 m^{-2}).
Scatterer volume density	ρ_v	Number m^{-3}	The number of scatterers per unit of sampled volume.
Scatterer areal density	ρ_a or ρ_A	Number m^{-2} or Number nautical mile^{-2}	The number of scatterers per unit of sampled area.
Scatterer abundance	n_b	Number	The number of scatterers within a sam- pled range and area.
Scatterer biomass	m_b	kg	The mass of scatterers within a sam- pled range and area.

1 Introduction

1.1 Scope and outline

Acoustic sampling has long been a standard survey tool for estimating the abundance and distribution of fish, zooplankton, and their seabed habitat (Kimura, 1929; Sund, 1935; Holliday, 1972a; Nielson *et al.*, 1980). Typically, acoustic surveys are conducted using multifrequency echosounders that transmit sound pulses down beneath the ship and receive echoes from animals and the seabed in the path of the sound waves (Simmonds and MacLennan, 2005). Generally, for surveys of animals, the backscatter signal is normalized to the range-dependent observational volume yielding the *volume backscattering coefficient*, which provides indications of the target type and behaviour. Objects scatter sound if their product of mass density and sound speed is different from that of the surrounding medium. A fish with a swimbladder has a large *acoustic-impedance contrast* (Foote, 1980), and thus has a large reflecting area, *backscattering cross-section*. Plankton, e.g. krill and salps, generally have much lower acoustic-impedance contrasts, but can produce large volume backscattering coefficients when they are aggregated in large densities (Hewitt and Demer, 1991, 2000). Under certain conditions, the summed and averaged volume backscattering coefficients are linearly related to the density of the fish or plankton aggregations that contributed to the echoes (Foote, 1983a). The *number density* can be estimated by dividing the *integrated volume backscattering coefficient* from an aggregation of target species by the average backscattering cross section from a representative animal (Ehrenberg and Lytle, 1972). An estimate of animal abundance is then obtained by multiplying the average estimated fish density and the survey area.

Increasingly, multifrequency echosounder surveys are being augmented with samples from other acoustic instruments such as multibeam echosounders (Gerlotto *et al.*, 1999; Simmonds *et al.*, 1999; Berger *et al.*, 2009; Colbo *et al.*, 2014), multibeam imaging sonars (Korneliussen *et al.*, 2009; Patel and Ona, 2009), and long-range scanning sonars (Bernasconi *et al.*, 2009; Nishimori *et al.*, 2009; Stockwell *et al.*, 2013)(Figure 1.1). Use of these instruments provides information on many more aspects of the biotic and abiotic environment, e.g. bathymetry, seabed classification (Humborstad *et al.*, 2004; Cutter and Demer, 2014), oceanographic fronts (Wade and Heywood, 2001), mixed-layer depths, anoxic regions, internal waves (Lavery *et al.*, 2010a), turbulence (Stanton *et al.*, 1994), currents, and methane seeps, all contributing to a broader ecosystem perspective (Demer *et al.*, 2009a). In each case, the quantitative use of the data requires that the acoustic instrument is calibrated.
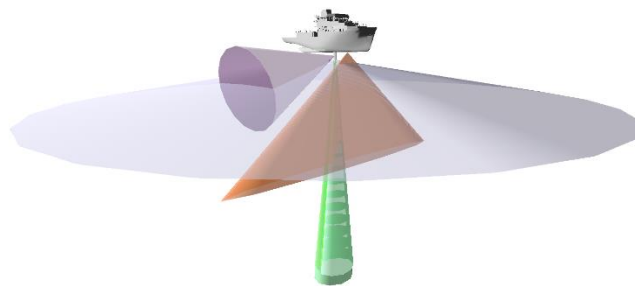
Figure 1.1. A conceptual image of acoustic-sampling beams projecting from a survey vessel equipped with multifrequency split-beam (green) and multibeam (orange) echosounders, multibeam imaging sonar (purple), and long-range scanning sonar (grey).

Instrument calibration involves the characterization of measurement accuracy (bias or systematic error) and precision (variability or random error). Sampling with the calibrated instrument involves additional systematic and random error (Demer, 2004). Calibration accuracy is estimated and optimized by comparing measured and assumed values for a standard, and correcting for the difference. The selection and characterization of a calibration standard is, therefore, paramount to the accuracy of an instrument calibration (Foote and MacLennan, 1984). Calibration precision is estimated by comparing multiple measures of a standard. Importantly, the performance of an instrument and thus its calibration accuracy and precision may change vs. time or the environment (Demer and Hewitt, 1993; Brierley *et al.*, 1998a; Nam *et al.*, 2007). Therefore, instruments should be calibrated frequently within the range of environments where they are used to make calibrated measurements (Demer and Renfree, 2008). If this is not possible, account should be made for any changes in the instrument or environment that appreciably affect the calibration accuracy and precision.

This report includes general instruction and current best practices for calibrating a selection of acoustic instruments commonly used to conduct fishery science and surveys. It also describes some less developed protocols for other acoustic instruments. For practical reasons, not all fishery acoustic instruments are included.

The remainder of Chapter 1 (i) summarizes some of the theoretical principles of acoustic instruments used to conduct fishery research and surveys, (ii) describes some commonly used instruments and their deployment platforms, and (iii) briefly introduces some common methods for calibrating acoustic instruments. Readers seeking only protocols for calibrating echosounders may wish to skip this and other sections and consult the Contents table to access information related to their interest and need.

Chapter 2, details the sphere calibration method. Chapter 3 explores uncertainty in sphere calibrations. Chapter 4 describes protocols for calibrating some commonly used echosounders. Chapter 5 describes emerging protocols for some other acoustic instruments. Chapter 6 acknowledges valuable contributions to this CRR by people not included in the list of authors.

1.2 Echosounder theory

The theory of sound transduction, propagation, and scattering is documented in numerous books and journal articles (see References). It is based on the same principles as radar theory (Rihaczek, 1969; Kerr, 1988), which is used for calibration and data processing in many commonly used acoustic instruments. Section 1.2.1 documents radar theory as it relates to these instruments; Section 1.2.2 highlights the calibration param-

eters; Section 1.2.3 summarizes the measurements that are typically derived from echosounder data; and Section 1.2.4 reconciles this radar theory with some aspects of sonar theory used by other systems. The content of these sections is largely a synthesis of Urick (1983), Kerr (1988), Simrad (1993), Medwin and Clay (1998), Bodholt (2002), Andersen (2006), and other references cited in the text. For simplicity and clarity, the theory is mostly presented in the linear domain, i.e., not in decibels.

1.2.1   Introduction

An echosounder generates, amplifies, and transmits an acoustic pulse (Figure 1.2), which propagates outward. When the pulse reaches a target object, e.g. zooplankton, fish, or the seabed, the interaction results in a reflected or scattered wave. Characteristics of the target modulate the scattered wave amplitude, shape, and frequency, and these changes may provide remote-sensing information. Part of this wave travels back to the echosounder where it is converted to voltage, amplified, filtered to remove noise, digitized, and thus received as backscatter (Furusawa, 1991). Real sonar systems may also include other steps such as heterodyning and demodulating. The delay between the pulse transmission and the backscatter reception is converted into an estimate of the target range using an estimate of the harmonic mean sound speed along the propagation path.
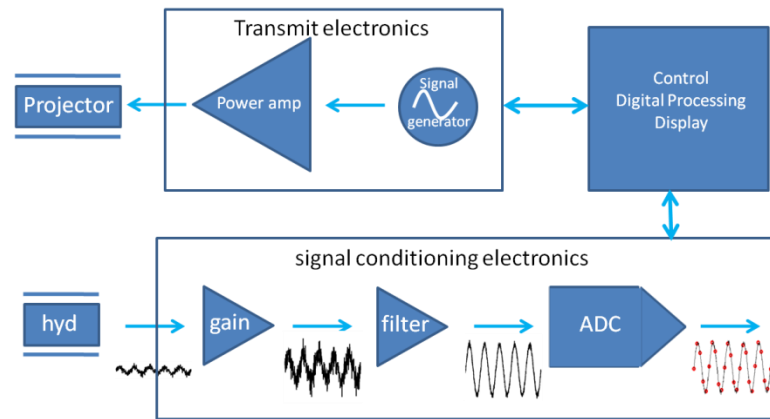
Figure 1.2. Diagram of a notional echosounder. Although a separate transmitter (projector) and receiver ("hyd"rophone) are shown (i.e. a bistatic system), most echosounders use a single transducer to transmit and receive (i.e. a monostatic system). The analogue-to-digital converter (ADC) digitizes the received, amplified and filtered voltage signal.

1.2.2   Transmission

1.2.2.1   Transmit power

A narrow bandwidth echosounder outputs sinusoidal pulses of mean *transmit electric power*, p_{et} (W), defined by the *root-mean-square* (rms) *transmit voltage*, u_{et} (V), and rms *transmit current*, i_{et} (A), applied to an electro-acoustic transducer with *transducer electrical impedance*, z_{et} (Ω). These variables are complex (having amplitude and phase), and are related by Ohm's Law:

$$p_{et} = \frac{u_{et}^2}{z_{et}} = i_{et}^2 z_{et} \,.$$

(1.1)

The transmit energy, equal to p_{et} integrated over time, increases with the pulse duration, τ (s). The resulting acoustic signal has a *frequency bandwidth*, $b_f \cong 1/\tau$ (Hz), about the signal *frequency*, f (Hz). In water with *sound speed*, c_w (m s^{-1}), the *acoustic wavelength*, λ (m), of the signal is:

$$\lambda = \frac{c_w}{f} \qquad .$$

(1.2)

Values for c_w and thus λ vary during the calibration and subsequent use of the echosounder, and modulate calibration accuracy and precision.

1.2.2.2 Intensity

Analogous to Ohm's law (Equation 1.1), the mean *transmit acoustic intensity*, i_t (W m^{-2}), of the plane wave is equal to the square of the rms *transmit acoustic pressure*, p_t (Pa = N m^{-2}), divided by the *water acoustic impedance*, z_{aw} (kg m^{-2} s^{-1}), which is the product of c_w and *mass density*, ρ_w (kg m^{-3}):

$$i_t = \frac{p_t{}^2}{z_{aw}} = \frac{p_t{}^2}{\rho_w c_w} = \frac{p_{at}}{a} .$$

(1.3)

By definition, i_t equals the mean *transmit acoustic power*, p_{at} (W), per unit *area*, a (m^2). Post-calibration variation in ρ_w values may also affect the calibration accuracy and precision.

The acoustic pressure of the resulting plane wave is often related to a *reference acoustic pressure*, ($p_{ref} = 1$ µPa, conventionally). Thus, the *reference acoustic intensity*, i_{ref} (W m^{-2}), is:

$$i_{ref} = \frac{p_{ref}{}^2}{\rho_w c_w} .$$

(1.4)

Unlike p_{ref}, values for i_{ref} may be modulated by variation in z_{aw}.

1.2.2.3 Directivity

The one-way *transducer directivity*, $d(\alpha, \beta)$ (dimensionless), describes the ratio of *acoustic intensity*, $i_t(\alpha, \beta)$ (W m^{-2}), and $i_t(\alpha, \beta)$ averaged over all directions, observed at a distant point, where α (°) and β (°) are orthogonal "alongships" and "athwartships" angles. The function $d(\alpha, \beta)$ is dependent on λ, which changes with c_w, following Equation (1.2). The one-way *transducer directivity pattern*, $b(\alpha, \beta)$ (dimensionless) is the ratio of $d(\alpha, \beta)$ and its maximum value (Figure 1.3).
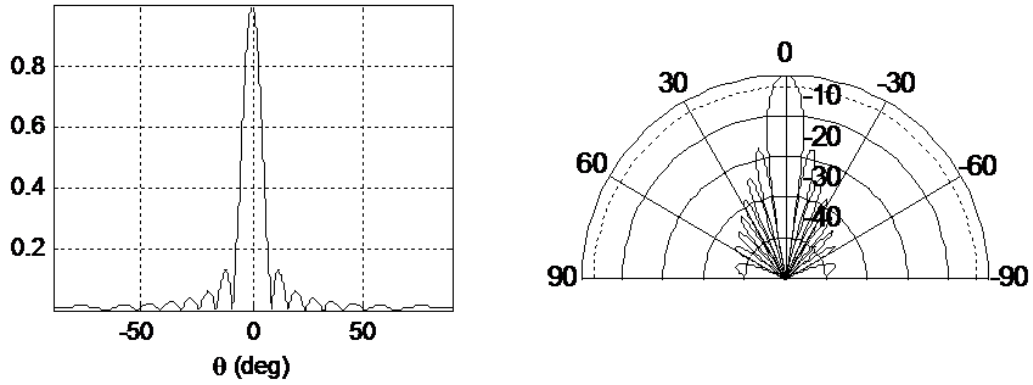
Figure 1.3. Equivalent representations of transducer directivity pattern, $b(\theta)$ (dimensionless) (left), and $B(\theta) = 10\log_{10}b(\theta)$ (dB re 1) (right), versus angle (θ) off the beam axis ($\theta = \alpha$, or β) of a piston transducer with a diameter equal to 50 wavelengths.

1.2.2.4 Gain

The *transducer gain, g* (dimensionless), is defined as the ratio of $i_t(\alpha, \beta)$ from a real transducer and an idealized lossless omnidirectional transducer, $i_{t\,omni}$ (W m^{-2}). It accounts for the *transducer efficiency, η* (dimensionless), which is the proportion of p_{et}, referred to a point on the electrical side of the transducer, converted to p_{at}:

$$g(\alpha, \beta) = \frac{i_t(\alpha, \beta)}{i_{t\,omni}} = \frac{p_{at}}{p_{et}}d(\alpha, \beta) = \eta d(\alpha, \beta) = g_0 b(\alpha, \beta) .$$

(1.5)

The *on-axis gain, g_0* (dimensionless), is the $g(\alpha, \beta)$ in the direction of maximum d (usually at $\alpha = 0°$, $\beta = 0°$). Both g_0 and $b(\alpha, \beta)$ are dependent on λ, which changes with c_w (Bodholt, 2002).

1.2.3 Propagation

1.2.3.1 Attenuation

As the transmitted pulse propagates to *range, r* (m), $p_{at}d(\alpha, \beta)$ is attenuated due to spreading of the wavefront (spherical spreading loss $= 1/4\pi r^2$) and conversion to heat in the water (absorption loss $= 10^{-\alpha_a r/10}$):

$$i = p_{at}d(\alpha, \beta)\frac{10^{-\alpha_a r/10}}{4\pi r^2} = p_{et}g(\alpha, \beta)\frac{10^{-\alpha_a r/10}}{4\pi r^2}$$

$$= \frac{u_{et}^2}{z_{et}}g(\alpha, \beta)\frac{10^{-\alpha_a r/10}}{4\pi r^2} = i_{et}^2 z_{et}g(\alpha, \beta)\frac{10^{-\alpha_a r/10}}{4\pi r^2},$$

(1.6)

where α_a (dB m^{-1}) is the *absorption coefficient*. Values for α_a, and their uncertainty, increase with f and vary with water temperature, salinity, pressure, pH, and λ (Urick, 1983).

1.2.3.2 Source intensity

Referring i to a *reference range, r_0* (m), conventionally 1 m, from the acoustic centre of the transducer in the direction of maximum d yields the *source intensity, i_s* (W m^{-2}):

$$i_s = p_{et}g_0\frac{10^{-\alpha_a r_0/10}}{4\pi r_0^2} = \frac{u_{et}^2}{z_{et}}g_0\frac{10^{-\alpha_a r_0/10}}{4\pi r_0^2} = i_{et}^2 z_{et}g_0\frac{10^{-\alpha_a r_0/10}}{4\pi r_0^2} .$$

(1.7)

The i_s is commonly expressed in decibels referred to the intensity of a plane wave with $p = 1$ µPa (p_{ref}), and termed *source level*, SL (dB re $\frac{p_{ref}^2}{\rho_w c_w}$ W m^{-2} at r_0):

$$SL = 10\log_{10}\left(\frac{i_s}{i_{ref}}\right) = 10\log_{10}\left(p_{et}g_0 \frac{10^{-\alpha_a r_0/10}}{4\pi r_0^2}\right) + 10\log_{10}\left(\frac{\rho_w c_w}{p_{ref}^2}\right)$$

$$= 10\log_{10}\left(\frac{u_{et}^2}{z_{et}} g_0 \frac{10^{-\alpha_a r_0/10}}{4\pi r_0^2}\right) + 10\log_{10}\left(\frac{\rho_w c_w}{p_{ref}^2}\right).$$

(1.8)

Assuming ρ_w = 1035 kg m^{-3}, c_w = 1500 m s^{-1}, and p_{ref} = 10^{-6} Pa,

$$SL = 10\log_{10}(i_s) + 181.91 = 10\log_{10}\left(p_{et} g_0 \frac{10^{-\alpha_a r_0/10}}{4\pi r_0^2}\right) + 181.91.$$

(1.9)

1.2.3.3 Backscattering cross section

When the transmitted wavefront encounters a target, the area effectively scattering the incident acoustic power is its *spherical scattering cross section*, σ_{sp} (m^2), which equals the *backscattering cross section*, σ_{bs} (m^2), multiplied by 4π (MacLennan *et al.*, 2002). Backscattering cross section is also known as the differential backscattering cross section (Medwin and Clay, 1998). As the reflected pulse travels between the target and the transducer, i is again attenuated due to spreading and absorption losses:

$$i = p_{et} g(\alpha, \beta) \frac{10^{-\alpha_a r/10}}{4\pi r^2} 4\pi\sigma_{bs} \frac{10^{-\alpha_a r/10}}{4\pi r^2} = \frac{p_{et}g(\alpha,\beta)\sigma_{bs}}{4\pi r^4 10^{\alpha_a r/5}}.$$

(1.10)

1.2.4 Reception

1.2.4.1 Effective receiving area

The *effective receiving area*, a_r (m^2), is the area of the transducer that transfers i to *received electric power*, p_{er} (W), referred to the same point on the electrical side of the transducer as p_{et} and $g(\alpha, \beta)$ (Kerr, 1988):

$$a_r = \frac{\lambda^2 g(\alpha,\beta)}{4\pi}.$$

(1.11)

Therefore,

$$p_{er} = i a_r = \frac{p_{et}g(\alpha,\beta)\,\sigma_{bs}}{4\pi r^4 10^{\alpha_a r/5}}\frac{\lambda^2 g(\alpha,\beta)}{4\pi} = \frac{p_{et}g(\alpha,\beta)^2\lambda^2\,\sigma_{bs}}{16\pi^2 r^4 10^{\alpha_a r/5}}.$$

(1.12a)

Values for p_{er} change with a_r, which changes with λ and thus c_w (Bodholt, 2002).

1.2.4.2 Effective pulse duration

To increase the signal-to-noise ratio, r_{sn}, (dimensionless), the transfer function of the receiver, including the transducer, receiver electronics, and digital filters, suppresses noise outside b_f and, in the process, delays, and distorts the echo pulse. Account must be made for this "filter delay" when estimating r from the sound propagation delay time, t (s), and c_w (see Simmonds and MacLennan, 2005). Correction for filter delay improves the accuracy of attenuation compensation, i.e. time-varied gain (Fernandes and Simmonds, 1996), and is especially critical for calibrations and measurements made at short ranges (Ona *et al.*, 1996). Modern echosounders generally correct for filter delay.

The receiver filter also modifies the amplitude and duration of the pulse, potentially altering the signal energy, $p_{er}\tau$. The perceived signal energy, discussed in MacLennan (1981), equals the measured instantaneous received power, $p_{er}(t)$ (W), a function of time, t (s), integrated over the period when it exceeds a threshold. For a single target, this period is the *effective pulse duration*, τ_{eff} (s) (see Sections 1.2.5.1 and 1.2.5.3).

1.2.5   Measurements

1.2.5.1   Range

The range to a scatterer is estimated by multiplying half of the propagation delay by an estimate of c_w for the propagation path. The maximum resolution of the range measurement is approximately equal to $c_w/2b_f$ (Burdic, 1991), assuming that the bandwidth of the receiver is larger than the transmitted signal bandwidth, b_f (Hz), and the Doppler shift in the scattered return from the target is negligible. For gated continuous wave (CW) signals with pulse duration, τ (s), $b_f \cong 1/\tau$. For frequency-modulated signals, b_f is larger and the range resolution is proportionately smaller.

1.2.5.2   Backscattering cross section

Values of σ_{bs} may be calculated by rearranging Equation (1.12):

$$\sigma_{bs} = \frac{p_{er}16\pi^2 r^4 10^{\alpha_a r/5}}{p_{et}g(\alpha,\beta)^2\lambda^2}.$$

(1.12b)

Some echosounders approximate p_{er} by the maximum measured received power, $\max[p_{er}(t)]$ (W), and account for any receiver gain or attenuation via the calibrated gain parameter (Simrad, 1993). Alternatively, p_{er} may be approximated by $\int_{\tau_{eff}} p_{er}(t)\,dt/\tau_{eff}$. Measurements of σ_{bs} are commonly presented in decibels referred to 1 m², termed *target strength, TS* (e.g. dB re 1 m²).

For a target on the beam axis, $g_0 = g(\alpha = 0°, \beta = 0°)$ (dB re 1), is obtained by rearranging Equation (1.12b):

$$g_0 = \left(\frac{p_{er}16\pi^2 r^4 10^{\alpha_a r/5}}{p_{et}\lambda^2\sigma_{bs}}\right)^{0.5}.$$

(1.12c)

The on-axis gain is the principle parameter estimated from a calibration, typically using a standard target (see Chapter 2).

In a *self-reciprocity calibration* (see Section 1.5.2.1), the transmitted acoustic pulse is received from a near-perfect reflector (e.g. a still air–water interface). Attenuation is calculated for one-way propagation from the transducer image. The *image range, r_i* (m), is twice the actual range from the transducer to the reflector, r ($r_i = 2r$):

$$p_{er} = p_{et}\,g_0\frac{10^{-\alpha_a r_i/10}}{4\pi r_i^2}\frac{\lambda^2 g_0}{4\pi} = \frac{p_{et}\lambda^2 g_0^2}{64\pi^2 r^2 10^{\alpha_a r/5}}.$$

(1.13a)

Rearranging:

$$g_0 = \left(\frac{p_{er}64\pi^2 r^2 10^{\alpha_a r/5}}{p_{et}\lambda^2}\right)^{0.5},$$

(1.13b)

which is independent of σ_{bs}. As self-reciprocity calibrations are typically made at short ranges, it is critical for estimates of r to be corrected for filter delay (see Simmonds and MacLennan, 2005) or measured physically.

1.2.5.3 Surface backscattering

The equivalent two-way beam angle, ψ (sr), is the solid angle subtended by an ideal conical beam that would produce the same volume integral as the square of the normalized real transducer directivity pattern. The area contributing to a received signal is the *sampled area*, a_s (m^2). The *surface backscattering coefficient*, s_s (m^2 m^{-2}), is the σ_{bs} per unit of a_s. Assuming a_s corresponds to the intersection of ψ and a sphere with radius equal to range r, centred on the transducer:

$$s_s = \frac{\delta \sigma_{bs}}{\delta a_s} = \frac{p_{er} 16\pi^2 r^2 10^{\alpha a r/5}}{p_{et} g(\alpha,\beta)^2 \lambda^2 \psi} .$$

(1.14)

This definition of s_s approximates normal incidence scattering from a flat seabed if the acoustic beam is narrow. Values of s_s are commonly expressed in decibels referred to 1 m^2 m^{-2}, and termed *Surface backscattering strength*, S_s (dB re 1 m^2 m^{-2}).

1.2.5.4 Volume backscattering

The *sample volume*, v_s (m^3), is the volume of water contributing to a received signal, corresponding to the intersection of ψ and a sphere of thickness $c_w\tau/2$ (Foote, 1991a). *Volume backscattering coefficient*, s_v (m^2 m^{-3}), is the total backscattering cross section per unit of sample volume:

$$s_v = \frac{\delta \sigma_{bs}}{\delta v_s} = \rho_v \sigma_{bs} = \frac{p_{er} 32\pi^2 r^2 10^{\alpha a r/5}}{p_{et} g(\alpha,\beta)^2 \lambda^2 c_w \tau \psi},$$

(1.15)

where ρ_v (number m^{-3}) is the *scatterer volume density*, and σ_{bs} is the mean backscattering cross section for the scatterers in the sampled volume. To account for the effects of the receiver filter, replace τ with τ_{eff}:

$$s_v = \frac{p_{er} 32\pi^2 r^2 10^{\alpha a r/5}}{p_{et} g(\alpha,\beta)^2 \lambda^2 c_w \tau \psi s_{a\,corr}^2} ,$$

(1.16)

where $s_{a\,corr} = (\tau_{eff}/\tau)^{0.5}$ (dimensionless) is the s_a *correction factor*. $s_{a\,corr}$ is squared in Equation (1.16) so that it relates linearly to gain. During calibration with a target near the beam axis, $s_{a\,corr}^2$ can be estimated from the ratio of the energies in the perceived signal, and a square pulse defined by $\max[p_{er}(t)]$ and τ:

$$s_{a\,corr}^2 = \frac{\tau_{eff}}{\tau} = \frac{\int_{\tau_{eff}} p_{er}(t)dt}{\max[p_{er}(t)]\tau} .$$

(1.17)

Values of s_v are commonly expressed in decibels referred to 1 m^2 m^{-3}, and termed *volume backscattering strength*, S_v (dB re 1 m^2 m^{-3}).

1.2.5.5 Area backscattering

Area backscattering coefficient, s_a (m^2 m^{-2}), is the integral of s_v over a measurement range, r_1 to r_2, often associated with a sampled depth range.

$$s_a = \int_{r_1}^{r_2} s_v dr .$$

(1.18a)

Nautical area backscattering coefficient, s_A (m^2 nautical mile^{-2}), is the same variable with different units and a legacy factor (4π) (MacLennan *et al.*, 2002).

$$s_A = 4\pi (1852)^2 \int_{r_1}^{r_2} s_v dr .$$

(1.18b)

1.2.5.6 Areal density

Scatterer areal density, ρ_a (number m^{-2}) or ρ_A [number (nautical mile)$^{-2}$], is the number of scatterers within the measurement range, e.g. depth range, per unit of sampled area, e.g. sea surface area:

$$\rho_a = \frac{s_a}{\sigma_{bs}}, \text{ and}$$

(1.19a)

$$\rho_A = \frac{s_A}{4\pi\sigma_{bs}}.$$

(1.19b)

1.2.5.7 Abundance

Scatterer abundance, n_b (number), is the number of target organisms within the measurement range, e.g. depth range, and the sampled area, a_s (m^2) or a_S (nautical mile^2):

$$n = \rho_a\, a_s, \text{ and}$$

(1.20a)

$$n_b = \rho_A\, a_S.$$

(1.20b)

Values for ρ_a and n_b may be converted from units of number to kg, i.e. mass or biomass, using an appropriate factor with units of kg number^{-1} (e.g. see Hewitt and Demer, 1993; Barange *et al.*, 1996; Demer *et al.*, 2012).

1.2.6 Sensitivities

As previously mentioned, many of the above terms and equations used to process echosounder data originated in radar theory. Below, some of these terms are equated with those from classical sonar theory.

1.2.6.1 Transmit sensitivity

Transmit voltage sensitivity, S_u (dB re 1 µPa V^{-1}) (also known as the transmit voltage response), is defined as the SL resulting from a 1-V rms continuous-wave signal applied to a point on the electrical side of the transducer (Figure 1.4). It is expressed by substituting u_{et}^2 with $(1\text{ V})^2$ in Equation (1.8):

$$S_u = 10\log_{10}\left(\frac{(1\text{ V})^2}{u_{et}^2}\frac{i_s}{i_{ref}}\right) = 10\log_{10}\left(\frac{(1\text{ V})^2}{z_{et}}g_0\frac{10^{-\alpha_a r_0/10}}{4\pi r_0^2}\frac{\rho_w c_w}{p_{ref}^2}\right), \text{ or}$$

(1.21a)

$$s_u = \frac{(1\text{ V})^2}{z_{et}}g_0\frac{10^{-\alpha_a r_0/10}}{4\pi r_0^2}\frac{\rho_w c_w}{p_{ref}^2}.$$

(1.21b)

Rearranging Equation (1.21a):

$$SL = S_u + 20\log_{10}\left(\frac{u_{et}}{1\text{ V}}\right).$$

(1.21c)

Rearranging Equation (1.21b):

$$g_0 = s_u\frac{z_{et}}{(1\text{ V})^2}i_{ref}4\pi r_0^2 10^{\alpha_a r_0/10}.$$

(1.21d)

Therefore, g_0 is a function of s_u and z_{et}.

Transmit current sensitivity, S_i (dB re 1 μPa A⁻¹) (also known as the transmit current response), is defined as the SL resulting from a 1–A rms continuous-wave signal applied to a point on the electrical side of the transducer (Figure 1.1). It is similarly expressed by substituting $i_{et}{}^2$ with $(1 \text{ A})^2$ in Equations (1.7) and (1.8):

$$S_i = 10\log_{10}\left(\frac{(1 \text{ A})^2}{i_{et}{}^2}\frac{i_s}{i_{ref}}\right) = 10\log_{10}\left((1 \text{ A})^2 z_{et}\, g_0 \frac{10^{-\alpha_a r_0/10}}{4\pi r_0{}^2}\frac{\rho_w c_w}{p_{ref}{}^2}\right), \text{ or}$$

(1.22a)

$$s_i = (1 \text{ A})^2 z_{et}\, g_0 \frac{10^{-\alpha_a r_0/10}}{4\pi r_0{}^2}\frac{\rho_w c_w}{p_{ref}{}^2}.$$

(1.22b)

Rearranging Equation (1.22a):

$$SL = S_i + 20\log_{10}\left(\frac{i_{et}}{1 \text{ A}}\right).$$

(1.22c)

Rearranging Equation (1.22b):

$$g_0 = s_i \frac{1}{(1 \text{ A})^2 z_{et}} i_{ref} 4\pi r_0{}^2 10^{\alpha_a r_0/10}.$$

(1.22d)
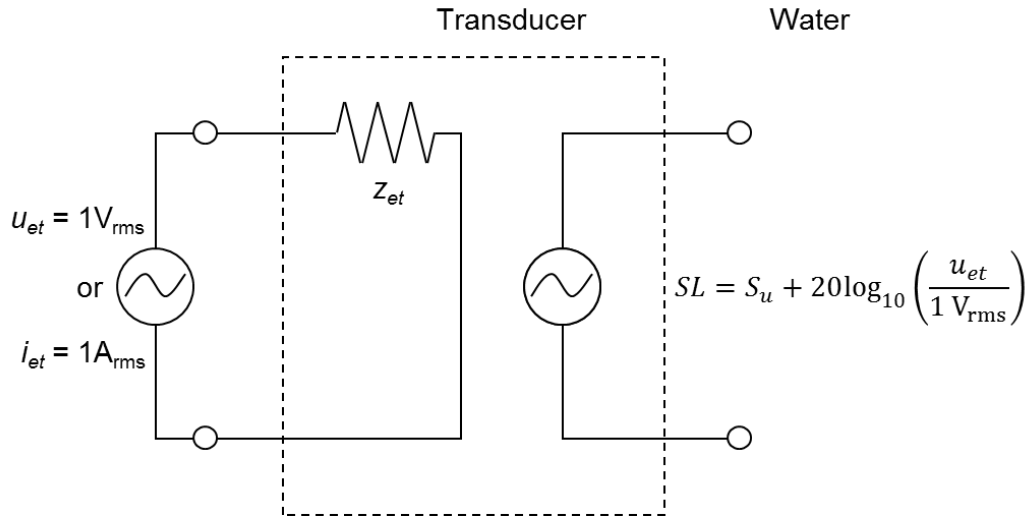
Figure 1.4. Transmit voltage (s_u) and current sensitivities (s_i) are defined as the source level (*SL*) resulting from a continuous-wave rms signal, u_{et} = 1 V or i_{et} = 1 A, respectively, applied to a point on the electrical side of the transducer.

1.2.6.2 Receive sensitivity

The *receive voltage sensitivity*, M_u (dB re 1 V μPa⁻¹) (also known as the open-circuit receiving sensitivity), is defined as the open-circuit rms voltage at a point on the electrical side of the transducer resulting from a plane wave with i_{ref} applied to the transducer surface (Figure 1.5) (Andersen, 2006) :

$$M_u = 20\log_{10}\left(\frac{u_{et}}{1 \text{ V}}\right) - 10\log_{10}\left(\frac{i}{i_{ref}}\right).$$

(1.23)

Transducer   Water

$$20\log_{10}\left(\frac{u_{et}}{1\ \text{V}_{\text{rms}}}\right) = M_u + 10\log_{10}\left(\frac{i}{i_{ref}}\right)$$

$$u_{et} \quad p = (i\rho_w c_w)^{0.5}$$
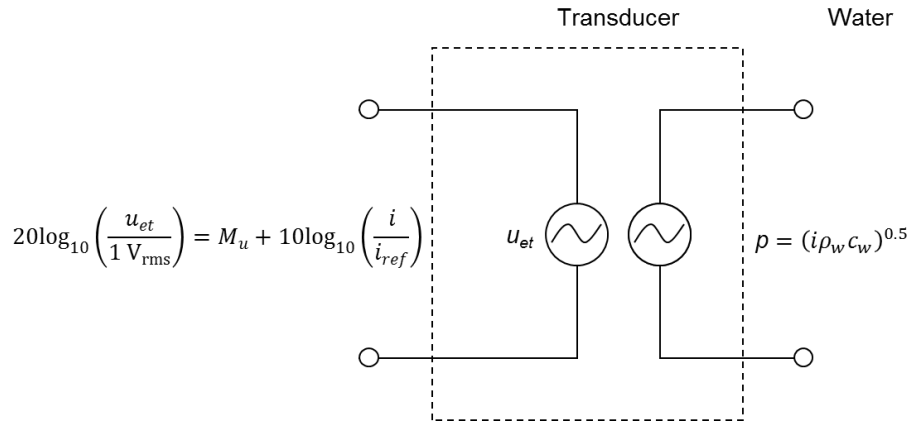
Figure 1.5. Receive voltage sensitivity (M_u) is defined as the open-circuit voltage at a point on the electrical side of the transducer resulting from a plane wave with an rms pressure of 1 μPa applied to the transducer surface.

When the transducer is connected to an echosounder receiver, the *received voltage*, u_{er} (V), is equal to the transducer voltage, u_{et} (V), electrically divided by z_{et} and the echosounder *receiver electrical impedance*, z_{er} (Ω) (Figure 1.6):

$$u_{er} = \frac{u_{et}z_{er}}{z_{er}+z_{et}}.$$

(1.24)

In the ideal case when $z_{er} = z_{et}$, the receiver is "matched" to the transducer and the p_{er}, proportional to $u_{er}{}^2$, is maximally transferred to the echosounder receiver.

$$u_{er} = \frac{u_{et}z_{et}}{2z_{et}} = \frac{u_{et}}{2}, \text{ and}$$

(1.25)

$$p_{er} = \frac{u_{er}{}^2}{z_{er}} = \frac{u_{et}{}^2}{4z_{et}}.$$

(1.26)

Echosounder   Transducer   Water

$$u_{er} = \frac{u_{et}Z_{er}}{Z_{er} + Z_{et}} \qquad Z_{er} \qquad Z_{et} \qquad u_{et} \qquad p = (i\rho_w c_w)^{0.5}$$

Figure 1.6. The voltage received by an echosounder (u_{er}) in response to an acoustic pressure on the transducer face is a fraction of the transducer voltage (u_{et}) defined by the echosounder receiver and transducer impedances (z_{er} and z_{et}, respectively).

The p_{er0} is expressed by combining Equations (1.1), (1. 3), (1.11) and (1.26):

$$p_{er0} = ia_r \text{ , and}$$

(1.27a)

$$\frac{u_{et}^2}{4z_{et}} = \frac{i\lambda^2 g_0}{4\pi} \text{ .}$$

(1.27b)

Dividing both sides by $(1\text{ V})^2$ and i_{ref}:

$$\frac{u_{et}^2}{(1\text{ V})^2 i_{ref} 4z_{et}} = \frac{i\lambda^2 g_0}{(1\text{ V})^2 i_{ref} 4\pi} \text{ .}$$

(1.27c)

Converting to decibels and rearranging:

$$20\log_{10}\left(\frac{u_{et}}{1\text{ V}}\right) - 10\log_{10}\left(\frac{i}{i_{ref}}\right) = 10\log_{10}\left(g_0 \frac{\lambda^2}{4\pi} i_{ref} \frac{4z_{et}}{(1\text{ V})^2}\right)$$
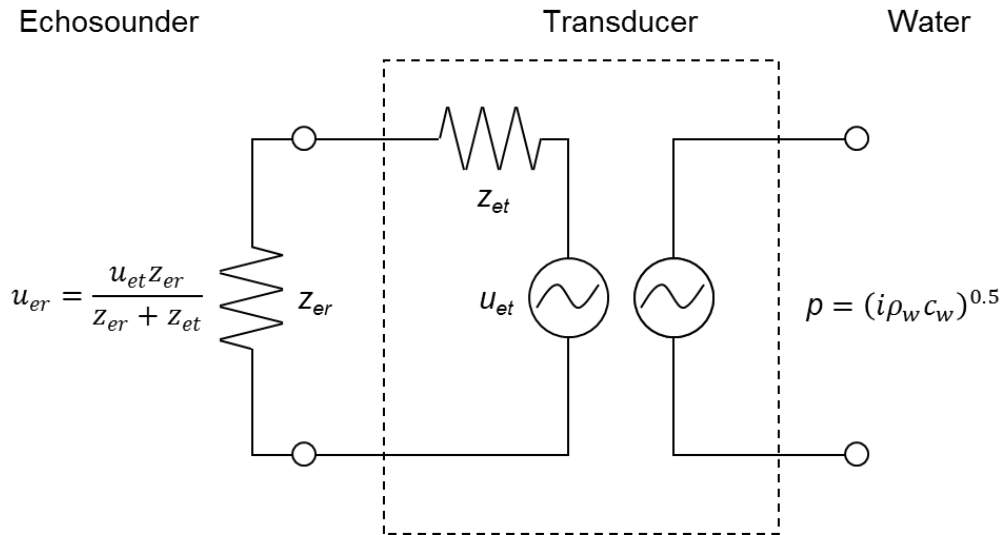
(1.27d)

Substituting Equation (1.23):

$$M_u = 10\log_{10}\left(g_0 \frac{\lambda^2}{4\pi} i_{ref} \frac{4z_{et}}{(1\text{ V})^2}\right), \text{ or}$$

(1.27e)

$$m_u = g_0 \frac{\lambda^2}{4\pi} i_{ref} \frac{4z_{et}}{(1\text{ V})^2} \text{ .}$$

(1.27f)

Rearranging:

$$g_0 = \frac{4\pi}{\lambda^2} \frac{(1\text{ V})^2}{4z_{et}} \frac{m_u}{i_{ref}} \text{ ,}$$

(1.27g)

which indicates that g_0 may be modulated by changes in m_u, ρ_w, c_w, and z_{et}, which may covary (Demer and Renfree, 2008).

The *reciprocity parameter*, j (dimensionless), is the ratio of the response of a reciprocal transducer acting as a receiver, i.e. m_u, to its response as a transmitter, i.e. s_i, (Foldy and Primakoff, 1945; Carstensen, 1947; Primakoff and Foldy, 1947; Urick, 1983). Substituting Equations (1.22b) and (1.27f), and ignoring absorption:

$$j = \left(\frac{m_u}{s_i}\right)^{0.5} = \left(\frac{i_{ref} g_0 \frac{\lambda^2}{\pi} \frac{z_{et}}{(1\text{ V})^2}}{(1\text{ A})^2 z_{et} g_0 \frac{1}{4\pi r_0^2} \frac{\rho_w c_w}{p_{ref}^2}}\right)^{0.5} \text{ .}$$

(1.28a)

Cancelling and rearranging:

$$j = \frac{2\lambda r_0 p_{ref}^2}{\rho_w c_w} \left(\text{W}^{-1}\right) \text{ .}$$

(1.28b)

Substituting $p_{ref} = 10^{-6}\text{Pa}$, $\text{Pa} = \text{kg m}^{-1}\text{s}^{-2}$, and $\text{W} = \text{kg m}^2\text{s}^{-3}$:

$$j = \frac{2\lambda r_0}{\rho_w c_w} 10^{-12} \left(\frac{\text{kg}}{\text{m}^4 \cdot \text{s}}\right)$$

(1.28c)

1.3 Common echosounder types

There are several types of echosounders that are now commonly used for fishery applications. These include single-beam, split-beam, and multibeam echosounders, and single-beam (conventional) and split-beam (interferometric or phase-measuring)

sidescan sonars. Less commonly used devices include acoustic Doppler current profilers (ADCPs), acoustic cameras, and scanning sonars (see Chapter 5). The method used to calibrate an echosounder generally depends on the system's ability to estimate the bearing angles, α, β, (°), to a target.

1.3.1 Single-beam

For single-beam echosounders, the bearing angles in the direction of the maximum transducer directivity pattern, conventionally $\alpha = 0°, \beta = 0°$ (see Figure 1.3) may be estimated by positioning a spherical target such that its echo is maximized. Then, if the sphere σ_{bs} and the $b(\alpha, \beta)$ are known for one or more colocated transducers, the off-axis elevation angles can be estimated from the differences in on-axis and off-axis measures of sphere σ_{bs} (Warren and Demer, 2010). For echoes from targets with unknown σ_{bs} values, the natural convolution of the target σ_{bs} values and $b(\alpha, \beta)$ causes ambiguity in the estimated bearing angles. However, if an ensemble of backscatter measurements is made randomly throughout the transducer beam, the $b(\alpha, \beta)$ can be deconvolved to estimate the probability density function (pdf) of the actual σ_{bs} values (Clay and Medwin, 1977).

1.3.2 Split-beam

Split-beam echosounders can more accurately estimate bearing angles to targets within the main lobe of the transducer, provided the targets are resolvable in range and constrained to a narrow range of angles compared to the beamwidth. Split-beam transducers are separated into subarrays (e.g. four quadrants for a circular transducer). The effective separation between the subarray centres (d_{eff}) produces small range differences to the target that are observed as phase-differences in the received signals between each pair of quadrants (Burdic, 1991). In two dimensions and using the notation defined by Figure 1.7, this electrical phase difference, φ_e (rad), is:

$$\varphi_e = 2\pi \frac{r_2 - r_1}{\lambda} \cong k d_{eff} \sin(\theta) = \Lambda \sin(\theta) \,,$$

(1.29)

where r_2 and r_1 are the ranges between the centres of each subarray and the target, λ is the acoustic wavelength at the transducer, k is the acoustic wavenumber ($k = 2\pi f / c_w$), and θ is the angle to the target relative to the transducer beam axis, i.e. α or β. The product $k d_{eff}$ is termed angle sensitivity, Λ (electrical°/geometric°). The d_{eff} is known *a priori* and the sound speed, c_w (m s⁻¹), at the transducer can be measured.
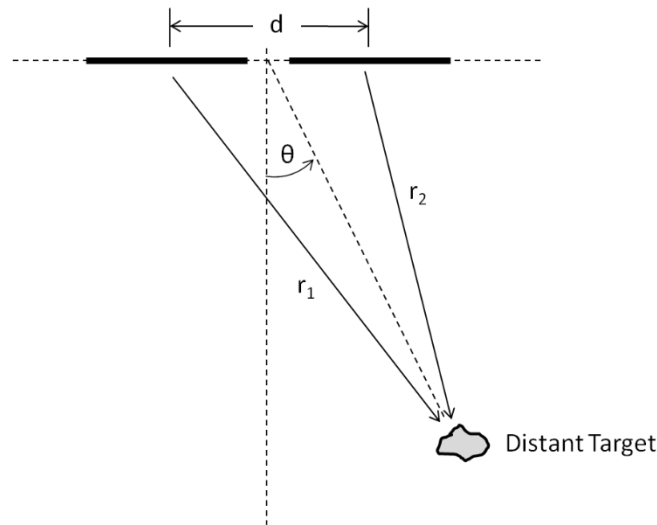
Figure 1.7. The geometry for a two-dimensional split-beam. The subarrays are represented as thick dark lines, separated by a distance d_{eff} (d in the figure).

If targets are not resolvable, measurements of φ_e may not be possible or accurate (e.g. Hewitt and Demer, 1991; Foote, 1996; Soule *et al.*, 1996; Demer *et al.*, 1999). Also, φ_e may not be measurable for targets away from the beam axis if the pulses are short and the targets are extended in range, because the pulses received on each subarray may not sufficiently overlap (Lurton, 2000). In general, the uncertainty associated with φ_e increases as the target occupies more of the beam (Jin and Tang, 1996) and the ratio of signal and noise intensities, r_{sn} (dimensionless), decreases (Demer *et al.*, 1999). For ideal point targets, the standard deviation (σ) for a phase-difference measurement is (Burdic, 1991; Demer *et al.*, 1999):

$$\sigma = \sqrt{2/r_{sn}} \ .$$

(1.30)

1.3.3   Sidescan

Sidescan sonars are a type of single-beam echosounder which have a transducer (stave) that is several tens of wavelengths long in one direction and a few wavelengths or less in the orthogonal direction, producing an asymmetric beam with an angular resolution that is typically ≤1° or ≥50°, respectively. Sidescan sonars have the same target-angle ambiguity as other single-beam echosounders. However, for imaging seabed backscatter, sidescan sonars use an estimate of the sound speed along the propagation path to convert propagation delays to target ranges and, assuming the seabed is flat and horizontal, or known from an independent source, to bearing angles.

There are also split-beam (interferometric) sidescan sonars that are constructed by stacking two or more single-beam transducers (Figure 1.8). The backscatter from a target constrained to a narrow range of the beamwidth is manifested as a split-beam phase difference that is used to estimate the bearing angle (see Section 1.3.2). Developed for seabed mapping, the bearing angles are only estimated in one plane (typically athwartships). The bearing angles in the orthogonal plane (typically alongships) are estimated as the direction of the beam axis (see Section 1.3.1).
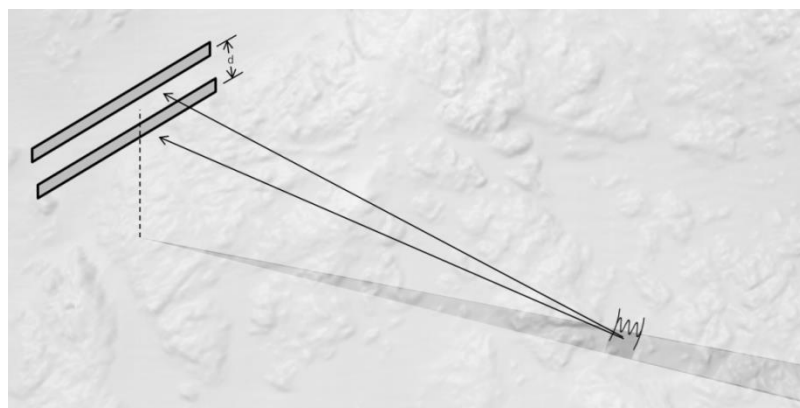
Figure 1.8. The geometry for bearing estimations using split-beam sidescan sonar. Two single-beam sidescan transducers, separated by a distance d_{eff} (d in the figure), are used to measure electrical phase differences and thus estimate the bearing angles to the seabed.

1.3.4   Multibeam

Multibeam echosounders are constructed from an array of transducer elements. In the common Mills cross configuration (Figure 1.9), for example, a line array (similar to a side-scan transducer) is used to transmit a fan beam, and an orthogonal array of elements is used to electronically form multiple, typically hundreds, of perpendicular receive beams. This combination of transmit and receive beams creates a swath of narrow, typically <1°, "pencil" beams.
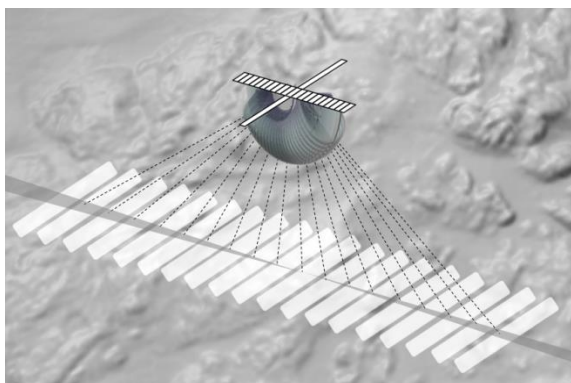
Figure 1.9. The geometry for a Mills cross hydrographic multibeam echosounder consisting of a line array which insonifies a narrow slice of the water column, and an orthogonal receive array that is steered to form many beams. The combination of the two creates multiple narrow beams that can be used to estimate ranges to targets along predetermined angles.

Multibeam transducers can also be constructed using two- or three-dimensional arrays of transducer elements arranged in a plane, cylinder, or other geometry. To transmit multiple beams, distinct frequencies or orthogonal phase-codes (unambiguous signals) are used for each beam to avoid cross-talk between beams. The number of transmit beams and their signal levels are limited by the power densities that can be achieved without non-linear effects (Tichy *et al.*, 2003; Korneliussen *et al.*, 2008) or damage to the transducer elements. To simultaneously steer and adjust the directivities of multiple receiver beams, the digitized signals from the transducer elements are typically "beam-formed" using complex weights, time delays, or both.

In multibeam echosounders, target-bearing angles are estimated in different ways depending on the nature of the target. For targets that span a small portion of the beamwidth, the beamforming may include subarrays and split-beam processing. For targets

that span a large portion of the beamwidth, the beamformer output is largest at the most probable bearing angle. Although extended to multiple beams, this filtering is analogous to bearing angle estimation in a single-beam echosounder.

1.3.5   Wide-bandwidth

Wide-bandwidth echosounders transmit signals spanning several octaves (Stanton *et al.*, 2010), and the backscatter vs. frequency (spectra) is often used to classify the acoustic targets (Woodd-Walker *et al.*, 2003; Imaizumi *et al.*, 2008; Johnsen *et al.*, 2009). For example, low-frequency backscatter spectra from fish may indicate mechanical resonances in their swimbladders (Hersey *et al.*, 1962), midfrequency spectra may differentiate backscatter from fish and zooplankton (e.g. Demer *et al.*, 2009b), and high-frequency spectra may differentiate backscatter from marine organism and turbulent microstructure (e.g. Lavery *et al.*, 2010a). Because the transceiver electronics, transducer characteristics, and sound propagation medium all affect the frequency spectra, it is necessary to quantify and deconvolve these effects from the target's backscattering spectra. For example, most acoustic transducers have frequency-dependent beamwidths and sensitivities (Rogers and Van Buren, 1978), which must be taken into account when calibrating a wide-bandwidth echosounder (Islas-Cital *et al.*, 2010).

1.3.6   Scanning

Scanning sonars electrically or mechanically steer acoustic beams to insonify and image scatterers throughout a large swath, potentially 360° horizontal, or hemisphere. The effective range of a scanning sonar depends on the signal type and bandwidth, and the scatterers. Scanning sonars have long been used by fishers to detect fish schools. They are used increasingly to observe fish behaviour and quantify their aggregation biomass.

1.3.7   Acoustic Doppler

An acoustic Doppler current profiler (ADCP) is an echosounder that measures relative water speed inferred from the shift in frequency content of the received vs. transmitted pulses. ADCPs typically have three or four narrow-beam transducers oriented in different directions to measure water velocity (speed and direction). The frequency shift is proportional to the velocity of the target relative to the ADCP beam axis. ADCP measurements are calculated with the assumption that the water speed is equivalent to that of the particulates or organisms contributing to the backscatter. ADCPs may also use echoes from the seabed to estimate movement of the instrument platform relative to earth. In addition to measuring current and platform velocities, most ADCPs measure echo intensity. However, the quality of echo intensity data from ADCPs is generally limited by a low dynamic range, temperature-sensitive gain, and the processing of wide-bandwidth signals. Because ADCPs are available on many research vessels, their data is often used opportunistically for various types of surveys, e.g. biomass or suspended sediment.

1.3.8   Imaging

An underwater acoustic camera uses echo intensity and propagation-delay data from an array of synchronous echosounder beams to create a two- or three-dimensional image of scatterers within the field-of-view. Some acoustic cameras use beamforming to amplify the signal in certain directions while suppressing the others. This method is fast and robust, but the beam sidelobes can produce ghost images. Alternatively, some acoustic cameras use acoustic lenses to create the receiver array. Acoustic cameras are used increasingly to observe animals in shallow and turbid water, and near the seabed.

1.4 Common transducer platforms

Echosounders and their transducers are mounted on a variety of platforms ranging from mobile research vessels and autonomous vehicles to relatively stationary landers and buoys. In each case, echosounder calibrations are generally performed using the sphere method (see Chapter 2).

1.4.1 Vessel

An acoustic system is generally installed on a vessel when its primary purpose is to survey targets spanning large areas, map their distributions, and estimate their abundance, e.g. using echo integration methods (Dragesund and Olson, 1965). On a vessel, transducers are mounted either on the hull or keel or over the side using a pole or towed-body. In most cases, the beam axis of each transducer is oriented downward, the cables are routed to minimize electrical interference and mechanical vibration, and calibration equipment is available to facilitate routine calibrations.

1.4.1.1 Hull

Transducers may be permanently mounted on a vessel hull or keel or on a small pod extending a short distance below the hull (Simmonds and MacLennan, 2005), optimally below any aerated water to provide low-noise operation. The main disadvantages of hull-mounted installations are cost and the signal loss due to motion-induced bubbles forced along the ship's hull in adverse weather conditions (Carstensen, 1947; Dalen and Lovik, 1981; Shabangu *et al.*, 2014). Hull mounting often requires architecture and engineering, dry docking, fabrication, installation, and testing. Therefore, it is done when the benefit of dedicating equipment to a vessel outweighs the installation costs.

1.4.1.2 Centreboard

It is now common to mount transducers on the bottom surface of a retractable centreboard. The centreboard positions the transducers at variable, user-defined depths below the hull, typically 5–10 m depth, to reduce vessel motion and noise from bubbles.

1.4.1.3 Pole

Transducers may be mounted on the end of a pole affixed to the side, bow, or stern of a vessel (Figure 1.10). Usually, the pole length positions the transducers a few metres below the water surface close to the depth of the vessel hull. The transducer depth may be fixed or adjustable. Transducers deployed deeply on a pole have advantages similar to centreboard-mounted transducers. However, poles are smaller than centreboards and can be retrofitted to small and large vessels (Gangl and Whaley, 2004; Cutter and Demer, 2007). Poles should be rigid during surveys and retractable for transiting and docking.

Figure 1.10. Pole-mounted transducers. Hydraulically retractable poles (left) are used to mount multibeam (starboard) and multifrequency split-beam transducers (port) on a small craft. A manually retractable pole is used aboard a fishing boat and other platforms of opportunity (right).

1.4.1.4 Towed and cast

Towed bodies and cast platforms may be used to deploy transducers alongside, behind, or beneath the vessel (Figure 1.11). They are portable and may be moved regularly among vessels that are not equipped with permanently mounted scientific echosounders, such as chartered commercial vessels. During surveys, towed-bodies are often positioned 4–6 m below the surface to avoid bubble noise and side-lobe echoes from the hull. However, when surveying fish or measuring backscattering cross sections at large depths, towed bodies or cast platforms may position the transducers 10s–100s of metres deep. Deep deployments reduce the ranges between the transducers and the acoustic targets, improving the spatial resolution of the measurements (Ona and Mitson, 1996).

Figure 1.11. Cast echosounder systems are used to position echosounders and deep-water transducers closer to demersal fish targets. In this case, the transducer is gimballed to provide vertical measurements, irrespective of platform tilt due to, e.g. water current.

1.4.2 Autonomous moving

Acoustic transducers may be deployed on autonomous underwater vehicles (AUVs), gliders, drifters, buoys, and landers. Such platforms may be used to collect data independently from a surface vessel and over large distances (e.g. several 1000 km), long time-scales (e.g. months), or both.

1.4.2.1 Propelled

AUVs are self-propelled and perform preprogrammed underwater missions (e.g. Fernandes *et al.*, 2003). They are often torpedo shaped, 2–10 m long, and 0.2–1.3 m in diameter (Figure 1.12). Echosounder transducers may be mounted on AUVs in down-, up- or side-projecting orientations (Scalabrin *et al.*, 2009).

Figure 1.12. An autonomous underwater vehicle (AUV) fitted with a split-beam echosounder and an acoustic Doppler current profiler.

Underwater gliders are autonomous vehicles that undulate along transects using wings for lift and low-power electro-mechanics to control pitch, roll, and buoyancy (Rudnick *et al.*, 2004). They may survey several thousand kilometres over several months (Eriksen *et al.*, 2001; Davis *et al.*, 2002). Sensors require low power and low hydrodynamic resistance (drag).

1.4.2.2 Drifting

Transducers mounted on drifters can be used to investigate organisms or processes that are dependent on oceanic currents. Once deployed, a Lagrangian drifter moves with water currents at the sea surface or at a specific water depth or density, depending on buoyancy. Some drifters can be programmed to change buoyancy and, therefore, may reside at user defined water depths throughout their deployment.

1.4.3 Autonomous stationary

Transducers may be mounted in a fixed location to observe the physical and biological environment vs. time. Stationary platforms facilitate observations on many temporal scales and do not require an operator or propulsion. Echosounder power may be supplied via cable from shore, or locally by batteries, perhaps recharged by photovoltaic cells or a wind generator.

1.4.3.1 Buoy

An echosounder system on a moored buoy may be used to monitor a selected location (Brierley *et al.*, 2006). Often, the echosounder transceiver, GPS receiver, computer, batteries, radio, and transducer are contained in the buoy float. The transducers, oriented horizontally or vertically, are positioned multiple metres below the sea surface to reduce bubble noise and the potential for biofouling (Figure 1.13).

Figure 1.13. Buoys fitted with dual-frequency and split-beam echosounders, and acoustic Doppler current profilers.

1.4.3.2 Lander

Landers are stationary platforms positioned on or near the seabed. Transducers mounted on landers usually project up or to the side. Landers are often used to make measurements spanning from near the seabed to the sea surface over long periods of time. They may also be used in areas where buoys are adversely subjected to weather or vandalism.

1.5 Calibration methods

Acoustic instrument calibrations estimate the accuracy (systematic error) and precision (random error) in the transduction processes and measurements of the resulting electrical signals. Each signal-processing step, from generation to digitization, may affect the system calibration. This does not necessarily mean that each process must be calibrated independently; it is generally more accurate and efficient to calibrate the whole echosounder system. In any case, acoustic instrument calibrations should be performed over the range of environmental conditions, particularly water temperature, t_w (°C), and pressure, p_w (mbar), or depth (Leroy and Parthiot, 1998) encountered during the measurements made using the instrument.

There are a number of methods to calibrate acoustic instruments (Urick, 1983; Bobber, 1988; Simmonds and MacLennan, 2005). These methods may be categorized as component or system calibrations.

1.5.1 Component

A component calibration requires identification and performance evaluation of each system component. It requires an assumption that the systematic errors from each component are independent and linearly sum to indicate the total systematic error (bias) in the measurement system. A component calibration may be useful to identify the major sources of systematic error and to confirm that the performance of each component is within the specification tolerance. However, a component calibration generally requires additional calibration instrumentation, expertise, and time, with its result affected by the accumulation of errors. Described below are some methods for characterizing some echosounder components, principally the transducer.

1.5.1.1 Transducer reciprocity

The sensitivities of a reciprocal transducer, i.e. one in which the energy losses on transmission are the same as on reception, may be measured by a reciprocity calibration (Schottky, 1926; Foldy and Primakoff, 1945). This involves three uncalibrated transducers including a projector, hydrophone, and the transducer to be calibrated (MacLennan and Simmonds, 1992). The three transducers are positioned in a triangle with distances between them being greater than their far-field ranges (Urick, 1983). For each set of measurements, the acoustic axes of each transducer pair must be aligned. For further details, see Urick (1983) and Bobber (1988). Reciprocity calibrations may be practical for calibrating echosounder transducers in tanks, but probably not in the field.

1.5.1.2 Transducer impedance

Echosounder transducers may be calibrated (MacLean, 1940; Sabin, 1956) and their performance monitored by measuring transducer impedance (Demer and Renfree, 2008). Transducer impedance and, therefore, transducer performance may change for a variety of reasons, e.g. due to changes in water temperature and pressure, electrical isolation, or damage to the piezoelectric elements. Impedance measurements may be made with an impedance analyser. However, some instruments have integrated tests for rapidly monitoring change in the transducer impedance.

1.5.1.3 Element analysis

Transducers have transmit- and receive-beam directivities that depend on the ratios of their sizes and the acoustic wavelengths. To increase the beam directivity and reduce its sidelobe intensities, and perhaps steer its axis, echosounder transducers are often composed of multiple elements that are electrically and spatially weighted, and beamformed, respectively (Wilson, 1988).

Some echosounder systems provide raw data from each transducer element. Therefore, theoretically, it is possible to characterize the performance of each transducer element and use those results to calculate the performance of the transducer for a variety of transmit and receive configurations. Practically, however, this strategy could require the characterization of numerous transducer elements and many assumptions about manufacturing tolerances; the resulting estimate of transducer performance would be subject to the accumulation of estimation errors.

More convenient are tools, available in many echosounders, that monitor the performances of individual elements and their transceiver channels during transmission and reception (e.g. Figure 1.14). This can be helpful as the beamforming performance of a numerous-element transducer array may not be obviously degraded by a few defective elements or transceiver channels.
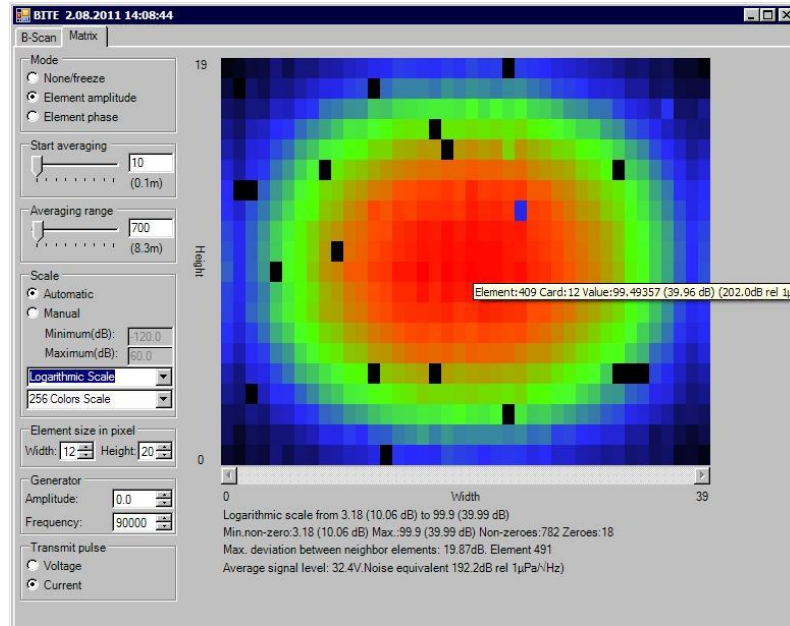
Figure 1.14. The ME70 BITE utility (Simrad, 2012) displays the average transmit level for each transducer element and transceiver channel. In this example, one element (blue) has a weak transmit level compared to surrounding elements. Elements associated with noisy channels on a transceiver (black) are disabled.

If one or more transducer elements or transceiver channels has become defective, the directivity pattern resulting from the functioning elements may be simulated to learn if the system performance has likely changed and, if so, what corrections may be applied or what maintenance actions are required (Figure 1.15).
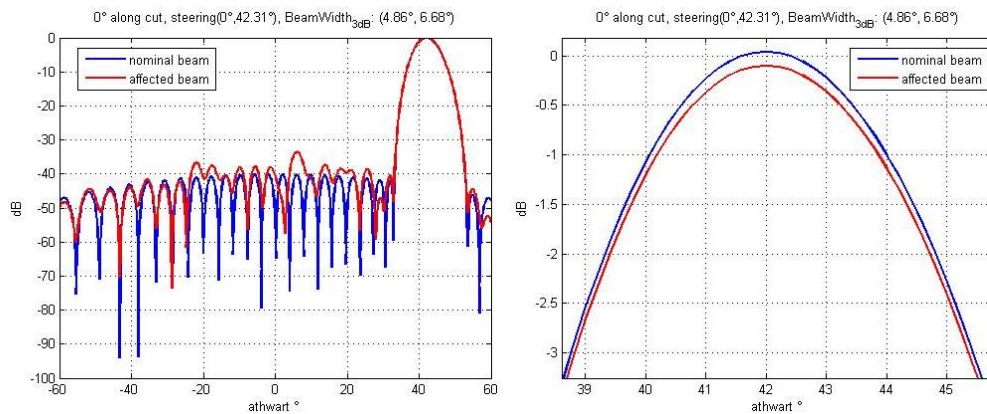
Figure 1.15. Beamforming simulation with and without the disabled elements shown in Figure 1.14. In this example, the sidelobe levels (left plot) have increased substantially (>6 dB), and exceed the specification. However, the loss of signal level in the main lobe (right plot) is small (~−0.14 dB), so the change in system performance may be negligible, depending on the application.

1.5.2　System

A system calibration evaluates the collective performance of the system components, such as the transmit and receive electronics, connectors, cables, and transducers. A system calibration can be performed following the recommended sphere method (Foote *et al.*, 1987), detailed in Chapter 2. When appropriate, other methods, briefly described below, can be used.

1.5.2.1 Self-reciprocity

A self-reciprocity calibration (Widener, 1980a, 1980b; Urick, 1983; Bobber, 1988) is analogous to a sphere calibration (Foote *et al.*, 1987; Sawada and Furusawa, 1993; Vagle *et al.*, 1996) when the echo from the target is replaced by the pulse transmitted from a virtual transducer (see Section 1.2.5.1). To do this, the transducer beam is accurately and precisely aligned perpendicularly to a mirror surface, e.g. a flat air–water interface that provides near-total reflection. Alignment is critical. Then, the received echo apparently originates from a virtual transducer that is twice the range between the real transducer and the reflecting surface (Carstensen, 1947; Urick, 1983; Bobber, 1988). Self-reciprocity calibrations may be performed in tanks, but they may not be practical for field calibrations because hull-mounted transducers are generally not oriented towards the sea surface.

The accuracy of a self-reciprocity calibration depends on the near-total reflection which may be degraded by misalignment and the roughness of the surface relative to the acoustic wavelength (Patterson, 1967). If the beam direction varies randomly about the perpendicular orientation, then a number of measurements may be averaged to obtain a precise, if inaccurate, calibration.

To grossly assess and compare echosounder performance, the seabed may be used as the reflecting surface (e.g. Stewart *et al.*, 1994). However, compared to an air–water interface, seabed reflectivity is lower and more unpredictable and unstable. This is because there are a multitude of substrate types; all have a lower impedance contrast relative to air and many have dynamic scattering properties due to physical (e.g. waves and currents) and biological (e.g. burrowing animals and shellfish) processes.

1.5.2.2 Reference

A reference transducer has well characterized (usually by the manufacturer) transmit response, receive sensitivity, and beam directivity vs. frequency. To calibrate an echosounder, the reference transducer is accurately and precisely positioned on the beam axis in the far-field of the echosounder transducer (see Section 2.1.2.4). The echosounder transmit response is calibrated when the reference transducer receives a transmitted signal. The echosounder receive sensitivity is calibrated when the reference transducer transmits a signal of known intensity. This method may be used to calibrate echosounders in a tank, but the uncertainties associated with positioning and aligning the reference transducer in the field make this method impractical for many studies (MacLennan and Simmonds, 1992; Hwang *et al.*, 2007).

Reference transducers are sometimes used to measure transmit pulse shape and source level, and to transmit and receive frequency responses. These parameters are relatively insensitive to the position of the reference transducer.

1.5.2.3 Comparison

The performance of an uncalibrated echosounder may be evaluated by comparing it to the performance of a calibrated echosounder. If the echosounders in the comparison are mounted on different platforms (e.g. Foote *et al.*, 1987; Fernandes *et al.*, 2000; De Robertis and Wilson, 2006; De Robertis *et al.*, 2008), then the comparisons may be affected by any differences in the echosounder specifications and settings (Jech *et al.*, 2005), the temporal and spatial distributions and behaviours of the target species, the temporal and spatial characteristics of the sampling, the radiated vessel noise (Mitson and Knudsen, 2003; De Robertis *et al.*, 2008), and the weather. Measurements from each

system may be statistically compared with a linear regression that accounts for the systematic and random errors in both sets of measurements. If the values from the different systems are statistically equivalent, then both systems may be calibrated to the same tolerances. If the measurements are statistically different, then other methods are required to understand the causes of the differences. Similarly, measurements made with uncalibrated echosounders have been compared to independent measures, e.g. net samples (see Section 5.5).

2 Sphere calibration

2.1 Introduction

A sphere calibration measures the overall performance of an echosounder using the reflection from a solid sphere of known backscattering cross section, σ_{bs} (m²), also known as target strength (*TS*; dB re 1 m²). The result is used to adjust the echosounder gain, g_0 (dimensionless), and the filter attenuation correction factor, $s_{a\,corr}$ (dimensionless), to optimize the accuracy of acoustic measurements of σ_{bs} and volume backscattering coefficient, s_v (m² m⁻³), also known as volume backscattering strength, S_v (dB re 1 m² m⁻³). In addition to providing these estimates, a conventional sphere calibration also provides a check of the beam-pattern characteristics. The details of the calibration procedure vary with the echosounder type, e.g. single-beam or split-beam, and transducer platform, e.g. vessel or towed body, but the aim and general procedure are the same.

Basically, a sphere of known σ_{bs} is placed into the beam of the acoustic transducer, and the echo received by the echosounder is recorded. The sphere is moved throughout the acoustic beam to measure its variation in sensitivity due to the beam directivity, $d(\alpha, \beta)$ (dimensionless). It is especially important to obtain data when the sphere is located in the centre of the acoustic beam (i.e. the axis of maximum sensitivity) where the sphere echo is strongest, as these measurements are used for estimating g_0 and $s_{a\,corr}$.

Sphere calibrations should be conducted often and over the range of water temperature, t_w (°C), salinity, s_w (psu), sound speed, c_w (m s⁻¹) and pressure, p_w (dbar), that the transducers will encounter during the measurements. At a minimum, calibrations should be performed before and after the acoustic instrument is used to make measurements.

The remainder of this section describes the equipment, procedures, and analysis for conducting calibrations of acoustic equipment using spheres. Chapter 3 explores the uncertainty in sphere calibrations. Chapter 4 provides additional details that are specific to some commonly used acoustic equipment.

2.1.1 Equipment

A sphere calibration requires some specialized equipment including a sphere, apparatus to suspend and move the sphere within the transducer beam, and sensors to measure t_w, s_w, c_w, and p_w at the transducer, at the sphere, and between them. Software is also needed to calculate estimates of g_0 and $s_{a\,corr}$ from the sphere-σ_{bs} measurements.

2.1.1.1 Sphere properties

A calibration sphere should have a known and stable σ_{bs} (MacLennan, 1981; Foote, 1982, 1983b). They are usually made from tungsten carbide with 6% cobalt (WC) or ≥99.99% electrical-grade copper (Cu). Cu spheres are machined to the desired sizes. WC spheres are manufactured using a powder-metallurgy and polishing process.

Generally, calibration spheres do not have traceable origins (i.e. materials and manufacturing) or documented metrological estimates of their σ_{bs} (i.e. measurements using national or international standards). Nevertheless, the precise composition of a calibration sphere is critical and should be verified since its σ_{bs} varies with the material properties (MacLennan, 1982; Foote and MacLennan, 1984). For example, the density of a WC sphere depends on the amount of cobalt binder. Calibration spheres should be weighed and their calculated densities compared to the values in Table 2.1.

The σ_{bs} of the sphere is calculated using a theoretical model for the reflection of sound by elastic spheres (MacLennan, 1981). The model requires estimates of the sphere size and its material properties (Foote and MacLennan, 1984; MacLennan and Dunn, 1984), the acoustic frequency, f (Hz), and the density, ρ_w (kg m^{-2}), and c_w of the surrounding water. A web-based application is available to calculate σ_{bs} using the model in MacLennan (1981) (http://swfscdata.nmfs.noaa.gov/AST/SphereTS/).

Table 2.1. Material properties for tungsten carbide with 6% cobalt binder (WC) and copper (Cu), from [1]Foote and MacLennan (1984) and [2]MacLennan and Dunn (1984). It is highly recommended to weigh spheres and validate their densities.

Property	Cu[1]	WC[1]	WC[2]
Density (kg m^{-3})	8 947	14 900	14 900
Longitudinal sound speed (m s^{-1})	4 760	6 864	6 853±19
Transverse sound speed (m s^{-1})	2 288.5	4 161.2	4 171±7

Sphere diameters are chosen to have stable and strong reflections throughout the echosounder frequency-bandwidth, and the expected water properties during calibration (Foote, 1982). The sphere-σ_{bs} can have large and abrupt changes in magnitude over small frequency ranges (MacLennan, 1981; Sun *et al.*, 1991) (Figure 2.1). Spheres with such regions close to the operating frequency of the echosounder should be avoided. Therefore, one or more different spheres may be needed to calibrate echosounders operating at different frequencies (e.g. Foote, 1990).
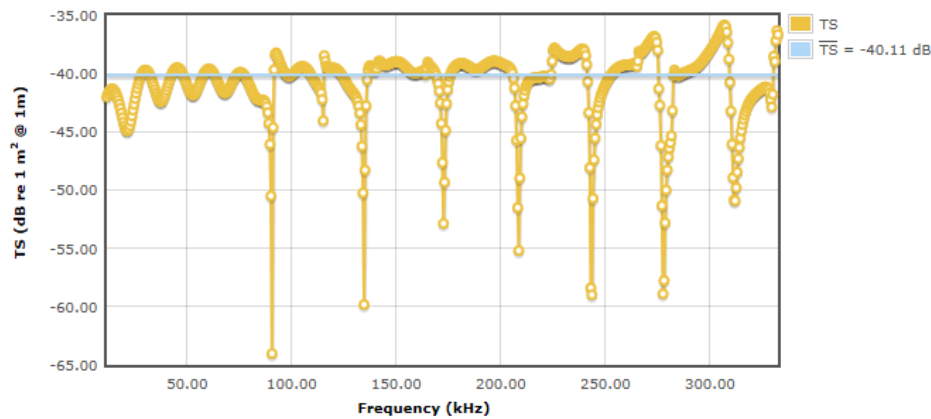
Figure 2.1. Theoretical target strength (*TS*; dB re 1 m^2 at 1 m) values for a 38.1-mm-diameter sphere made from tungsten carbide with 6% cobalt (WC), at $t_w = 13.5$ °C, $s = 33.3$ psu, pressure = 25.0 dbar, $c_w = 1500$ m $\cdot$ s^{-1}, and $\rho_w = 1025.0$ kg $\cdot$ m^{-3}. The mean *TS*, $\overline{TS}$, is calculated in the linear domain, over the displayed bandwidth (12-333 kHz). This image is from http://swfscdata.nmfs.noaa.gov/AST/SphereTS/, an application that implements the sphere *TS* model in MacLennan (1981).

Use the fewest number of spheres necessary to accomplish the calibration. Deploying multiple spheres sequentially takes time and, during the transitions, the suspension lines may become caught or tangled. Deploying multiple spheres simultaneously, one above the other, can save time, but may increase calibration error due to forward scattering (MacLennan, 2011).

Commonly used sphere sizes and materials are given in Table 2.2. These are for narrow-band systems and have been chosen such that their σ_{bs} values are insensitive to small changes in f, t_w, and acoustic pulse duration, τ (s) (Table 2.3) (Foote, 1982, 2007; Miyanohana *et al.*, 1993).

Table 2.2. Recommended spheres for calibrating common echosounder frequencies. The spheres are made from copper (Cu) or tungsten carbide with 6% cobalt binder (WC).

Frequency (kHz)	Material/diameter (mm)
12	Cu/45.0
18	WC/38.1, Cu/64.0, Cu/63.0
27	Cu/42.0
38	WC/38.1, Cu/60.0
50	Cu/45.0
70	WC/38.1, Cu/32.0
120	WC/38.1, Cu/23.0
200	WC/38.1, Cu/13.7
333	WC/22.0

Calibration spheres should have σ_{bs} values (see Table 2.3) which provide a signal-to-noise ratio, r_{sn} (dimensionless), that is ≥100 (20 dB) at the calibration location. The spheres should not have nicks, scratches, dents, or corrosion. They should be cleaned and dried after each use and stored in a protective container. Spheres are occasionally lost overboard during calibrations, so it is prudent to have spare spheres available.

Table 2.3. Approximate theoretical target strength, TS (dB re 1 m^2 at $r_0 = 1$ m), of common calibration spheres with various diameters (mm), made from tungsten carbide with 6% cobalt (WC), and copper (Cu), at $t_w = 13.5\,°C$, $s_w = 33.3$ psu, $p_w = 25.0$ dbar, $c_w = 1500\ \mathrm{m\cdot s^{-1}}$, and $\rho_w = 1025.0\ \mathrm{kg\cdot m^{-3}}$. Green indicates there are no nulls within or near the signal bandwidth ($b_f \approx f \pm 0.5(1/\tau)$), where f is frequency (Hz) and τ is pulse duration (s). Yellow indicates a null close to the b_f, and red indicates a null within the b_f.

Material	Diameter (mm)	$f \cdot 10^{-3}$ (Hz)	$\tau \cdot 10^{-6}$ (s) 64	128	256	512	1024	2 048	4 096	8 192
WC	20.0	18								
		38			−49.7	-49.7	−49.7	−49.7	−49.7	
		70		-47.6	−47.8	-47.8	-47.8	-47.8		
		120	−45.8	-45.6	−45.6	−45.5	−45.5			
		200	-45.2	−45.1	-45.0	−45.0	−45.0			
		333								
WC	21.0	18								
		38			−49.8	−49.9	−49.9	−49.9	−49.9	
		70		−47.3	−47.4	−47.5	−47.5	−47.5		
		120	−46.0	−46.2	−46.3	−46.3	−46.3			
		200			−45.5	−45.5	−45.5			
		333		−44.4	−44.4	−44.4	−44.4			
WC	22.0	18								
		38			−49.6	−49.6	−49.7	−49.7	−49.7	
		70		−46.1	−46.2	−46.3	−46.3	46.3		
		120	−45.9	−46.2	−46.3	−46.4	−46.4			
		200								
		333	−44.1	−44.1	−44.1	−44.1	−44.1			
WC	38.1	18				−42.6	−42.6	−42.6	−42.6	−42.6
		38			−42.2	−42.4	−42.4	−42.4	−42.4	
		70			−41.3	−41.4	−41.4	−41.4		
		120				−39.5	−39.5			
		200			−39.1	−39.1	−39.1			
		333								
Cu	60.0	18				−35.4	−35.4	−35.4	−35.4	−35.4
		38			−33.7	−33.6	−33.5	33.5	33.5	
		70								

Material	Diameter (mm)	$f \cdot 10^{-3}$ (Hz)	$\tau \cdot 10^{-6}$ (s)							
			64	128	256	512	1024	2 048	4 096	8 192
Cu	60.0	120								
		200								
		333								

2.1.1.2 Sphere suspension

Suspend the sphere by one or more monofilament lines. The line may be attached to the sphere by either gluing a loop of line into a small hole, or constructing a net bag (Figure 2.2). Holes may be drilled into Cu spheres, but must be spark-eroded into WC spheres as they are extremely hard. In either material, the hole should be small (e.g. 2-mm diameter by 3-mm deep) such that it has negligible effect on the sphere σ_{bs} (e.g. Foote, 1982).
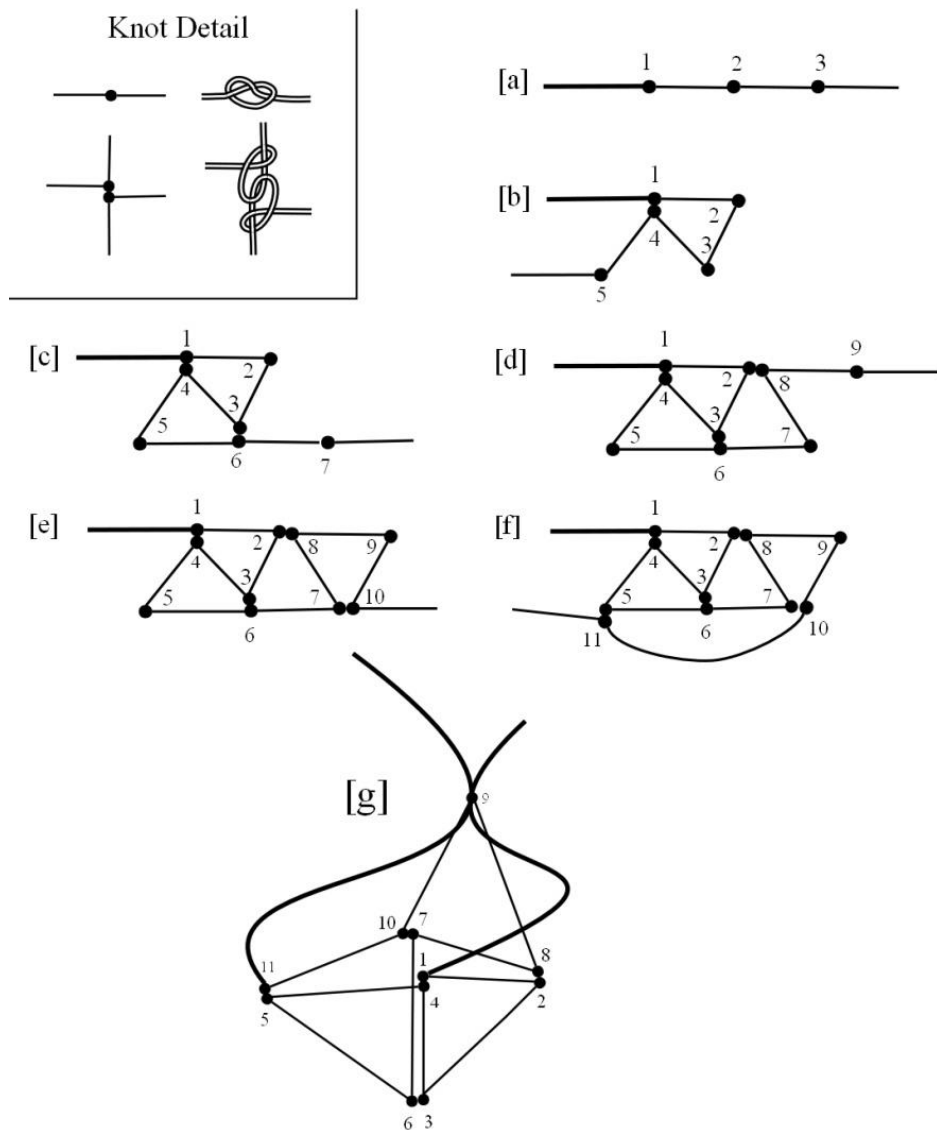
Figure 2.2. A method for tying a net around a sphere. Proceed from step (a) to (g). Tie the knots in numbered order. The interknot distance should equal one-fourth of the sphere circumference. This graphic is a revision of Figure 4 in Foote et al. (1987).

The sphere suspension method depends on the transducer mount and platform. Generally, the sphere is suspended from three monofilament lines run from reels and outrigger poles mounted on the railings of the ship (see Figure 2.3). Outriggers are used

to keep the monofilament lines from rubbing on the hull and for moving the sphere during the calibration. The line lengths are adjusted to precisely move the sphere within the acoustic beam.

Outriggers may be manual or motorized fishing outriggers with line-length indicators. Alternatively, outriggers may be constructed with manual or electric fishing reels, each attached to the inboard end of a rigid rod and the monofilament line fair-led through a ring or pulley on its outboard end. Motorized outriggers may be controlled remotely and by computer. In lieu of a mechanical or electronic line-length indicator, the line may be marked incrementally with colour.

Fill each outrigger reel with mostly non-elastic line (e.g. Dyneema, Spectra, or stainless steel). To each line, attach (i) a small swivel, (ii) monofilament line attached to the sphere, and (iii) monofilament line attached to a stabilizing weight (see Figure 2.3). To reduce uncertainty in the sphere-echo intensity and position caused by phase noise from the monofilament attachments, the three monofilament lines should be attached to three different points on the net bag. If echoes from the lines are not a concern, e.g. when calibrating lower-frequency echosounders, then loops in the monofilament lines extending from each downrigger may be joined to the loop on the sphere and a loop in a monofilament extension line attached to the weight. In any case, echoes from the swivels, sphere, and weight must be acoustically resolvable (separated). Thus, the vertical distances between the swivels, sphere, and weight should be $\geq c_w \tau$, e.g., $\geq (1500$ m s^{-1})(0.001 s) = 1.5 m.
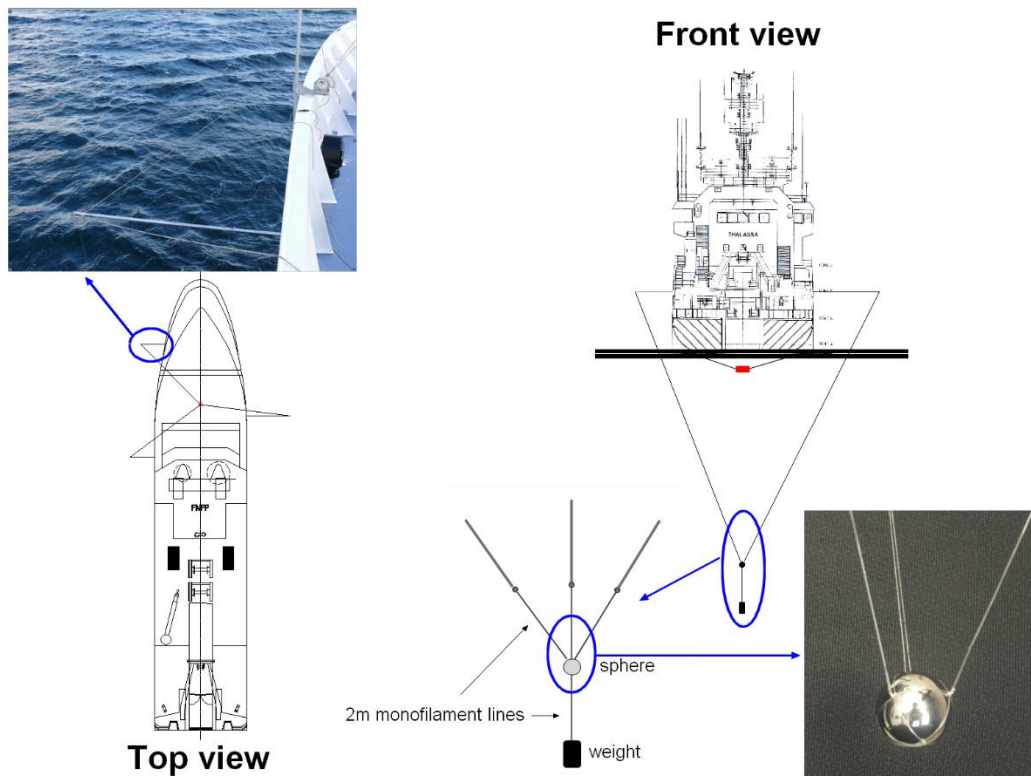
Figure 2.3. The three-line method for suspending a sphere below a hull-mounted transducer. The monofilament lines should be attached to the mesh bag at different locations to minimize phase noise at high frequencies (i.e. >100 kHz). Note, if the weight is too heavy, the net bag may break and the sphere could be lost.

Forward scatter from the swivels, lines, and knots must be negligible or else the sphere-echo intensity and phase will be degraded, especially at high frequencies (MacLennan,

2011). To minimize forward scatter, the swivels and knots should be small and the monofilament line thin, yet strong enough to withstand the deployment, movement, and retrieval of the sphere and weight. Also, to shed bubbles, dip the sphere, swivels, knots, and lines in soapy water before deploying.

An alternative to the three-line method is to run a single monofilament line under the vessel from one side to the other. Suspend the sphere from the midpoint of the line. Adjust the sphere athwartships by releasing line on one side of the ship and retrieving an equal amount of line on the other side. Adjust the sphere alongships by moving both ends of the line forward or aft.

2.1.2   Calibration procedure

This section provides guidance on the general sphere-calibration procedure. Subsequent sections in this chapter detail each operation.

1) Stabilize the transducer, e.g. by positioning the vessel in a sheltered area (see Section 2.1.2.1).
2) Measure transducer impedance, the receiver test amplitude, or both (see Section 2.1.2.2).
3) Choose an appropriate sphere (see Tables 2.2 and 2.3).
4) Suspend the sphere in the transducer beam using outriggers and monofilament (see Sections 2.1.2.3 and 2.1.2.4).
5) Measure the t_w, s_w, and c_w at the transducer, sphere, and between them (see Section 2.1.2.5).
6) Position the sphere in the centre of the beam, then move it throughout the beam (see Section 2.1.2.6).
7) Analyse the calibration data and results (see Section 2.1.2.7).
8) Retrieve the sphere and stow the gear (see Section 2.1.2.8).

2.1.2.1   Calibration location

As much as possible, calibration experiments should be conducted over the range of environmental conditions, i.e. t_w, s_w, c_w and p_w, encountered during the survey measurements (Demer and Renfree, 2008). Calibrations should be performed in areas where the water is well mixed and relatively void of biological scatterers. The experiment should be scheduled for slack tide. The water depth should be sufficient to place the sphere in the far-field of the transducers (see Section 2.1.2.4), accounting for tides.

Depending on the location, traffic, wind, swell, and current, the sphere calibration may be conducted while the vessel drifts in the open ocean or anchored from one or more points. If the wind speed is < ~15 knots and the swell is < ~2m, drifting may be most convenient. More often, however, anchoring in a sheltered bay or fjord is a better option. For portable echosounders, a wharf or large tank of water may be more convenient.

If the vessel is drifting or anchored from a single point, usually the bow, vessel, and tethered sphere tend to move in unison with any current. However, if the wind and current are from different directions, the vessel may be anchored from multiple points, e.g. the bow and stern, to keep it from swinging.

2.1.2.2   Transducer impedance

Prior to each sphere calibration, measure the transducer impedance and compare it to the manufacturer's specifications and any previous measurements. The electrical im-

pedance of the transducer (Wilson, 1988; Sherman and Butler, 2007) affects the efficiency of the conversion between transducer voltage and acoustic pressure in the water. Changes in transducer impedance can change echosounder performance (Demer and Renfree, 2008).

The measurement of transducer impedance is most conveniently made using an electrical impedance meter, but can also be accomplished using a signal generator, oscilloscope, and inductive current probe (see Demer and Renfree, 2008). Regular measurements of impedance provide a useful diagnostic tool to help explain large changes in echosounder calibrations. Large changes in transducer impedance may indicate a faulty transducer and avoid a time-consuming and ultimately unsuccessful calibration. Abrupt changes in impedance may result from damage to the transducer or associated cabling, or bio-fouling on the transducer face. Some echosounders have built in functions to monitor transducer impedance.

2.1.2.3 Sphere suspension

This section describes the three-outrigger method for sphere suspension beneath a large vessel (Figure 2.3). It can be readily adapted for other situations.

1) Locate the transducer(s) using hull drawings, sketches, or photographs. In some cases, divers may be needed to locate the transducers and to help initially position the sphere beneath them.
2) Attach a weight to the middle of a messenger line that is at least threefold the vessel's beam. With the ends of this line affixed to each side of the bow, throw the weight forward and clear of the vessel. As the line sinks, untie the line and move the two ends aft until it is aligned with the transducer(s) to be calibrated. If needed, a skiff may be used to assist with this step.
3) If appropriate, anchor the vessel.
4) Attach three outrigger poles to the ship in positions approximating an equilateral triangle centred on the transducer(s). At the fore-aft position of the transducer (where the line is now located), place one outrigger on one side of the ship (e.g. starboard in the following example). If the transducer(s) are not centred athwartships, place the single downrigger on the side farthest from the transducers. On the other side of the ship (e.g. port in this example), place each of the other outriggers approximately equal distances fore (port-forward) and aft (port-aft) of the transducer. For transducers centred athwartships, these distances may be ~0.58 times the vessel width.
5) Attach the starboard outrigger line to the messenger line.
6) While maintaining slack in the line so that it does not catch on the hull, release line from the starboard outrigger and retrieve it on the port side. Continue until the starboard outrigger line is secured on the port side. Detach and stow the messenger line.
7) Bring the port-aft line to meet the port-forward line.
8) Bring all three lines together and attach the sphere and stabilization weight (see Figure 2.3).
9) Immerse the calibration sphere and monofilament line in a mixture of roughly 2/3 water and 1/3 liquid dishwashing soap to shed bubbles from the sphere and knots.
10) Carefully lower the weight and sphere over the side of the vessel and into the water without contacting the hull.
11) To initially position the sphere, release the same amount of line on all three outriggers. Port-forward and port-aft lines should be released at the same time to

ensure that the calibration sphere does not make contact with the hull. Lines running against the hull may become caught, abraded, or cut on protrusions such as anode blocks, bilge keels, or barnacles. If a line is caught, try to release it by moving the line forward or aft. If it cannot be released, it may be necessary to cut the caught line, retrieve the sphere with the other lines, and start again, perhaps using longer outrigger poles.

12) Let out line incrementally until the sphere is visible at a suitable range on the echosounder display. Avoid letting the sphere, or weight if used, hit the seabed. When the sphere is in the transducer beam, its echo should be received at a constant range (see Figure 2.4).
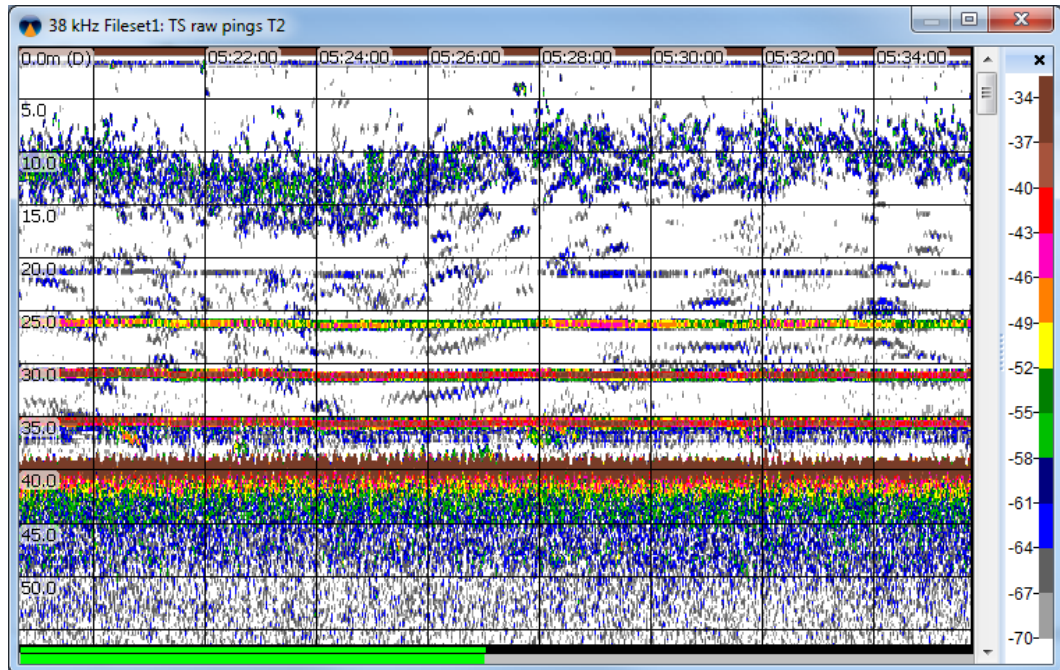
Figure 2.4. An echogram during a sphere calibration of a 38-kHz echosounder. The vertical axis is depth below the transducer (m), and the horizontal axis is time (hh:mm:ss). The red band at 0 m is the transmit pulse. Echoes are from organisms (~10–15 m), swivels (~21 m), a 38.1-mm diameter WC sphere (~26 m), a 60-mm diameter Cu sphere (~30 m), a stabilizing weight (~35 m), and the seabed (~39 m). Forward scatter from organisms, swivels, monofilament knots, and even other spheres can degrade the measurements of sphere position and the calibration accuracy, particularly at higher frequencies (MacLennan, 2011).

2.1.2.4 Sphere range

At short ranges, compensation of the sphere echo for spreading loss can vary significantly with small changes in the estimated range. Therefore, measurements of sphere σ_{bs} (or any other quantitatively sampled backscatter) should not be made at short ranges. Simmonds and MacLennan (2005) recommend that the range to the sphere is at least twofold the near-field range, r_{nf} (m). For a circular piston projector:

$$r_{nf} = \frac{d_t^2}{\lambda},$$

(2.1a)

where d_t (m) is the diameter of the transducer and λ is the acoustic wavelength (m). Medwin and Clay (1998) recommend that the range to the sphere is at least threefold the r_{nf}:

$$r_{nf} = \frac{\pi d_t^2}{4\lambda} \, ,$$

(2.1b)

where d_t (m) is the largest distance across the active elements in a circular piston projector. The recommendation by Medwin and Clay (1998) is 0.356-fold more conservative than that by Simmonds and MacLennan (2005).

The −3 dB points on the main lobe of a transducer directivity pattern occur at off-axis angle $\theta_{-3\,\text{dB}}/2 \cong \sin^{-1}(3.2/kd_t)$, where $k = 2\pi/\lambda$ is the wave number (Sherman and Butler, 2007). Therefore, d_t can be estimated from the beamwidth, $\theta_{-3\,\text{dB}}$, using:

$$d_t \cong \frac{3.2}{k\sin(\theta_{-3\,\text{dB}}/2)} \, .$$

(2.2)

Combining Equations (2.1b) and (2.2), the recommended minimum range for the sphere (Medwin and Clay, 1998) is estimated for a selection of frequencies and transducer beamwidths (Figure 2.5).
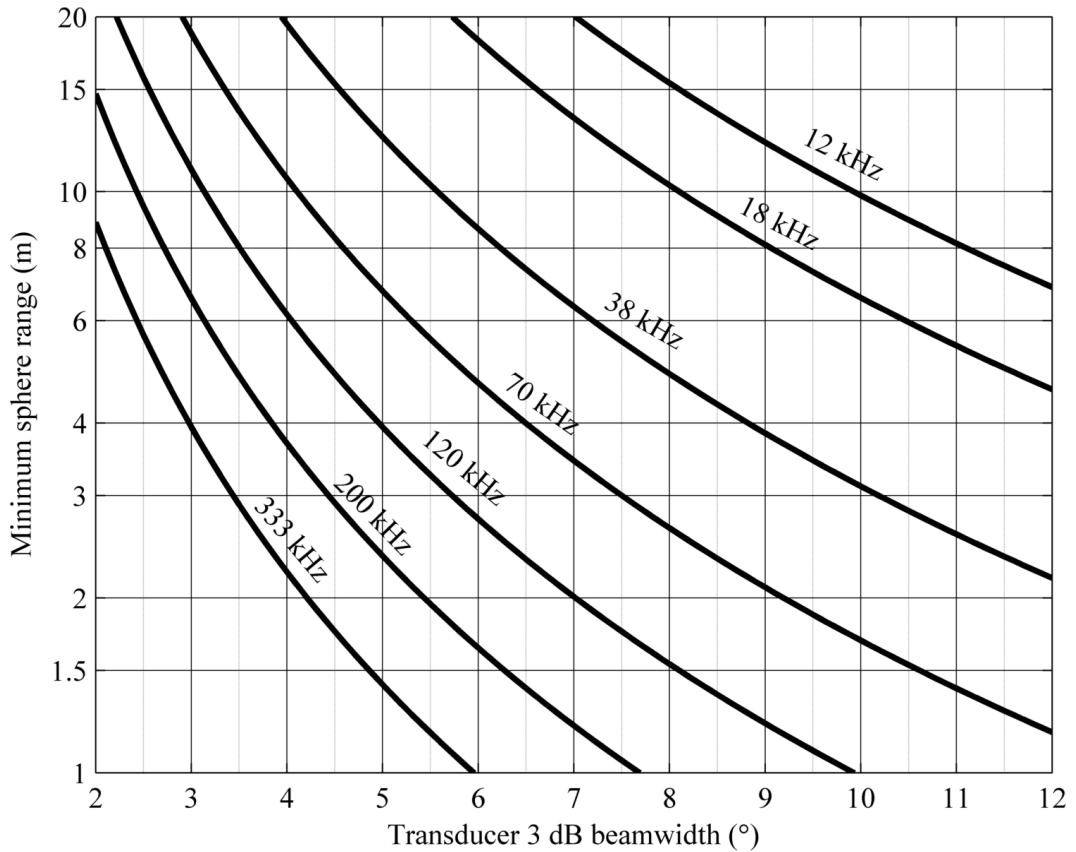
Figure 2.5. Minimum recommended range for the calibration sphere [= $3r_{nf}$, as calculated in Equation (2.1b)] vs. transducer −3 dB beamwidth, $\theta_{-3\,\text{dB}}$, and acoustic frequency, f, for a circular-piston transducer and water sound speed, $c_w = 1470\,\text{m s}^{-1}$.

Just as the sphere must be sufficiently outside of the transducer's near-field, the transducer must be sufficiently outside of the sphere's near-field. To estimate $3r_{nf}$ for the sphere, substitute the sphere diameter for the transducer diameter in Equation (2.1b). Furthermore, the sphere must approximate a point target, so the beam diameter must be large compared to the sphere diameter at the measurement range. For example, if $\theta_{-3\,\text{dB}} = 7°$, $r = 15$ m, and the sphere diameter = 0.0381 m, then the sphere diameter is

1/48th or 2.1% of the beam diameter. This requirement may be important when calibrating multibeam sonars with small values of $\theta_{-3\,dB}$.

Even if the near-field range criteria are met for both the transducer and the sphere, sphere echoes can cause saturation in some echosounder receivers, particularly if they are designed for measuring long-range or small σ_{bs} targets. When this happens, the received sphere-echo power remains constant vs. range. In such cases, attenuate the echo, for example by moving the sphere to a larger range than indicated in Figure 2.5.

2.1.2.5 Measurement environment

Measure t_w and s_w between the transducer and calibration sphere. These measurements are used to calculate the c_w at the transducer and the sphere, e.g. using the equations in Leroy (1969), Del Grosso (1974), Mackenzie (1981), Fofonoff and Millard (1983), Leroy *et al.* (2008), or Figure 2.6, and the mean c_w for the propagation path between the transducer and the sphere. The c_w at the transducer should be used to calculate the equivalent two-way beam angle, ψ (sr) (see Section 2.1.2.7.2). The c_w at the sphere should be used to calculate the sphere σ_{bs}.

The mean sound speed for the propagation path should be calculated by weighting the sound speed values measured in each range (e.g. depth) increment by the time the wave spends in that range increment (Demer, 2004). This harmonic mean sound speed, $\overline{c_w}$, is calculated by weighting the i-th sound speed, c_{wi} (m s^{-1}), by the incremental time, Δt_i (s), spent by the sound wave in the i-th range increment, $\Delta r_i = r_i - r_{i-1}$ (m) (Weinberg, 1971; De Moustier, 2001):

$$\overline{c_w} = (r_{\max} - r_{\min})\left[\sum_{i=1}^{N}\frac{1}{g_i}log_e\left(\frac{c_{wi+1}}{c_{wi}}\right)\right]^{-1},$$

(2.3a)

where g_i (s^{-1}) is the gradient $\partial c_w/\partial r$ in Δr_i, and $r_{\max}$ (m) and $r_{\min}$ (m) are the maximum and minimum ranges (e.g. depths), respectively. If $\partial c_{wi}/\partial r_i$ is approximately zero, then the time spent in the i-th increment is calculated using a constant sound speed (De Moustier, 2001). If a constant sound speed is assumed for all of the increments, then Equation (2.3a) can be approximated by (Seabird, 2013):

$$\overline{c_w} \cong \frac{\sum_{i=1}^{N}\Delta r_i}{\sum_{i=1}^{N}\Delta r_i/c_{wi}}.$$

(2.3b)
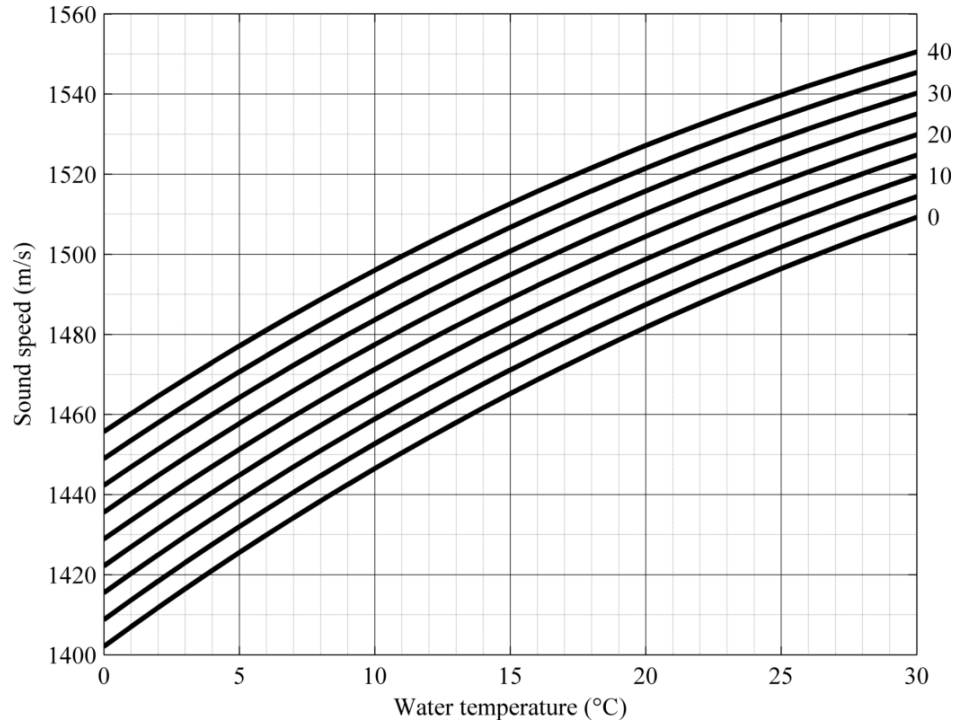
Figure 2.6. Variation of sound speed with water temperature, t_w (°C), and salinity, s_w (psu, as indicated on the right axis). Calculated from the nine-term equation in (Mackenzie, 1981).

The measurements of t_w and s_w are also used to calculate the mean absorption coefficients, α_a (dB re 1 m⁻¹), for the propagation path, e.g. using equations in (Francois and Garrison, 1982a), Ainslie and McColm (1998), Doonan *et al.* (2003), or Figure 2.7 and 2.8.

Figure 2.7. Variation of absorption with frequency and salinity (psu, as indicated on the right axis) for frequencies <100 kHz. Calculated using the formula given by Francois and Garrison (1982a) using a temperature of 10°C and pH = 7.0 for salinity <10 and pH = 8.0 otherwise.

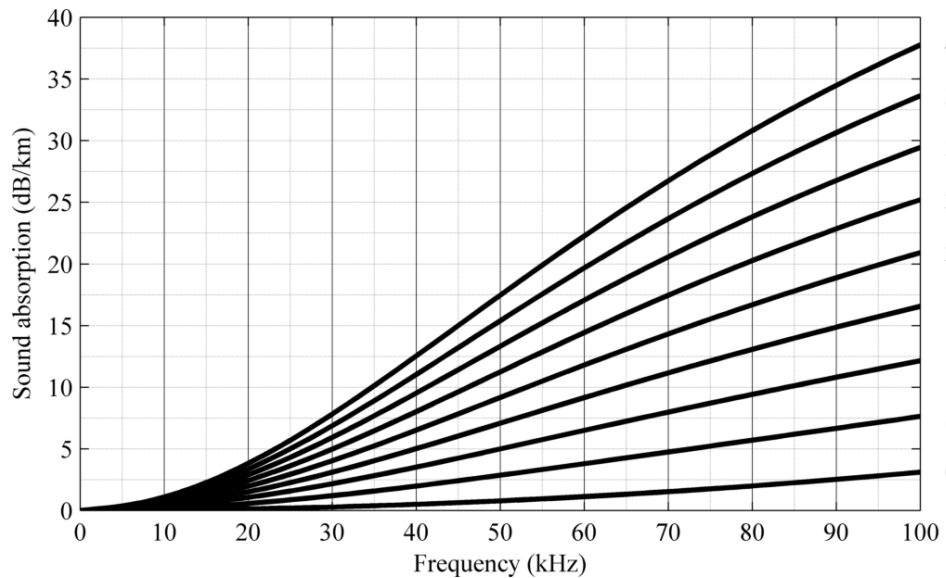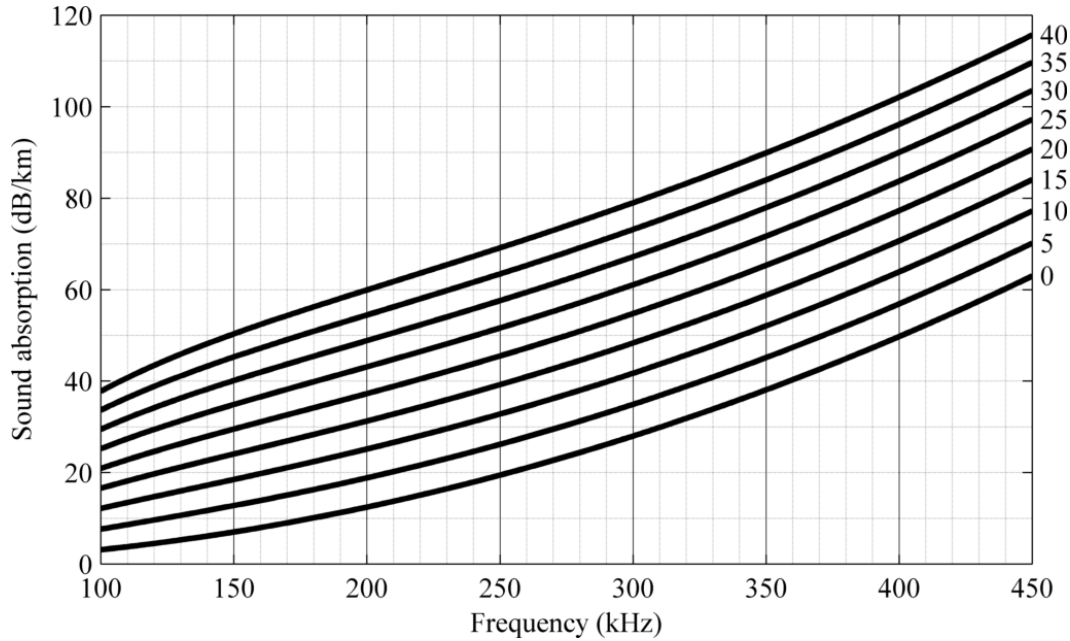**Figure 2.8. Variation of absorption with frequency and salinity (psu, as indicated on the right axis) for frequencies between 100 and 450 kHz. Calculated using the formula given by Francois and Garrison (1982a) using a temperature of 10°C and pH = 7.0 for salinity <10 and pH = 8.0 otherwise.**

2.1.2.6 Sphere positioning

Considering the geometry of the outriggers and transducer, calculate the line lengths required to place the sphere directly beneath the transducer, at $r \geq 3r_{nf}$ (Equation 2.1b). Then, adjust the line lengths to position the sphere on the beam axis. This procedure is greatly facilitated by the angular coordinates of the sphere, (α, β), provided by a split-beam echosounder.

To position the sphere on the beam axis of a single-beam echosounder, the sphere position must be adjusted until the maximum intensity is measured. When the sphere is located on the beam axis, movement in any direction will result in lower echo intensity.

If a split-beam transducer is located in close proximity to a single-beam transducer, the split-beam sphere-position estimates may be translated, using knowledge of the relative transducer locations, to position the sphere in the centre of the single-beam (Demer *et al.*, 1999; Simrad, 2001).

Measure σ_{bs} for the sphere on the beam axis. To expedite subsequent calibrations, mark or record the outrigger line lengths used to place the sphere in the centre of the beam for each transducer. Then, measure $\sigma_{bs} b(\alpha, \beta)^2$ as the sphere is methodically move throughout the beam, to at least $\pm \theta_{-3\text{ dB}}/2$.

The sphere is efficiently moved throughout the beam by moving one line at a time. For example, place the sphere in the centre of the beam, then retrieve the line that is abeam of the transducer until the sphere reaches one edge of the beam. Release twice that amount of line until the sphere has reached the opposite edge of the beam. Then, shift the sphere forward or aft by shortening or lengthening the forward line and lengthening or shortening the aft line, respectively. Repeat the process with the line abeam, moving the sphere to the opposite edge of the beam. Repeat the process until sphere-*TS* measurements are made throughout the beam.

Positioning the sphere may be difficult if the tethers are too long, particularly if the current is strong. In this case, add a ballast weight beneath the sphere (see Figure 2.3).

Sphere positioning will be difficult if the outrigger geometry is incorrect. In this case, remeasure the geometry and adjust the positions of the outrigger(s) appropriately.

If part of the transducer is not transmitting or receiving, the sphere may not be detected even when it is physically located in portions of the beam. In this case, the sphere echoes measured in the other parts of the beam will be weaker than expected, and the fitted beam model will be significantly distorted. These symptoms may be caused by faulty electrical wiring between the transceiver and transducer or a faulty transducer or transceiver.

Current, vessel movement, animal echoes, or low tide can sometimes make it difficult to complete a calibration. In these situations, consider doing the calibration later, at a different location, or both. Persevering in difficult conditions often yields a poor quality calibration.

2.1.2.7 Sphere retrieval

After the calibration, update the echosounder and analysis software with the new calibration values (see Section 2.1.2.8). The calibration sphere may then be retrieved from under the vessel using the following steps:

1) Release line on the side with two outriggers until the outrigger line on the other side of the vessel hangs perpendicular to the water surface.

2) While retrieving the sphere and weight on the side with one outrigger, continue to release line on the side with two outriggers. Avoid touching the hull with the lines or calibration sphere as they can easily become entangled.

3) Untie the lines, temporarily stow the sphere and weight, and retrieve the other downrigger lines. If there is a current or if the lines are buoyant, a small weight may be attached to each of the lines before releasing them to keep them from catching on the hull while they are being retrieved.

4) Rinse the calibration sphere and weight in freshwater, allow them to dry, and store the sphere in its protective case.

2.1.2.8 Calibration analysis

2.1.2.8.1 Beam directivity

A split-beam echosounder estimates α and β, the alongships and athwartships target-bearing angles, θ (geometric°), from phase angles of electrical signals received by transducer sub-arrays, φ_e (electrical°):

$$\varphi_e = k d_{eff} \sin(\theta) = \Lambda \sin(\theta) ,$$

(2.4)

where Λ (electrical°/geometric°) is the transducer angle sensitivity, a function of wavelength and thus c_w. Bodholt (2002) showed that one estimate of angle sensitivity, Λ', measured at a certain sound speed, c_w', can be adjusted to the local sound speed, c_w, using:

$$\Lambda = \Lambda' \frac{c_w'}{c_w} .$$

(2.5)

As the sphere is moved throughout the transducer beam, the split-beam angular coordinates, α and β (°), can be used to measure $\sigma_{bs} b(\alpha, \beta)^2$. For a real circular- or elliptical-beam transducer, $b(\alpha, \beta)^2$ can be modelled by:

$$b(\alpha,\beta)^2 = 10^{0.60206\left(\left(\frac{2\alpha}{\alpha_{-3\,\text{dB}}}\right)^2 + \left(\frac{2\beta}{\beta_{-3\,\text{dB}}}\right)^2 - 0.18\left(\frac{2\alpha}{\alpha_{-3\,\text{dB}}}\right)^2\left(\frac{2\beta}{\beta_{-3\,\text{dB}}}\right)^2\right)}, \tag{2.6}$$

where $\alpha_{-3\,\text{dB}}$ and $\beta_{-3\,\text{dB}}$ are the alongships and athwartships –3 dB beamwidths. Bodholt (2002) also showed that one estimate of beamwidth, $\alpha_{-3\,\text{dB0}}$, measured at a certain sound speed, $c_w{}'$, can be adjusted to the local sound speed, c_w, using:

$$\alpha_{-3\,\text{dB}} = \alpha_{-3\,\text{dB}}{}'\frac{c_w}{c_w{}'}, \text{ and}$$
$$\tag{2.7a}$$

$$\beta_{-3\,\text{dB}} = \beta_{-3\,\text{dB}}{}'\frac{c_w}{c_w{}'}.$$
$$\tag{2.7b}$$

The values for $\alpha_{-3\,dB}$ and $\beta_{-3\,\text{dB}}$ can be estimated from a regression of Equation (2.6) and the measures of $\sigma_{bs}b(\alpha,\beta)^2$. It is important to exclude echoes from other sources (e.g. fish) and noise (e.g. crosstalk from other echosounders), as these can bias the model regression.

Proper system function is indicated by an undistorted beam model that has small deviations from the measurements (e.g. Figures 2.9 and 2.10). Conversely, if one quadrant of a circularly-symmetric, split-beam transducer is not functioning, then the beam model will be more oval than circular, and the system gain will be significantly different from the nominal value that is indicated by the manufacturer.
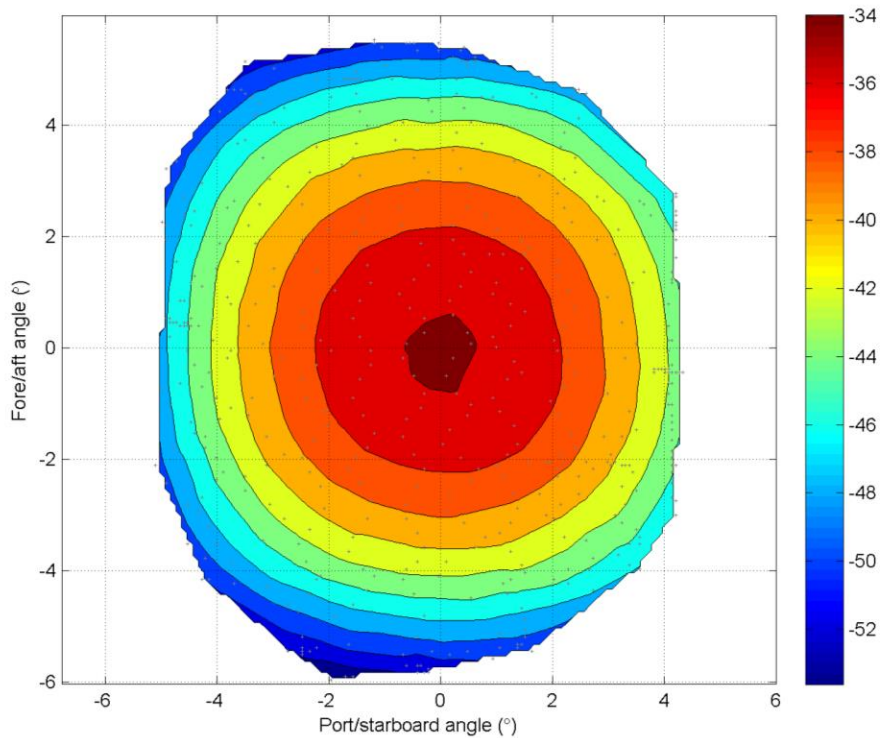
Figure 2.9. Example of the beam model for a 7°-beamwidth, 38-kHz transducer, estimated using *TS* measurements of a 60.0-mm diameter copper sphere. Indications of a good quality calibration are: uniform coverage of the sphere-*TS* measurements (+), and smooth, circular, and concentric contours. The colours indicate the observed (beam uncompensated) sphere *TS* (dB).
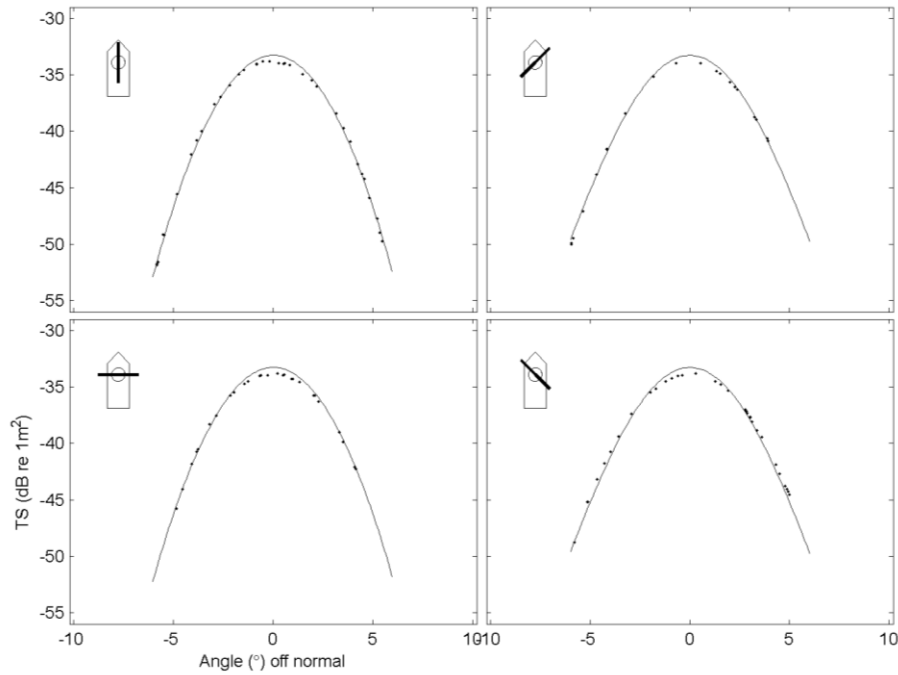
Figure 2.10. Example of *TS* measurements of a 60.0-mm diameter copper sphere (dots) and the fitted beam model for the 7°-beamwidth 38-kHz transducer (solid line). The orientation of each beam cross section is indicated in the legend. Note that the sphere *TS* measurements near the beam axis may be lower than the model of $b(\alpha, \beta)^2$ in Equation (2.6) (Pedersen, 2007).

Because both Λ and θ_{-3dB} vary inversely with c_w, the directivity pattern model, Equation (2.6), is insensitive to changes in c_w (Bodholt, 2002). This assumes that $\sin(\theta_{-3dB}) \cong \theta_{-3dB}$, which is valid for small angles. However, if α and β are calculated using nominal values for Λ_α and Λ_β, the regression estimates of $\alpha_{-3\,dB}$ and $\beta_{-3\,dB}$ are not estimates of the true beamwidths. Nevertheless, if they are used in Equation (2.6), the resulting $b(\alpha, \beta)^2$ can be used to correctly normalize measurements of σ_{bs} to the beam axis:

$$\sigma_{bs} = \frac{p_{er} 16\pi^2 r^4 10^{\alpha_a r/5}}{p_{et} g_0 b(\alpha,\beta)^2 \lambda^2} \ .$$

(2.8)

2.1.2.8.2 Equivalent beam angle

Because >99% of the transmitted energy is in the main lobe (Simmonds, 1984a, 1984b), the equivalent two-way beam angle, ψ (sr), can be estimated from accurate estimates of the transducer beamwidth (Urick, 1983),

$$\psi \simeq (\alpha_{-3\,dB} \cdot \beta_{-3\,dB})/5800 \ .$$

(2.9)

Because the regression values of $\alpha_{-3\,dB}$, and $\beta_{-3\,dB}$, (see Section 2.1.2.7.1) are not estimates of the true beamwidths, they should not be used in Equation (2.9) to estimate ψ. Instead, values for ψ, adjusted for the local sound speed, c_w, may be estimated from the transducer specific value, ψ', measured by the echosounder manufacturer at sound speed, c_w' (Bodholt, 2002):

$$\psi = \psi' \frac{c_w^2}{c_w'^2} \ .$$

(2.10)

The transducer mounting may also affect ψ (Simmonds, 1984b; Foote, 1987), but this affect is commonly and conveniently assumed to be negligible. Accurate estimates of ψ, Λ_α, Λ_β, α_{-3dB}, and β_{-3dB}, all functions of c_w, require sphere-position estimates, (r, α, β), that are independent of those reported by a split-beam echosounder (Simmonds, 1984b; Reynisson, 1998). Such measurements require specialized equipment, a controlled environment, or both, and are generally not part of a sphere calibration.

Summarizing, it is recommended that a value for ψ is estimated from the transducer specific measurement made by the manufacturer in controlled conditions (e.g. a test tank) at a known sound speed, c_w', adjusted for the local c_w (Bodholt, 2002). Furthermore, it is recommended that nominal values are used for Λ_α and Λ_β, and then $\alpha_{-3\,dB}$ and $\beta_{-3\,dB}$ are estimated from the sphere calibration results. If this procedure is followed, the beamwidth values may not be the true values, but the directivity-pattern compensation will be correct (Bodholt, 2002).

2.1.2.8.3 On-axis gain

The calibrated g_0 is calculated from the arithmetic mean of sphere-σ_{bs} measurements made on the beam-axis, $\overline{\sigma_{bs}}$:

$$g_0 = \widehat{g_0} \left(\frac{\overline{\sigma_{bs}}}{\sigma_{bs}} \right)^{0.5},$$

(2.11)

where $\widehat{g_0}$ is the uncalibrated g_0, and σ_{bs} is that calculated for the sphere (see Section 2.1.1.1). Because it is often difficult to make sphere-σ_{bs} measurements exactly on the beam axis, $\overline{\sigma_{bs}}$ is generally estimated as the arithmetic mean of the sphere-σ_{bs} measurements made near the beam-axis, where $b(\alpha, \beta)^2 \simeq 1$, e.g. $\leq 0.5°$. It is important to remove noise (e.g. echoes from swivels, biological scatterers, and the weight), as they can bias $\overline{\sigma_{bs}}$. Once g_0 has been calculated and entered into the echosounder, check that $\overline{\sigma_{bs}} \cong \sigma_{bs}$, within the echosounder's measurement accuracy.

A large change in the calibrated gain, e.g. $\geq 12\%$, could be caused by (i) high acoustic absorption on the transducer face, perhaps due to bio-fouling or bubbles (follow the manufacturer's recommendation for cleaning the transducers); (ii) high acoustic absorption between the transducer and the sphere, perhaps due to air bubbles or suspended organic matter; or (iii) a damaged transducer, transceiver, cable, or connector (in some cases, the directivity pattern may still appear to be correct).

2.1.3 Alternative platforms

Depending on the transducer platform, the three-line method may be modified or replaced by another method. For example, to calibrate a system with a horizontally-projecting transducer, the sphere may be moved within the beam using two reels and outriggers. To calibrate a pole-mounted system, it may be necessary to extend the outrigger nearest to the transducer pole. If this is not possible, the calibration sphere may be positioned below the transducers using a single monofilament line. In this case, the sphere may be moved within the acoustic beams intentionally by moving the line or pseudo-randomly as a result of vessel motion.

For some platforms, it may be more appropriate to hold the sphere relatively stationary (e.g. suspended from one or more lines) while the transducer is pitched and rolled. For platforms with vertically-projecting transducers, it is sometimes advantageous to suspend the sphere in the beam throughout the measurements, e.g. buoyed above a lander with a float or by gravity beneath a towed body. The latter method provides concurrent

measurements of σ_{bs} from the sphere and targets and monitors changes in g_0 vs. d_w or p_w (Dalen *et al.*, 2003) (e.g. Figure 2.11). However, forward scatter from the sphere can affect the measurements of the targets (MacLennan, 2011), and vice versa. These effects can be reduced by increasing the range between the sphere and biological targets.
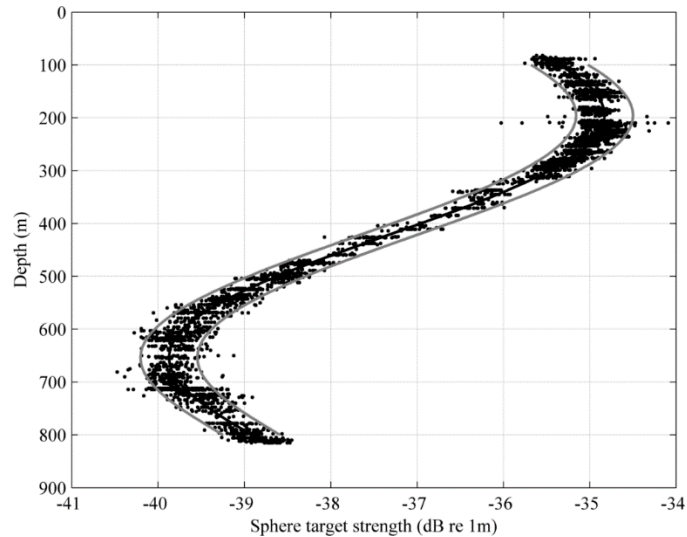
Figure 2.11. Near-axis $[b(\alpha,\beta)^2 \leq 0.5$ dB] measurements of target strength, *TS* (dB re 1 m²), made with a constant g_0 setting in the echosounder (Simrad EK60), from a 38.1-mm WC sphere suspended below a 120-kHz transducer (Simrad 120-7DD) during one descent to over 800-m depth. Overlaid is a 5th-order polynomial fit to the data (black line) with upper and lower 95% confidence intervals (grey lines).

Transducers mounted in deep-towed bodies should be designed specifically for deep deployments. Air-backing or rubber faces on some transducers will exhibit hysteresis in g_0 vs. d_w (e.g. see Figure 8.1 in Ona, 1999). Such transducers should be calibrated and operated within a narrow range of shallow depths.

For echo-integration-based studies with a deeply deployed transducer, ψ should also be quantified vs. d_w. Foote (1987) and Bodholt (2002) described the dependence of ψ on c_w, which generally changes with d_w, but further work is needed to determine how ψ changes vs. p_w.

Optimally, calibrations should be conducted with the echosounder system installed in the survey platform. If this is not possible, they may be calibrated in a controlled environment, e.g. in a test tank, and separately from the platform (Scalabrin *et al.*, 2009).

3   Calibration uncertainty

3.1   Introduction

There are two types of uncertainty in measurement of any quantity: (i) precision (random error) and (ii) accuracy (systematic error or bias). The former indicates the relative variability, or repeatability, of the measurements; the latter indicates the closeness of the measurements to the true value (Figure 3.1). This chapter explores uncertainty in acoustic system calibrations.
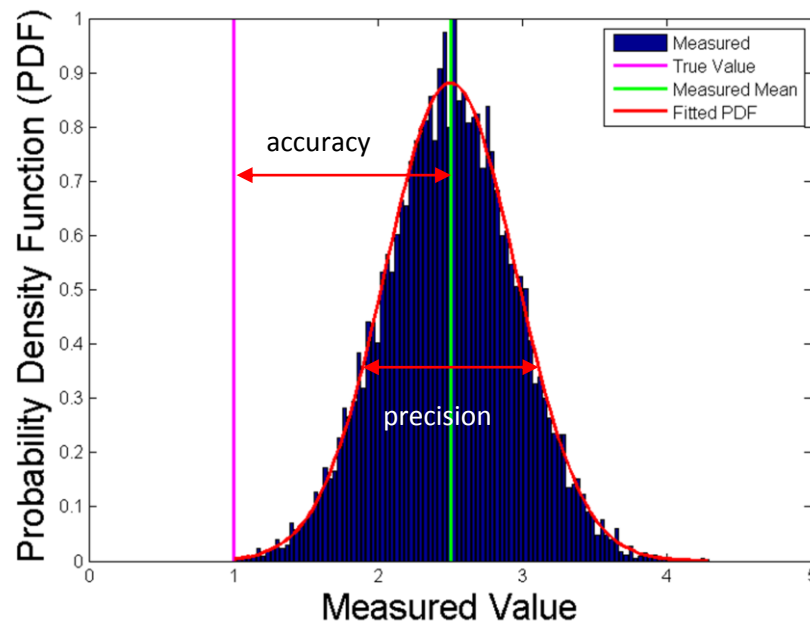
Figure 3.1. Illustration of accuracy and precision. The measurements in this example have a normal or Gaussian distribution with mean = 2.5 and standard deviation = 0.44. The deviation of the mean from the true value represents the measurement accuracy (bias or systematic error). The standard deviation represents the measurement precision (variability or random error).

3.2   Random error

Random noise resulting from system electronics (electric noise) and ambient conditions [acoustic noise; Wenz (1962)] may cause random error in echosounder measurements. This noise may be measured with the echosounder operating in passive mode without transmitting pulses. Calibration spheres are selected to have σ_{bs} values such that the signal-to-noise-ratio at the calibration site is larger than 100 (20 dB). In this case, ambient noise is generally a negligible source of calibration error.

Random error in measurements of beam-compensated sphere σ_{bs} is often estimated as the root-mean-square (rms) deviation of the measured sphere σ_{bs} from the directivity-pattern model. With good practice and accounting for the environment, modern scientific echosounders may have calibrated g_0 values that are precise to about ±0.1 dB over multiple years (Simmonds, 1990; Knudsen, 2009). Although this estimate may increase with increasing frequency, the random error due to calibration is likely a minor contributor to the total error in an acoustic survey (Demer, 2004; O'Driscoll, 2004; Loland *et al.*, 2007; Woillez *et al.*, 2009).

3.3 Systematic error

The systematic error or accuracy in a system calibration depends foremost on the accuracy of the backscattering cross section, σ_{bs} (m²), estimated for the calibration sphere. It also depends on the accuracy of many other parameters in Equation (1.12b). Furthermore, each of these parameters and, therefore, the system response may change after the system is calibrated, e.g. due to changes in the operating environment (Demer, 2004; Demer and Renfree, 2008). In the following subsections, we explore the relative magnitudes of calibration uncertainties potentially contributed by these parameters.

3.3.1 Sphere target strength

First explored is the accuracy of sphere σ_{bs}, based on a theoretical model of backscattering from solid elastic spheres (Faran, 1951; MacLennan, 1981). A Matlab (The Mathworks, USA) implementation of the model is <u>available</u>. The model is exact, so the accuracy of the computed σ_{bs} depends on the accuracy of the estimated physical and geometric model parameters relative to the actual sphere.

3.3.1.1 Material properties

The material properties of an elastic sphere include the density of the sphere, ρ_s (kg m⁻³), the compressional (or longitudinal) wave sound speed, c_c (m s⁻¹), and the shear (or transverse) wave sound speed, c_s (m s⁻¹). Nominal values for tungsten carbide with 6% cobalt binder (WC) and copper (Cu) are listed in Table 3.1.

Table 3.1 Nominal parameters for calculating the σ_{bs} values of spheres made from tungsten carbide with 6% cobalt binder (WC), and copper (Cu). Percent bandwidth, $\%f$ (%), is the percentage of the frequency over which the average is taken.

Property	Symbol	WC	Cu
Sphere material density	ρ_s (kg cm⁻³)	14.90×10⁻³	8.95×10⁻³
Sphere compressional wave speed	c_c (m s⁻¹)	6 853.0	4 760.0
Sphere shear wave speed	c_s (m s⁻¹)	4 171.0	2 288.5
Sphere depth	d_w (m)	30	30
Water temperature	t_w (°C)	10	10
Water salinity	s_w (psu)	35	35
Percent bandwidth	$\%f$ (%)	1.0	1.0

The variation of theoretical sphere target strength, $TS = 10\log_{10}(\sigma_{bs})$ (dB re 1 m²), was simulated for a 38.1-mm-diameter sphere made from tungsten carbide with 6% cobalt (Figure 3.2). In computations for six frequencies, f (Hz), that are commonly used in fishery acoustics surveys, the ρ_s, c_c, and c_s were each varied within $\pm4\%$ of their nominal value (Table 3.2) while the other parameters were held constant at their nominal values (Table 3.1).

Figure 3.2. Theoretical target strength (*TS*; dB re 1 m²) vs. frequency, *f* (Hz), for a 38.1-mm-diameter sphere made of tungsten carbide with 6% cobalt, calculated with ±4% variations in (a) density, ρ_s (kg m⁻³), (b) compressional-wave sound speed, c_c (m s⁻¹), and (c) shear-wave sound speed, c_s (m s⁻¹). Nominal values (Table 3.1) were used for the other parameters. Because there is a null near *f* = 200 kHz, the minimum *TS*, calculated with c_s = 1.04, is >13 dB lower than the nominal *TS*.

Variation in ρ_s affects the mean σ_{bs}, $\overline{\sigma_{bs}}$, but it has relatively little effect on the normalized frequency response, $\sigma_{bs}(f)/\overline{\sigma_{bs}}$, e.g. the positions of the peaks and nulls (Figure 3.2a). The c_c and c_s values affect both $\overline{\sigma_{bs}}$ and $\sigma_{bs}(f)/\overline{\sigma_{bs}}$ values (Figure 3.2b-c). The σ_{bs} values are most sensitive to changes in c_s, and this sensitivity increases with f.
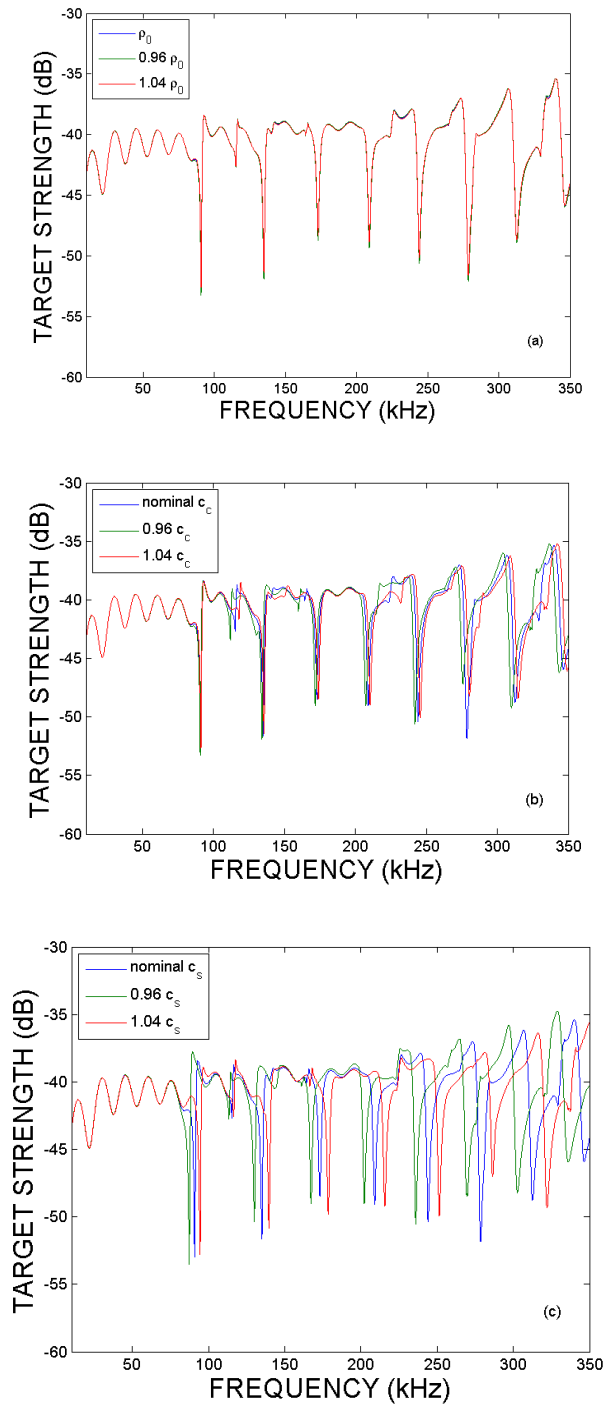
Table 3.2. Theoretical target strength (TS; dB re 1 m²) vs. material properties for a 38.1-mm-diameter sphere made of tungsten carbide with 6% cobalt, calculated with ±4% variations in density, ρ_s (kg m⁻³), (b) compressional-wave sound speed, c_c (m s⁻¹), and (c) shear-wave sound speed, c_s (m s⁻¹). Nominal values (Table 3.1) were used for the other parameters and to calculate the nominal TS. Values for TS range = maximum TS – minimum TS ≥0.1 dB re 1 m² (≥2.3% variation) are bold.

Parameter	TS	Frequency (Hz)/1 000					
		18	38	70	120	200	333
Density	Minimum	−42.75	−42.41	−41.29	−39.50	−39.27	−36.85
ρ_s	Nominal	−42.70	−42.39	−41.29	−39.48	−39.23	−36.73
	Maximum	−42.66	−42.37	−41.29	−39.46	−39.19	−36.60
	Range	0.09	0.04	0.00	0.05	0.09	0.25
Compress-ional speed	Minimum	−42.70	−42.40	−41.33	−39.73	−39.30	−43.41
	Nominal	−42.70	−42.39	−41.29	−39.48	−39.23	−36.73
c_c	Maximum	−42.70	−42.39	−41.27	−38.95	−39.16	−36.26
	Range	0.00	0.01	0.06	**0.78**	0.14	**7.16**
Shear speed	Minimum	−42.70	−42.42	−41.32	−39.75	−52.64	−46.71
	Nominal	−42.70	−42.39	−41.29	−39.48	−39.23	−36.73
c_s	Maximum	−42.70	−42.36	−41.29	−39.20	−39.04	−34.81
	Range	0.00	0.05	0.04	**0.55**	**13.61**	**11.90**

3.3.1.2 Sphericity

The accuracy in machining or sintering the sphere is normally better than 0.1 mm. The acoustic wavelength is >4 mm for frequencies <350 kHz. Therefore, the sphericity of the calibration target likely has negligible effect on the sphere TS.

3.3.1.3 Temperature, salinity, and pressure

Sphere σ_{bs} varies with temperature because c_c, c_s, and water sound speed, c_w (m s⁻¹), are functions of temperature (more discussion in Section 3.2.10.1). However, the temperature dependences of c_c and c_s are not well characterized. Shown are the TS values of a 38.1-mm-diameter sphere made from tungsten carbide with 6% cobalt vs. t_w = 5, 10, and 20°C; water salinity, s_w = 0, 30, 33, and 35 psu; and water pressure = 0, 10, 30, and 100 dbar (Table 3.3).

Table 3.3. Theoretical target strength (TS; dB re 1 m²) vs. water temperature, t_w = 5, 10, and 20°C; water salinity, s_w = 0, 30, 33, and 35 psu; and water pressure, p_w = 0, 10, 30, and 100 dbar for a 38.1-mm-diameter sphere made from tungsten carbide with 6% cobalt. Nominal values (Table 3.1) were used for the other parameters. Range values ≥0.1 dB re 1 m² (≥2.3% variation) are bold.

Parameter		Frequency (Hz)/1 000					
		18	38	70	120	200	333
Temperature (°C)	5	−42.87	−42.29	−40.96	−39.54	−39.50	−36.89
	10	−42.70	−42.39	−41.29	−39.48	−39.23	−36.73
t_w	20	−42.44	−42.39	−41.64	−39.78	−38.80	−36.71
	Range	**0.44**	**0.11**	**0.68**	**0.30**	**0.69**	**0.18**
Salinity (psu)	0	−43.08	−42.06	−40.51	−39.89	−39.44	−36.87
	30	−42.75	−42.37	−41.19	−39.48	−39.34	−36.80

Parameter		Frequency (Hz)/1 000					
		18	38	70	120	200	333
s_w	33	–42.72	–42.38	–41.26	–39.48	–39.27	–36.76
	35	–42.70	–42.39	–41.29	–39.48	–39.23	–36.73
	Range	0.38	0.33	0.78	0.41	0.21	0.14
Pressure (dbar) p_w	10	–42.70	–42.39	–41.29	–39.48	–39.24	–36.73
	30	–42.70	–42.39	–41.29	–39.48	–39.23	–36.73
	100	–42.69	–42.40	–41.31	–39.48	–39.21	–36.71
	Range	0.01	0.00	0.02	0.00	0.03	0.02

3.3.1.4 Measurement bandwidth

The bandwidth of a pulsed sinusoidal signal, b_f (Hz), is approximately equal to the inverse of the pulse duration, τ (s). The sphere σ_{bs} should be calculated and averaged over b_f, before being expressing as target strength (TS; dB re 1 m²) (Table 3.4).

Table 3.4. Theoretical target strength (TS; dB re 1 m²) vs. bandwidth, percent of frequency, f (Hz), for a 38.1-mm-diameter sphere made of tungsten carbide with 6% cobalt. The model parameters were nominal values (Table 3.1). The receiver bandwidth is assumed to be much larger than %f. Values for TS Range ≥0.1 dB re 1 m² (≥2.3% variation) are bold.

Bandwidth (%f)	Frequency (Hz)/1 000					
	18	38	70	120	200	333
0	–42.70	–42.39	–41.29	–39.48	–39.23	–36.73
0.5	–42.70	–42.39	–41.29	–39.48	–39.23	–36.69
1.0	–42.70	–42.39	–41.29	–39.48	–39.23	–37.11
1.5	–42.70	–42.39	–41.29	–39.49	–39.23	–37.49
2.0	–42.70	–42.38	–41.28	–39.49	–39.22	–37.79
Range	0.00	0.01	0.01	0.01	0.01	**1.10**

3.3.1.5 Sphere suspension

The contribution of the sphere suspension line to the uncertainty of the TS measurement depends on its thickness, the sphere attachment method, and the echosounder frequency. The monofilament line should have a diameter that is much smaller than the wavelength; it should be as thin as possible to support the sphere and perhaps a stabilizing weight. The knots should be at least $c_w\tau$ metres from the sphere. Typically, the uncertainty introduced by the tether is negligible at 18 and 38 kHz, but increases with frequency and is significant (~0.5 dB or more) at 200 kHz and higher.

3.3.2 Sound speed and absorption

The received power is compensated, as a function of propagation range, for attenuation due to spherical spreading and absorption. The range estimate is a function of sound speed, which is a function of temperature, salinity, and pressure. The equations used to estimate sound speed values are mostly heuristic and empirical.

There are a number of algorithms for estimating sound speed in seawater (Wilson, 1960; Del Grosso, 1974; Chen and Millero, 1977; Mackenzie, 1981; Speisberger and Metzger, 1991; Millero and Li, 1994; Leroy and Parthiot, 1998), but the algorithm pro-

posed by Chen and Millero (1977) is used most (Fofonoff and Millard, 1983). It is endorsed by the UNESCO/SCOR/ICES/IAPSO Joint Panel on Oceanographic Tables and Standards and SCOR Working Group 51. However, Pike and Beiboer (1993) compared algorithms and recommended the Chen and Millero (1977) algorithm for water depth <1000 m, and the Del Grosso (1974) algorithm for water depth >1000 m. The two algorithms differ mainly due to pressure (Table 3.5).

Table 3.5. Sound speed in seawater calculated using algorithms by Chen and Millero (1977) and Del Grosso (1974) at different pressures.

Pressure (dbar)	Chen and Millero (ms⁻¹)	Del Grosso (ms⁻¹)	Difference (ms⁻¹)
0	1 489.79	1 489.82	–0.03
10	1 491.38	1 489.99	1.40
50	1 497.78	1 490.65	7.14
100	1 505.82	1 491.47	14.35
500	1 571.36	1 498.07	73.29
1000	1 654.84	1 506.34	148.50
1500	1 737.52	1 514.64	222.88

Sound absorption in seawater results from shear and bulk viscosities, and chemicals (Thorp, 1967; Fisher and Simmons, 1977; Francois and Garrison, 1982a, 1982b; Ainslie and McColm, 1998; Doonan *et al.*, 2003). The sound absorption coefficient for seawater ($t = 4°C$, $s = 35$ psu, $p = 300$ dbar, $pH = 8$, $Lat = 48°N$) is calculated vs. f using multiple algorithms (Table 3.6). The algorithm by Francois and Garrison (1982a) is probably the most used, but other formulae were validly obtained by fitting different sets of measured data.

The algorithm by Ainslie and McColm (1998) is a simplified version of that by Francois and Garrison (1982a), so it gives essentially the same results. Doonan *et al.* (2003) reprocessed the data in Francois and Garrison (1982a) and, ignoring the boric acid component, proposed another algorithm that gives essentially the same results for f between 10 and 120 kHz, and $t_w < 20°C$. However, values computed by other algorithms (Thorp, 1967; Fisher and Simmons, 1977) differ more, e.g. >1.5 dB km⁻¹ at 38 kHz and >4.5 dB km⁻¹ at 200 kHz.

Table 3.6 Seawater absorption coefficients, α_a (dB km⁻¹), computed with algorithms from various authors, each parameterized with: $t_w = 4°C$, $s_w = 35\,psu$, $p_w = 300$ dbar, $pH = 8$, Lat = 48°N.

Reference	Frequency (kHz)					
	18	38	70	120	200	333
Francois and Garrison (1982a)	3.15	10.33	20.23	29.86	42.93	72.42
Ainslie and McColm (1998)	3.19	10.42	20.37	30.11	43.55	74.17
Doonan *et al.* (2003)	2.67	9.38	19.61	30.16	43.92	73.75
Fisher and Simmons (1977)	2.35	8.56	19.51	32.08	47.62	78.72
Thorp (1967)	3.43	12.00	25.54	38.68	52.02	75.81

3.3.3   Directivity pattern

The directivity pattern, $b(\alpha, \beta)$ (dimensionless), and equivalent beam angle, ψ (sr), vary as the ratio of the transducer size to the acoustic wavelength, λ (m). The latter varies with sound speed, c_w (m s⁻¹). Therefore, as sound speed changes from one value, c_{w0}

(m s⁻¹), to another, c_w, the beamwidth and equivalent beam angle change, the transmit power is more or less focused, and the on-axis gain, g_0 (dB re 1), is changed by the factor $(c_{w0}/c_w)^2$ (Bodholt, 2002). For example, if c_w changes from 1500 to 1450 m s⁻¹, g_0 will change by 7%.

3.3.4   Equivalent beam angle

Normally, ψ is expressed in decibels, Ψ (dB re 1 sr). Assuming backward radiation is negligible and the signal-to-noise ratio, r_{sn} (dimensionless), is infinite, Ψ is calculated by integrating $b(\alpha, \beta)^2$ over a hemisphere (half space). Realistically, the r_{sn} is less than ideal, and the integration should, therefore, be performed over the space corresponding to the actual r_{sn}. Values of Ψ were computed for a circular piston transducer with nominal beamwidths ranging from 6.6 to 7.4°, and integration spaces corresponding to various *snr* values (Table 3.7).

Table 3.7. Equivalent beam angle, Ψ (dB re 1 sr), vs. beamwidth $\theta_{-3 \text{ dB}}$ (°) and the integration space, which depends on the signal-to-noise ratio, r_{sn} (dimensionless).

$\theta_{-3 \text{ dB}}$ (°)	Integration space (r_{sn})				
	3 dB	6 dB	12 dB	20 dB	Infinity
6.6	−22.44	−21.82	−21.58	−21.38	−21.34
6.8	−22.17	−21.56	−21.33	−21.12	−21.08
7.0	−21.92	−21.31	−21.08	−20.87	−20.84
7.2	−21.68	−21.07	−20.83	−20.63	−20.59
7.4	−21.44	−20.83	−20.59	−20.39	−20.35

3.3.5   Linearity and dynamic range

In fishery acoustics applications, the term *linearity* confusingly refers to (i) the summation of echoes from individual targets in an observation volume (Foote, 1983a), (ii) the echosounder-receiver response over its dynamic range, or (iii) the propagation of high-intensity sound pulses (Tichy *et al.*, 2003; Pedersen, 2007; Korneliussen *et al.*, 2008). The latter two are relevant to acoustic system calibrations.

In the linear region of the echosounder response, the output values are proportional to the input values. Uncertainty in this proportionality is commonly expressed as the deviation from a linear input–output relationship, expressed as a percentage of full scale. Because sphere calibrations are typically conducted with one transmit power and one sphere at one range, they are only valid for the linear region that was calibrated.

Dynamic range is the ratio of the maximum to minimum possible values of a variable quantity. Optimally, the linear range spans the dynamic range. When calibrating with targets at short ranges, particularly when conducting a self-reciprocity calibration, it is important to assure that the echo signals are not outside the dynamic range, i.e. the echosounder receiver is not saturated, and the measurements are in the linear region.

When sound propagation is non-linear, power is shifted from the signal frequency to its harmonics. This can occur when the power density is too high. When this occurs, the echosounder response is nonlinear. To avoid non-linear propagation, use sufficiently low transmit-power densities (Table 4.5) [Table 1 in Korneliussen *et al.* (2008)].

3.3.6   System stability

System gain may change between the time an echosounder is calibrated and used, due to changes in the environmental and system parameters (Van Buren *et al.*, 1999). For

example, Demer and Renfree (2008) demonstrated that temperature can change the impedance and thus performance of some transducers. For applications involving a towed or cast acoustic system, the on-axis system gain and directivity pattern may change significantly with changes in pressure (Beamiss *et al.*, 2002). The performance of system electronics and transducers may change over time, gradually or abruptly (Blue, 1984). Biofouling over the course of a survey may cause signal attenuation and degrade the calibration accuracy. Therefore, it is important to characterize such changes and apply any necessary corrections. A sudden change in system performance indicates a problem with the system. Frequent calibrations will monitor for gradual changes.

3.4   Total error

3.4.1   Backscattering cross section

To assess the systematic error or bias in on-axis gain, g_0 (dimensionless), due to bias in the aforementioned parameters, rearrange Equation (1.12c), and substitute $r = c_w t_r/2$, where t_r (s) is the time corresponding to scattering at range, r (m):

$$g_0 = \frac{\pi f c_w {t_r}^2 10^{\alpha_a c_w t_r/20}}{{\sigma_{bs}}^{0.5}} \left(\frac{p_{er}}{p_{et}}\right)^{0.5}.$$

(3.1)

Ignoring parameter covariance, the relative bias in g_0 can be estimated by:

$$\frac{\Delta g_0}{g_0} = \frac{\Delta f}{f} + \frac{\Delta c_w}{c_w} + \frac{2\Delta t_r}{t_r} - \frac{\Delta \sigma_{bs}}{2\sigma_{bs}} + \frac{\Delta p_{er}}{2p_{er}} - \frac{\Delta p_{et}}{2p_{et}} + \log_e(10)\left(\frac{\Delta c_w t_r \alpha_a}{20} + \frac{c_w \Delta t_r \alpha_a}{20} + \frac{c_w t_r \Delta \alpha_a}{20}\right).$$

(3.2)

Grouping similar terms, we obtain:

$$\left|\frac{\Delta g_0}{g_0}\right| \le \frac{|\Delta \sigma_{bs}|}{2\sigma_{bs}} + \frac{\log_e(10)}{20} c_w t_r |\Delta \alpha_a| + \left(\frac{\log_e(10)}{20}\alpha_a t_r + \frac{1}{c_w}\right)|\Delta c_w|$$
$$+ \frac{|\Delta f|}{f} + \frac{|\Delta p_{er}|}{2p_{er}} + \frac{|\Delta p_{et}|}{2p_{et}} + \left(\frac{\log_e(10)}{20}\alpha_a c_w + \frac{2}{t_r}\right)|\Delta t_r|.$$

(3.3)

To estimate the relative bias in g_0 after a system calibration with a sphere, solve Equation (3.3) using a relevant scenario, perhaps assuming that the:

1) sphere is manufactured to specifications;
2) sphere material is homogeneous (or any deviations are negligible);
3) sphere is perfectly spherical (or any deviations are negligible);
4) sphere materials change negligibly vs. pressure (or depth);
5) effect of the sphere tether is negligible;
6) sound propagation is linear;
7) echosounder response is linear; and
8) environmental conditions vary as those encountered during ocean surveys.

For example, consider the following hypothetical scenario:

The difference in the absorption coefficient, $\Delta \alpha_a$, is the difference between the values from (Francois and Garrison, 1982a) and those from Ainslie and McColm (1998), with the parameters given in Table 3.6. The σ_{bs} is for a 38.1-mm-diameter sphere made from tungsten carbide with 6% cobalt; it is a function of t_w, s_w, p_w, ρ_s, c_c, c_s, and b_f:

$$\Delta \sigma_{bs} = \text{maximum} \begin{bmatrix} \sigma_{bs}\left(t_w', s_w', p_w', \rho_s', c_c', c_s', b_f'\right) \\ -\sigma_{bs}\left(t_w, s_w, p_w, \rho_s, c_c, c_s, b_f\right) \end{bmatrix},$$

(3.4)

where each parameter and its prime counterpart indicate the values within that parameter's expected range which yield, in combination with those values for the other parameters, the maximum difference in σ_{bs} values, $\Delta\sigma_{bs}$. Values for ρ_s, c_c, c_s were varied $\pm2\%$ about their nominal values (Table 3.1); $t_w = 10 \pm 5°C$; $b_f = 1$ kHz; $\Delta t_r = 1$ µs; $\Delta f/f = 0.01$; and $\Delta p_{er}/p_{er} = \Delta p_{et}/p_{et} = 0.01$.

The results of this simulation, conditioned by the aforementioned assumptions and scenario, indicates that the uncertainty in g_0 is mostly due to relative bias in σ_{bs} and α_a, then c_w. Their relative contributions depend on f (Table 3.8). Because co-occurrence of extreme relative bias in each parameter is improbable, the distribution of total relative bias in g_0 should be calculated by estimating the distributions of each parameter and solving Equation (3.3) by Monte Carlo simulation (Demer, 1994, 2004; Rose, 2003; O'Driscoll, 2004). This was not done here due to a lack of knowledge about the parameter distributions.

Table 3.8 Components of relative bias for gain, g_0 (dimensionless), vs. frequency, f (Hz). The total relative bias in g_0 should be calculated by estimating the distributions of each parameter and solving Equation (3.3) by Monte Carlo simulation (Demer, 1994, 2004; Rose, 2003; O'Driscoll, 2004). Measurements of backscattering cross section, σ_{bs} (m² m⁻²), involve $g_0{}^2$, and, therefore, have twice the relative bias for g_0.

Relative uncertainty	Frequency (Hz) / 1 000					
	18	38	70	120	200	333
$|\Delta\sigma_{bs}|$	0.0407	0.0247	0.0808	0.0254	0.0687	2.4771
$|\Delta\alpha_a|$	0.0073	0.0311	0.0518	0.0518	0.1036	0.4145
$|\Delta c_w|$	0.0130	0.0133	0.0139	0.0146	0.0153	0.0164
$|\Delta f|$	0.0100	0.0100	0.0100	0.0100	0.0100	0.0100
$|\Delta p_{er}|$	0.0050	0.0050	0.0050	0.0050	0.0050	0.0050
$|\Delta p_{et}|$	0.0050	0.0050	0.0050	0.0050	0.0050	0.0050
$|\Delta t_r|$	0.0001	0.0001	0.0001	0.0001	0.0001	0.0001

3.4.2 Volume backscattering coefficient

The calibration for measurements of volume backscattering coefficient, s_v (m² m⁻³), involves both $g_0{}^2$ and a correction factor, $s_{a\,corr}{}^2$. Comparing Equations (1.12b) and (1.16) and substituting $r = c_w t_r/2$ and Equation (1.13):

$$s_v = \sigma_{bs} \frac{2}{s_{a\,corr}{}^2 \tau c_w \psi r^2} = \sigma_{bs} \frac{8}{\tau_{eff} c_w{}^3 \psi t_r{}^2} = \sigma_{bs} k_{s_v},$$

(3.5)

where k_{s_v} is a substitute for the quotient $8/\tau_{eff} c_w{}^3 \psi t_r{}^2$. Therefore, the relative bias in measurements of s_v include the relative bias in $g_0{}^2$, i.e. twice the values shown in Equation (3.3), plus the relative bias in k_{s_v}, which can be estimated by:

$$\left|\frac{\Delta k_{s_v}}{k_{s_v}}\right| \leq \frac{|\Delta\tau_{eff}|}{\tau_{eff}} + \frac{3|\Delta c_w|}{c_w} + \frac{|\Delta\psi|}{\psi} + \frac{2|\Delta t_r|}{t_r}.$$

(3.6)

This equation may also underestimate the total relative bias because it does not account for parameter covariance. A hypothetical scenario could include the following values for the parameters in Equation (3.5): $\left|\Delta\tau_{eff}\right|/\tau_{eff} = 0.05$, $|\Delta c_w| = 20\,\text{m s}^{-1}$, $|\Delta\psi|/\psi = 0.07$ (Table 3.7), and $\Delta t_r = 1$ µs. The distribution of total relative bias should be calculated by estimating the distributions of each parameter and solving Equations (3.3) and

(3.6) by Monte Carlo simulation (Demer, 1994, 2004; Rose, 2003; O'Driscoll, 2004). In that case, the relative bias in calibration for measures of s_v can be approximated as $2|\Delta g_0/g_0| + |\Delta k_{s_v}/k_{s_v}|$.

4 Calibration protocols

This section presents calibration protocols for several commonly-used acoustic instruments including scientific and commercial echosounders (Simrad EK60, ES60, and ES70) and a multibeam sonar (Simrad ME70). Protocols are presented for systems with vessel-mounted transducers, either mounted on the hull or in a centreboard. With minor modification, these protocols can be adapted to systems with other transducer-mount configurations (see Section 1.4).

4.1 Simrad EK60, ES60, and ES70

4.1.1 Introduction

The EK60 scientific echosounder (Simrad, 2008) replaced the EK500 (Simrad, 1997) in 2003. Hereafter, EK60 refers to a complete single-frequency echosounder system including the General Purpose Transceiver (GPT), connectors and cable, transducer, computer, and the ER60 control and data-logging software (Simrad, 2008). Calibration.exe refers to the ER60 calibration utility that may be run from, or independently from, the ER60.

The ES60 commercial echosounder (Simrad, 2004) and its successor, the ES70 (Simrad, 2010), are composed of EK60-generation transceiver hardware, but have different firmware, software, and features. They too can be calibrated and used effectively in certain research situations. ES60 and ES70 refer to the respective echosounder systems and their software with the same names.

Most of the calibration protocols presented in this document apply generically to EK60, ES60, and ES70 systems. System-specific procedures are highlighted. Protocols are presented for both single-beam and split-beam systems.

These echosounders are most commonly calibrated using the sphere method (Chapter 2). The results of a sphere calibration are relevant to the entire echosounder system. Therefore, if the GPT, transducer, cable, or connector are changed or altered, the system should be recalibrated. The parameters to be quantified for a calibrated system are shown in Table 4.1.

Table 4.1. EK60, ES60, or ES70 parameters estimated from nominal values, measurements in a tank (e.g. by the manufacturer), or sphere calibrations.

Parameter	Symbol	Units	Purpose	Description	Source
On-axis gain	G_0	dB re 1	Estimating target strength (TS)	On-axis efficiency	Measured
s_a correction	$s_{a\,corr}$	dB re 1	Estimating volume backscatter coefficients (s_v) and integrated s_v (s_a)	Difference in energy of the nominal and actual received pulses	Measured
Beamwidth	$\alpha_{-3\,dB}$ and $\beta_{-3\,dB}$	Degree	Estimating TS and school dimensions	Angle between half-power points	Nominal, adjusted for local c_w or measured

Parameter	Symbol	Units	Purpose	Description	Source
Angle offset	α_o and β_o	Degree	Estimating TS and school dimensions	Bias in phase detection	Nominal or measured
Angle sensitivity	Λ_α and Λ_β	(Electrical°/ geometric°)	Estimating $\alpha_{-3\,dB}$, $\beta_{-3\,dB}$, α_o, β_o, TS, and school dimensions	Factor to convert electrical phase angle to off-axis angle	Nominal or measured
Equivalent two-way beam angle	Ψ	dB re 1 sr	Echo integration		Nominal or measured
Sound speed	c_w	m s⁻¹	All measures	Sound propagation rate in water	Measured, or calculated using measures of temperature and salinity vs. depth
Frequency-specific absorption coefficient	α_a	dB m⁻¹	All measures	Sound attenuation due to viscous and chemical properties of water	Calculated using measures of temperature, salinity, and pH

The ER60 Calibration.exe utility is used to model the transducer directivity pattern and thereby provide estimates of on-axis gain, G_0 (dB re 1), s_a correction, $S_{a\,corr}$ (dB re 1), 3-dB beamwidths, $\alpha_{-3\,dB}$ and $\beta_{-3\,dB}$ (°), and angle offsets, α_o and β_o (°). In this chapter, the advantages and limitations of this application, and alternative approaches, are presented.

4.1.1.1 Data

The EK60, ES60, and ES70 echosounder systems output data in two formats that can be used for quantitative acoustic measurements: (i) raw data (.raw); and, converted to volume backscattering strength, S_v (m² m⁻³) and resampled, (ii) legacy (EK500) or ek5 data (.ek5 or Q-telegram).

For each echosounder transmission (ping), the raw data include received echo power, p_{er} (W), phase angles in two orthogonal planes, α, β (°) (for split-beam systems), and the following GPT settings: frequency, f (kHz), transmit power, p_{et} (W), pulse duration, τ (s), G_0, $S_{a\,corr}$, and equivalent two-way beam angle, Ψ (dB re 1 sr). These data and settings are used to calculate and display S_v and target strength, TS (dB re 1 m²):

$$S_v = P_{er} + 20\log_{10}(r) + 2\alpha_a r - 10\log_{10}\left(\frac{(p_{et}\lambda^2 g_0^2 c_w \tau \psi)}{32\pi^2}\right) - 2S_a corr \text{ , and} \quad (4.1)$$

$$TS = P_{er} + 40\log_{10}(r) + 2\alpha_a r - 10\log_{10}\frac{(p_{et}\lambda^2 g_0^2)}{16\pi^2} - 20\log_{10}\left(\frac{g(\alpha,\beta)}{g_0}\right) \text{ ,} \quad (4.2)$$

where r (m) is the range to the sphere, P_{er} (dB re 1 W) is the received power, p_{et} (W) is the transmit power, α_a (dB m⁻¹) is the absorption coefficient, g_0 (dimensionless) is the transducer on-axis (peak) gain, $g(\alpha, \beta)$ (dimensionless) is the transducer gain in the direction of off-axis angles α and β (°), λ (m) is the wavelength, f (Hz) is the frequency, c_w (m s⁻¹) is the water sound speed, τ (s) is the transmit pulse duration, ψ (sr) is the

equivalent two-way beam angle, and $S_a corr$ (dB re 1) is the S_a correction factor. Software (e.g. LSSS by IMR in Bergen, Norway; or Echoview by Myriax in Hobart, Tasmania) can be used to convert raw data to echograms of S_v or TS.

Although the ek5 data are less voluminous than the raw data, they do not contain the GPT settings (important metadata) and may contain quantization errors. For ER60 versions prior to 2.2.0, all versions of ES60, and possibly some or all versions of ES70, there is a quantization error in ek5 data that can cause significant (>4 dB) errors in the calibration results. This quantization error is extreme for measurements of highly reflective objects at a fixed range (e.g. a calibration sphere). Therefore, always record raw data and, unless you use ER60 version 2.2.0 or higher, always calibrate using raw data. If desired, ek5 data may be logged concurrently and independently.

Table 4.2. Key features of the EK60, ES60, and ES70 systems relevant to data outputs and calibration.

Feature	EK60	ES60	ES70
Primary purposes	Scientific echosounder	Fishery echosounder	Fishery echosounder
Simrad supports as a scientific instrument	Yes	No	No
System type	Split-beam (except 12 kHz and custom units)	Split- and single-beam	Split- and single-beam
Outputs raw data	Yes	Yes (V1.4.3.64+)	Yes
Outputs ek5 data	Yes, to file and Ethernet	Yes, to Ethernet; log with Echolog500 (www.echoview.com); quantization error can affect calibrations, but may not affect sampling	Yes, to file and Ethernet. Uncertain if ek5 data have quantization error
Calibration tools	Yes	No	No
Triangle-wave error sequence (TWES; Section 4.1.1.2)	No	Yes	Yes
Record of GPT parameters	Calibration.exe updates trlist.ini	Manually update trlist.ini	Manually update trlist.ini

4.1.1.2 Triangle-wave error

The raw data from ES60 and ES70 echosounders are modulated with a triangle-wave error sequence (TWES) with a 1-dB peak-to-peak amplitude and a 2720-ping period (Figure 4.1) (Ryan and Kloser, 2004). The TWES averages to zero over a complete period, so its contribution to sampling error may be insignificant. However, the TWES

may bias calibration results as much as ±0.5 dB. Therefore, prior to calibrations, the TWES should be removed from ES60 or ES70 P_{er} data.

To remove the TWES, it is first necessary to determine its phase. This is done by analyzing P_{er} data collected during and shortly after the transmit pulse (the first few metres of the echogram) from at least 1360 continuous pings (half the period of the TWES). The TWES phase is defined relative to the first ping in the file. The p_{er} data are corrected by subtracting the phase-aligned TWES from P_{er} data from each transmission in each file. This procedure can be conveniently accomplished using the batch processing feature of ES60adjust.jar (an open source utility developed by CSIRO Marine and Atmospheric Research, available from the ICES website).
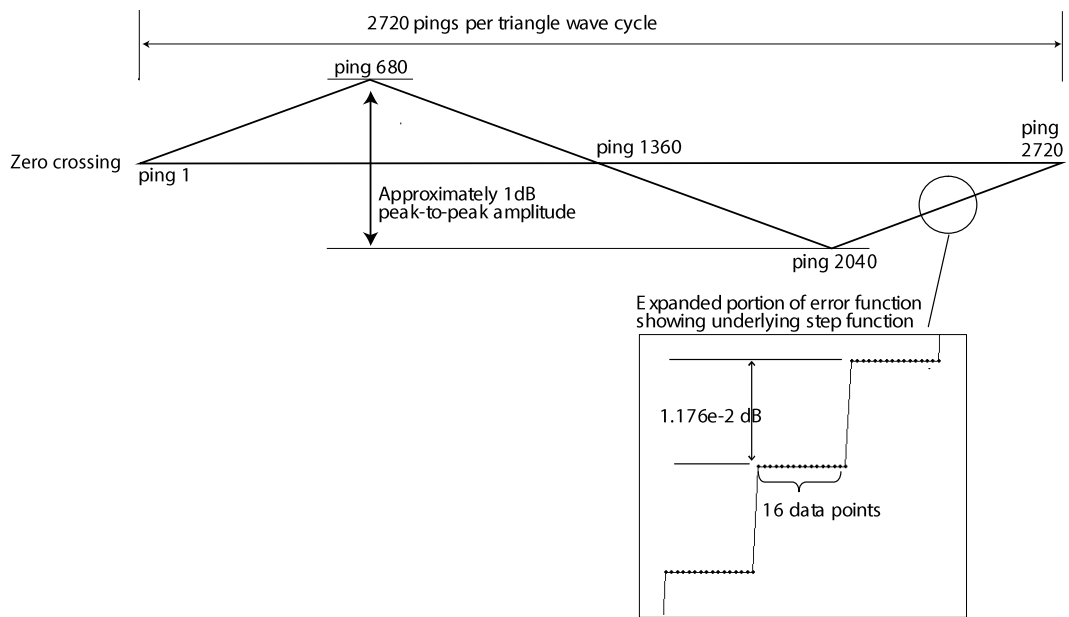
Figure 4.1. The ES60 and ES70 triangle wave error sequence (TWES) showing the 1-dB peak-to-peak amplitude and 2720-pings period. The expanded portion shows an underlying step function, due to sampling quantization, with 16-ping width and 1.176×10^{-2} – dB height.

4.1.1.3 Settings

Nominal values for the GPT settings (Table 4.1) are listed in the TRList.ini file for each combination of transducer, transceiver, and pulse duration (Table 4.3). This file is located in the echosounder-software installation directory. TRList.ini can be updated through the ER60 menu or manually.

Table 4.3. Excerpt from a TRList.ini file showing nominal settings for a 38-kHz split-beam GPT, an ES38B transducer, and five pulse lengths (i.e. durations).

GPTTRANSCEIVER "GPT-Q38(1)-F 1"
BEAMTYPE=SPLIT
MARKETSEGMENT=FISHERY
MINMEDMAXTXPULSELENGTH=0.000256 0.000512 0.001024 0.002048 0.004096
ENDGPTTRANSCEIVER
TRANSDUCER="ES38B"
FREQUENCY=38000
BEAMTYPE=SPLIT
EQUIVALENT2WAYBEAMANGLE=−20.6
GAIN=24.00 26.00 26.50 26.50 26.50
SACORRECTION=0.00 0.00 0.00 0.00 0.00
MAXTXPOWER=4000.0
THREEDBBEAMWIDTHALONGSHIP=7.10
THREEDBBEAMWIDTHATHWARTSHIP=7.10
ANGLESENSITIVITYALONGSHIP=21.90
ANGLESENSITIVITYATHWARTSHIP=21.90
OFFSETALONGSHIP=0.00
OFFSETATHWARTSHIP=0.00
ENDTRANSDUCER

For each scientific echosounder transducer, Simrad measures the beamwidths, θ_{-3dB}' (°), and angle sensitivities, Λ' (electrical ° / geometrical °), under controlled, freshwater tank conditions (Table 4.4). Simrad then uses the estimated $\alpha_{-3\,dB}'$ and $\beta_{-3\,dB}'$ values to estimate the equivalent two-way beam angle [$\Psi' = 10\log_{10}(\alpha_{-3\,dB}'\,\beta_{-3\,dB}'/5800)$]. However, once the transducer is relocated to a different environment and mounted in a platform (e.g. the hull of a ship, centreboard, or towed body), these values may be different (Simmonds, 1984a, 1984b; Reynisson, 1998). This is because the local c_w affects λ, Λ, $\theta_{-3\,dB}$, ψ, and g_0, and, therefore, measures of TS and S_v (Bodholt, 2002):

$$\Lambda = \Lambda'(c_w'/c_w)\,;$$

(4.4)

$$\theta_{-3dB} = \theta_{-3dB}'(c_w/c_w')\,;$$

(4.5)

$$\psi = \psi'\left(c_w^2/c_w'^2\right)\,; \text{ and}$$

(4.6)

$$g_0 = g_0'\left(c_w'^2/c_w^2\right)\,.$$

(4.7)

Measures of Λ and $\theta_{-3\,dB}$ require echosounder-independent measures of the target location (Reynisson, 1990, 1998). Because such measures are difficult to make routinely (Simmonds, 1984a), use the nominal value for Λ, and derive ψ from Equation (4.6) using a measure of local c_w, and ψ' from the manufacturer's measurements at c_w' (e.g. Table 4.4). Then, estimate values for $\alpha_{-3\,dB}$ and $\beta_{-3\,dB}$ from the calibration results. In this case, the estimates of $\alpha_{-3\,dB}$ and $\beta_{-3\,dB}$ may not indicate the true beamwidths, but their use in the directivity-pattern model will correctly compensate measures of σ_{bs} for the directivity pattern (Bodholt, 2002).

Table 4.4. An example report of Simrad's freshwater tank measurements for a Simrad ES38 B transducer.

TRANSDUCER MEASUREMENTS	Part 1	Part 2	Part 3	Part 4	All Parts
Measured at: f (kHz)	38,0	38,0	38,0	38,0	38,0
Beamwidth					
Longitudinal: ß1 (deg)					6,8
Transversal: ß2 (deg)					6,9
Directivity index (dB): 10 log(2.5/(sin(ß1/2)*sin(ß2/2)))					28,5
Equivalent two way beam angle (dB): 10 log(ß1*ß2/5800)					-21,0
Impedance					
|Z| (ohm) :	63,4	61,4	66,2	62,4	15,8
Phase (deg) :	-2,7	-2,3	-6,0	0,8	1,5
Transmitting response (at 1 metre)					
Si (dB re 1 µPa/A):	208,6	208,7	209,5	208,7	209,1
Su (dB re 1 µPa/V):	172,6	172,9	173,1	172,8	185,1
Receiving sensitivity					
Theoretical open circuit (Si-354.1-20 log f): (dB re 1 V/µPa)	-177,0	-177,0	-176,2	-177,0	-176,6
Leaking resistance (Mohm) :	OK	OK	OK	OK	OK
Type: ES38-B					
Serial no: 30595					
Watertemp: 21,0 °C					
Tested by: BK Date: 21. jun. 2005					

4.1.1.4 Preparation

Before a calibration, Simrad (2001) recommends checking the internal test signal for each frequency (channel) to identify any major operational issues with the echosounder receiver. If the internal test signal has not been disconnected by the manufacturer, with the transceiver channel set to "Test" mode, record the Noise Est(imate) displayed in the "Numerical View". Acceptable test values are –70 ±1 or –64 ±1 dB re 1 W for a single- or split-beam system, respectively.

Record the ambient noise at each frequency to compare with conditions at historical or future calibration sites. With the transceiver channel set to "Passive" mode, record the range of background noise values estimated under "Environment" in the "Numerical View" (ER60 software only).

Deploy a conductivity–temperature–depth probe (CTD) at the calibration site to obtain depth profiles of salinity and temperature. Calculate the mean salinity and temperature, and harmonic mean sound speed (see Section 2.1.2.5) for the range between the transducer and the calibration sphere. In the "ER60 Install-Environment" dialog box, input these values and calculate absorption coefficients for each frequency (Francois and Garrison, 1982a). For ES60 and ES70 echosounders, input the harmonic mean sound speed (see Section 2.1.2.5) calculated from the measured salinity and temperature and indicate if the environment is fresh- or salt water. Note, these values may be set or changed when later processing the raw data, e.g. with Echoview (Myriax, 2014).

The effects of non-linear harmonic distortion can affect the transducer directivity pattern and limit the sound energy radiated into the water (Tichy *et al.*, 2003; Korneliussen

et al., 2008). These non-linear effects generally increase with frequency. To mitigate these effects, (Korneliussen *et al.*, 2008) recommended maximum p_{et} for several Simrad transducers (Table 4.5).

Table 4.5. Recommended maximum transmit power (p_{et}) for 60% electro-acoustic efficiency, for some common transducer sizes (Korneliussen *et al.*, 2008).

Frequency (Hz)/1 000	18	38	70	70	120	200	333	400
Transducer area (10^{-3} m^2)	200	100	30	12	10	4.4	1.6[a]	1.1
Nominal $\theta_{-3\,\text{dB}}$ (°)	11	7	7	11	7	7	7	7
Maximum p_{et} (W)	5 000	2 500	750	300	250	110	40	28

Generally, echosounders should be calibrated in the configuration that they will be used for sampling. If multiple echosounders with different frequencies will be used during sampling, those echosounders should also be active during calibration. To reduce the time necessary to calibrate, the transmit rate may be maximized, generally without deleterious effects. However, if the transmit rate is too rapid, echoes from a previous ping might alias into data from the current transmission, introducing "phantom seabed" or "false bottom" echoes in the echograms for one or more frequencies. If this occurs, adjust the transmit rate until the aliased reverberation is avoided.

Generally, when calibrating, a single sphere is suspended below the transducer. If multiple spheres are suspended concurrently (e.g. to efficiently calibrate multiple systems), MacLennan (2011) cautions that forward scatter may introduce some measurement error.

4.1.2 Split-beam EK60

This section describes three approaches to calibrating a split-beam EK60 with a sphere including: (i) the recommended ER60 Calibration.exe utility, (ii) an alternative ExCal script, and (iii) an on-axis method. The differences, advantages, and limitations of each approach are discussed.

4.1.2.1 Calibration.exe

Measurements of *TS* from a sphere are made as it is moved throughout the transducer beam. Calibration.exe uses these measures to estimate $\alpha_{-3\,\text{dB}}$, $\beta_{-3\,\text{dB}}$, α_o, β_o, G_0, and $S_{a\,corr}$. The steps are detailed below and in Simrad (2008).

4.1.2.1.1 Data collection

Calibration.exe requires measurements of *TS* from a sphere throughout all the transducer-beam quadrants. The apparatus and procedure to map the directivity pattern are described in Chapter 2.

To measure the sphere *TS*, it generally suffices to use the default parameters for single-target detection (i.e. minimum echo length = 0.8, maximum echo length = 1.8, maximum phase deviation = 8.0, maximum gain compensation = 6.0, minimum echo spacing = 1.0). However, the minimum *TS* threshold should be set ~10 dB below the theoretical *TS* value (TS_{theory}) for the reference sphere value. For example, for a sphere with TS_{theory} = –42.2 dB, set the minimum *TS* threshold to –52 dB). If it is difficult to locate

the sphere, lower the minimum TS threshold, find the sphere, and then restore the threshold to the recommended level.

Launch Calibration.exe from the ER60 "Single Target Detection" dialogue box. Input the TS_{theory} (Chapter 2), set the allowable TS deviation = 5 dB, and set the upper and lower ranges equal to the on-axis sphere range ±3 m. These settings allow most of the sphere echoes to be recorded. Spurious echoes from other scatterers (e.g. fish, swivels, and weights) may be filtered during data processing. To assure that the transducer beam is sufficiently mapped, Calibration.exe displays the positions of the TS measurements. To precisely estimate the $\alpha_{-3\,\text{dB}}$, $\beta_{-3\,\text{dB}}$, α_o, β_o, G_0, and $S_{a\,corr}$ values, at least 100 TS detections should be evenly distributed throughout the $\alpha_{-3\,\text{dB}}$, and $\beta_{-3\,\text{dB}}$ (e.g. to ±3.5° for each axis of a 7°-beamwidth transducer), and ten or more detections should be near the beam axis (Simrad, 2008).

If the transducers to be calibrated are mounted sufficiently close to each other or the ranges to the sphere are sufficiently large, or both, TS data can be collected simultaneously at multiple frequencies (Demer *et al.*, 1999; Conti *et al.*, 2005a; Korneliussen *et al.*, 2008). Then, each channel may be calibrated by replaying the same raw data file and rerunning Calibration.exe. For example, data used to calibrate 38-, 70-, 120-, and 200-kHz echosounders may be collected at the same time by moving a 38.1-mm-diameter sphere made from tungsten carbide with 6% cobalt throughout the overlapping beams. In this case, the Calibration.exe should be first configured for the most centrally located transducer, and the TS data should be collected to the edges of its beam. Then, in succession, the raw data file(s) can be repeatedly replayed, each time configuring Calibration.exe for each one of the other transducers. If one or more of the beams are insufficiently mapped, collect more TS data and replay again using both raw-data files.

4.1.2.1.2   Data processing

After sufficient TS data are collected, save the file, fit the beam model, and inspect and edit the results. The beam model has a theoretical basis and, with a properly functioning system, is less susceptible to noise than the polynomial model. However, if the system is dysfunctional, the polynomial model can provide additional diagnostic information (Figure 4.2).

Calibration.exe displays the TS data overlaid on the selected beam model. Optional views are polar or one of several planar slices. TS outliers can be deselected with a click of the mouse cursor, and the beam model can be refitted. The root-mean-square (rms) error generally increases with frequency. An rms error <0.4 indicates an acceptable model fit. Fits with larger rms values should be scrutinized and perhaps discarded. Examinations of the polar and planar views can confirm that the system is working properly. For example, the plot view of the beam model for a circularly symmetrical transducer should display concentric circles. If it displays ellipsoids with the major axis at 45° or 135°, the transducer or receiver might have a dysfunctional quadrant (e.g. Figure 4.2). If non-circular shapes are paired with large offset angles, the transducer may be wired incorrectly. See Simrad (2008) for additional troubleshooting guidance. If the estimated G_0 differs from that of recent calibrations conducted under similar environmental conditions by >0.5 dB (ICES, 1994), the system should be evaluated for proper function, the calibration should be repeated, or both.
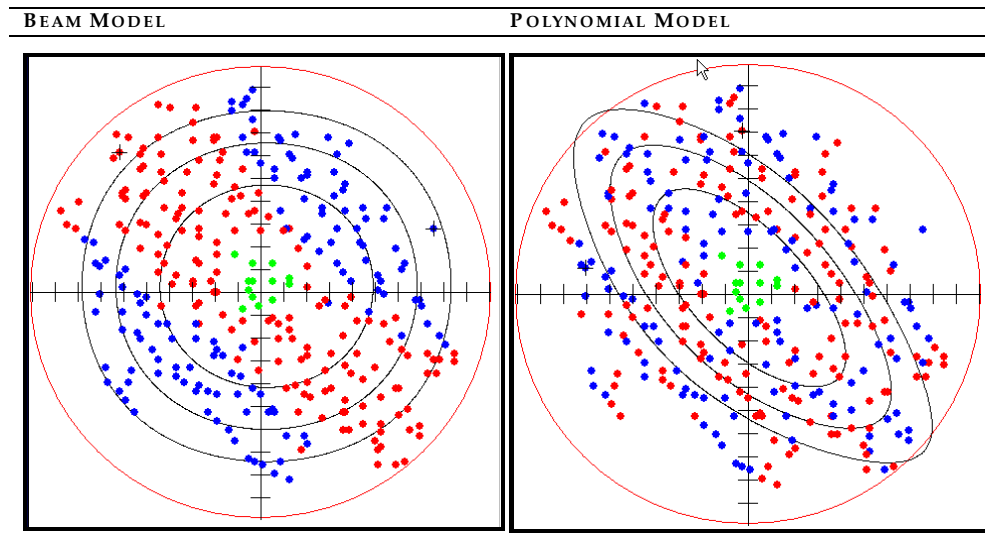
BEAM MODEL	POLYNOMIAL MODEL

Figure 4.2. Example beam maps for a transducer with a disconnected upper-right quadrant. In this case, *TS* **measurements could not be made towards the edges of the upper-right and lower-left quadrants. The beam model (left) has concentric lines, but banding in the positive (red) and negative residuals (blue) indicates a problem. The polynomial model (right) shows slanted ellipsoids with more randomly distributed residuals, also indicating a problem with the transducer or receiver.**

4.1.2.1.3 Echosounder update

The EK60 can be configured with the updated calibration parameters by selecting "Update Beam Data" in Calibration.exe. Optionally, record the calibration parameters manually and exit Calibration.exe without updating the beam data; then set the transducer parameters through "Install Transducer Parameters" in the ER60. Both of these methods update the calibration values in the TRlist.ini file (Section 4.1.1.3). A third option is to make a backup copy of Trlist.ini (e.g. named Trlist.ini.bak) and then manually update the TRlist.ini file using a text editor. If desired, a simplified version of Trlist.ini file may be created by deleting all of the >5000 lines of text that are not relevant to the system being calibrated. A fourth option is to simply retain the current values in the echosounder and then calibrate the raw data while processing, e.g. using an .ecs file in Echoview (Myriax, 2014). With this latter option, however, the EK60 will not display calibrated data.

4.1.2.1.4 Advantages and limitations

The following are advantages of Calibration.exe:

- a simple application designed for EK60 calibrations;
- runs within the ER60 in normal and replay modes;
- runs outside the ER60 for analysing calibration data sets;
- provides model-fit rms error to judge the quality of calibrations; and
- readily configures the EK60 with the calibration results.

The following are limitations of Calibration.exe:

- records only the first *TS* value measured in each cell of a 25 x 25 array spanning the −6 dB points of the beam;

- the beam-model is fitted with equally weighted TS measurements, perhaps resulting in a fit that exceeds all of the near-axis TS measurements;
- TS measurements must span the beam, which may be time-consuming or unachievable in poor conditions or when the sphere movement is otherwise physically constrained; and
- noisy or biased TS data (e.g. echoes from the sphere among biota) cannot be readily filtered and might bias the calibration results.

4.1.2.2 ExCal

ExCal is a free open-source Matlab (The Mathworks, MA, USA) script for estimating calibration parameters for EK60, ES60, and ES70 echosounders. It reads raw data files.

4.1.2.2.1 Advantages and limitations

The following are advantages of the ExCal utility:

- offers convenient exclusion of all undesired TS data;
- uses more TS data than Calibration.exe to calculate G_0 and $S_{a\,corr}$;
- provides options to filter TS and thereby allow better utilization of noisy data;
- estimates G_0 and $S_{a\,corr}$ using maximum, mean, or model-fit TS values;
- plots the calibration data and results for use in calibration reports; and
- is open source code that can be modified to test other algorithms.

The following are limitations of the ExCal utility:

- does not update the EK60 with new calibration parameters; and
- requires a Matlab license and familiarity with Matlab.

4.1.2.3 On-axis calibration

A third approach to estimating G_0 and $S_{a\,corr}$ is to make measurements of TS and S_a with the sphere positioned on the beam axis. This is most accurately accomplished using split-beam angle measurements to position the sphere and a post-processing application, e.g. Echoview (Myriax, 2014), to filter the measurements and calculate mean S_a. To position the sphere on the axis of a single-beam transducer, it is necessary to iteratively maximize the measured TS (Section 4.1.4).

4.1.2.3.1 Data collection

To position the sphere on the beam axis, surround the sphere echo with a 5-m wide active layer in the ER60 "Echogram" view and monitor the location of the sphere in the beam using the ER60 "Single Target Position" view. This procedure restricts the targets appearing in the "Single Target Position" view to only those within the layer that meet the "Single Target Detection" criteria (Section 4.1.2.1). Calculate the mean of approximately 100 sphere-TS measurements and compare it to TS_{theory}. Using an appropriate sphere for each frequency, repeat this process for each transducer. Collect separate raw data files for each on-axis calibration.

4.1.2.3.2 Data processing

Using an application to process the raw data, e.g. Echoview (Myriax, 2014), adjust the "Single Target Detection" criteria (Table 4.6) to detect sphere echoes. Filter echoes that are not from the sphere and restrict the sphere-TS measurements to those exactly or approximately on the beam axis.

Table 4.6. Recommended "Single Target Detection" criteria for Echoview (Myriax, 2014) processing of *TS* measurements of a 38.1-mm-diameter WC sphere at 38 kHz. These values might require adjustments for different spheres, frequencies, and environmental conditions.

"Single Target Detection" criteria	Recommended setting
TS threshold	−50.0 dB
Pulse length determination level	6.0
Minimum normalized pulse length	0.20*
Maximum normalized pulse length	1.50
Beam compensation model	Simrad LOBE
Maximum beam compensation	3.0 dB
Maximum standard deviation of minor axis angles	0.60°
Maximum standard deviation of major axis angles	0.60°
Filter beam compensation	0.1 dB**

*Less than the ER60 default value.
**Increase in noisy conditions.

Calculate the mean on-axis sphere TS by averaging in the linear domain. Estimate the new G_0 using the following equation.

$$\text{new } G_0 = \frac{TS - TS_{\text{theory}}}{2} + \text{old } G_0$$

(4.8)

Calculate the theoretical on-axis S_a ($S_{a\,\text{theory}}$) for the sphere (see Chapter 2). Use the mean measured sphere S_a and the following equation to estimate the new $S_{a}corr$.

$$\text{new } S_{a\,\text{corr}} = (\text{old } G_0 + \text{old } S_{a\,\text{corr}}) - \frac{10\log\left(\frac{S_{a\,\text{theory}}}{S_a}\right)}{2} - \text{new } G_0$$

(4.9)

Update the echosounder settings using any of the manual options described in Section 4.1.2.1.

4.1.2.3.3 Advantages and limitations

The following are advantages of on-axis calibrations:

- data can be filtered using raw data-processing software, e.g. Echoview (Myriax, 2014);
- calibration is quicker and more successful when conditions or apparatus prevent beam mapping; and
- $S_{a\,\text{corr}}$ is estimated using more data than used in Calibration.exe.

The following are limitations of on-axis calibrations:

- requires that the sphere is centred stably on the beam axis;
- uses existing $\theta_{-3\,dB}$, θ_o, and Λ settings to calculate the sphere position;
- does not estimate beam shape, $\theta_{-3\,dB}$ or θ_o values;
- does not automatically update the ER60 with the new calibration settings; and
- does not verify the function of all quadrants in a split-beam system (e.g. Figure 4.2).

4.1.3 Split-beam ES60 and ES70

ES60 and ES70 software packages do not include a calibration utility. Nevertheless, these echosounders may be calibrated. This section outlines the calibration procedures that are unique to ES60 and ES70 echosounders.

4.1.3.1 Data collection

The apparatus for calibrating and a method for positioning the sphere are described in Chapter 2. Calibrate the echosounders using the same p_{et} and τ to be used for acoustic sampling. Assure that p_{et} does not exceed the values in Table 4.5.

Position and monitor the sphere within the acoustic beam using the "Echo Trace" display in the ES60 or the "Fish Position" display in the ES70. To display only the sphere detections, adjust the start and stop ranges in the "Echogram" display. Check that adjustments to the sphere position are mimicked in the echosounder measurements. Methodically move the sphere and record its TS uniformly throughout the beam. If software is not available to track the sphere movements, either note on a piece of paper where the sphere has been or tape clear plastic over the "Echo Trace" or "Fish Position" display and mark the sphere locations with a pen. For each calibration, start a new file and assure that the raw data includes more than 1360 pings so that the TWES (Section 4.1.1.2) can be removed prior to data processing.

4.1.3.2 Data processing

ES60 and ES70 calibration data can be processed using one of the methods described for EK60 calibrations (Section 4.1.2). To use Calibration.exe or the on-axis approach, first generate new raw files with the TWES removed (Section 4.1.1.2). Uncorrected raw files can be processed directly with ExCal, as it can remove the TWES.

4.1.3.3 Echosounder update

The calibration settings in split-beam ES60 and ES70 echosounders can be updated by manually editing the TRlisit.ini file (Section 4.1.2.1). Alternatively, the uncalibrated raw data may be calibrated using processing software, e.g. Echoview (Myriax, 2014).

4.1.3.4 Advantages and limitations

The advantages and limitations of ES60 and ES70 calibrations are the same as for the three approaches to EK60 calibrations (Section 4.1.2), except that the update of calibration settings is not automated.

4.1.4 Single-beam ES60 and ES70

Single-beam echosounders do not measure the angular positions of the sphere within the transducer beam. Therefore, to position the sphere on the beam axis, the sphere is moved until the beam-uncompensated TS is maximized (Chapter 2). Values for G_0 and $S_{a\,corr}$ are then estimated (see Section 1.2.2).

4.1.4.1 Data collection

Adjust the display range and colour scale to highlight the sphere echo in the ES60 or ES70 Echogram window. The colour-scale resolution is only 3 dB, but other software applications, e.g. Echoview Live Viewing (Myriax, 2014) can provide better display resolution. Start a new file and assure that the raw data from the calibration include more than 1360 pings so that the TWES (Section 4.1.1.2) can be removed prior to data processing.

4.1.4.2 Data processing

First remove the TWES from the raw data (Section 4.1.1.2). Then, apply a single-target detection algorithm to the corrected data and, using processing software, e.g. Echoview (Myriax, 2014), export the sphere-TS measurements in csv-format file. Using these data, estimate the mean on-axis sphere-TS by averaging the largest 5% of the TS measurements. Estimate the new G_0 (Section 4.1.2.3). Next, calculate the mean on-axis S_a using the sphere-S_v measurements that correspond to the largest 5% of the TS measurements. Calculate the new $S_{a\,corr}$ (Section 4.1.2.3.2).

4.1.4.3 Echosounder update

The calibration settings in single-beam ES60 and ES70 echosounders can be updated by manually editing the TRlisit.ini file (Section 4.1.2.1). Alternatively, the uncalibrated raw data may be calibrated using processing software, e.g. Echoview (Myriax, 2014).

4.1.4.4 Advantages and limitations of ES60 and ES70 single-beam calibrations

The advantages and limitations of single-beam calibrations are the same as for on-axis calibrations (Section 4.1.2.3.2).

4.1.5 Measurement error

Calibration uncertainty is presented in Chapter 3. Details specific to EK60, ES60, and ES70 systems are discussed here. The chosen approach (e.g. Calibration.exe, ExCal, or on-axis) can result in different estimates of G_0 and $S_{a\,corr}$. In most instances, however, the various estimates of G_0 vary by approximately ±0.1 dB. One reason for small discrepancies is that the fitted beam model often exceeds slightly the measurements near the beam axis (e.g. Figure 4.3).
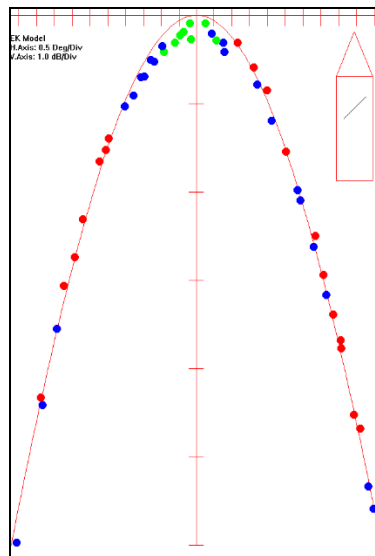

Figure 4.3. The beam-model fit to sphere-TS measurements made with an EK60 configured with an ES38B transducer. In this example, the TS measurements near the beam axis are all below the model.

Knudsen (2009) estimated the precision of sphere-calibration estimates of G_0 to be ±0.1 dB for an EK60 configured with a Simrad ES38-B transducer (Figure 4.4). Calibrated G_0 may be a little less precise for higher frequencies, e.g. 70, 120, and 200 kHz.
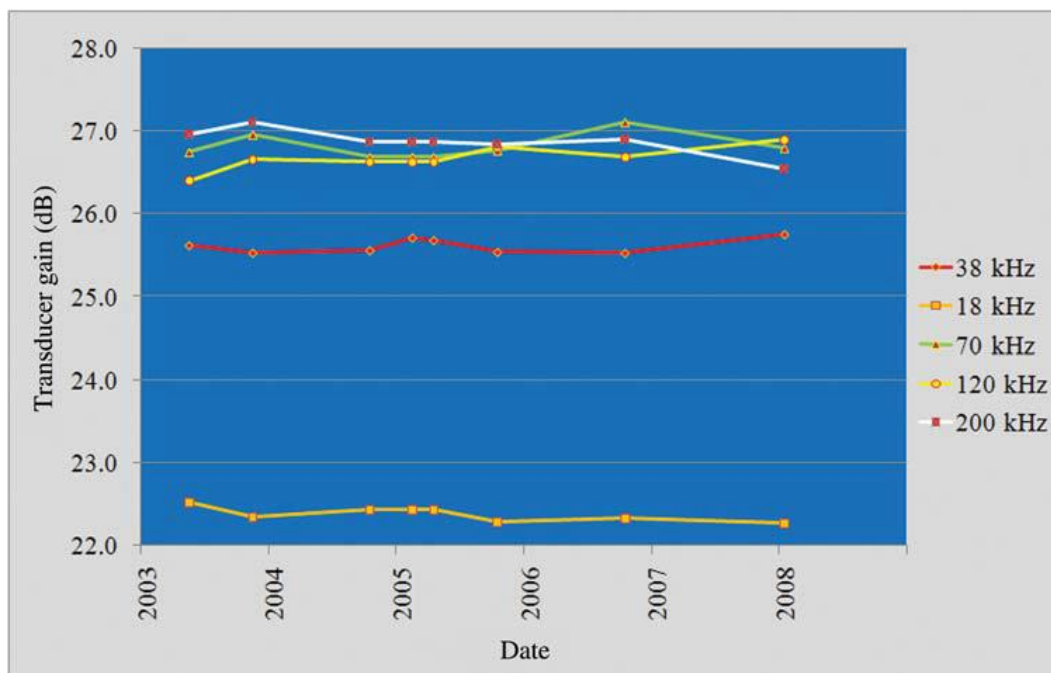
Figure 4.4. Time-series of gain (G_0) for a five-frequency EK60 system configured with Simrad transducers (composite, 70 kHz and higher) on R/V "G. O. Sars" (Knudsen, 2009).

The aforementioned estimates of precision for G_0 were for contemporary calibrations made in low-noise conditions (i.e. low sea state and resolvable sphere echoes). Demer *et al.* (1999) showed that the precision of split-beam angle measurements decreases with the signal-to-noise ratio. Accordingly, Pedersen (2007) found that the standard error in some beam-model parameters (i.e. $\alpha_{-3\,\text{dB}}$, $\beta_{-3\,\text{dB}}$, α_o, and β_o) increased with ambient noise level. Changes in temperature also affect transducer performance (Demer and Renfree, 2008). Of the 10 Simrad transducers they tested, the composite transducers were less sensitive to changes in temperature than the older models, and the ES120-7 was most sensitive. Transducer performance is also affected by changes in pressure (Chapter 2). For example, Dalen *et al.* (2003) observed a 2 dB change in sphere-*TS* when a Simrad ES38DD transducer was lowered from near the surface to 500 m. It is, therefore, important to calibrate echosounder systems under the range of conditions (i.e. temperature, salinity, and pressure) to be encountered during the acoustic sampling.

4.1.6   Documentation

Calibration metadata provide a record that is useful for quality control and comparisons of the results. These metadata (Anon., 2014) can be organized by physical environment (site and water column), equipment and settings, and calibration results (Table 4.7).

Table 4.7. Recommended calibration metadata.

Site	Platform name, location, latitude, longitude, seabed depth
	Sea-state at start and end of exercise
	Date and time at start and end of calibration, with time zone
	Comments (e.g. anchoring notes)
Water column	CTD data including model, configuration, and filename
	Water temperature, salinity, and sound speed at the transducer and sphere depths
	Harmonic-mean sound speed between the transducer and the sphere
	Mean absorption coefficient between transducer and sphere, for each frequency
	Estimated noise, for each frequency
	Comments (e.g. other scatterers present)
Equipment	Transducer model, frequency, serial number, and depth
	GPT model, frequency, serial number, and firmware version
	Echosounder software version
	Sphere identification, material, diameter, range from transducer, and TS_{theory}
Settings (by frequency)	Transmit power, p_{et} (W)
	Pulse length (duration), τ (ms)
	On-axis gain, G_0 (dB)
	S_a correction, $S_{a\ \text{corr}}$ (dB)
	Bandwidth, b_f (Hz)
	Sample interval (m)
	Equivalent two-way beam angle, Ψ (dB re 1 sr)
	Absorption coefficient, α_a (dB km^{-1})
	Water sound speed, c_w (m s^{-1})
	Angle sensitivity alongships, Λ_α (electrical°/geometric°)
	Angle sensitivity athwartships, Λ_β (electrical°/geometric°)
	3-dB beamwidth alongships, $\alpha_{-3\ \text{dB}}$ (°)
	3-dB beamwidth athwartships, $\beta_{-3\ \text{dB}}$ (°)
	Angle offset alongships, α_o (°)
	Angle offset athwartships, β_o (°)
	Single-target detection parameters
Results	Internal test oscillator readings
	On-axis data-collection start and end times
	Beam map start and end times
	Processing software name and version
	On-axis results including mean TS and mean S_a
	Beam model results including estimated $\alpha_{-3\ \text{dB}}$, $\beta_{-3\ \text{dB}}$, α_o, β_o, G_0, and $S_{a\ \text{corr}}$, and model fit rms error

4.1.7   Quick start

The following is a guide to using ER60 and its Calibration.exe utility to calibrate EK60 split-beam systems. Similarly, ES60 or ES70 split-beam systems may be calibrated by replaying TWES-corrected raw data (Section 4.1.1.2) in ER60 and Calibration.exe.

1) Record metadata (Section 4.1.6) throughout the calibration.

2) Anchor in sheltered water with few biota (there may be fewer during daytime).

3) Set the "Raw Data Collection Range" to include the seabed. Ensure that the "Display Range" and "Bottom Detection Range" do not exceed "Data Collection Range".

4) Maximize the ping rate.

5) Set the ER60 "Single-Target Detection" parameters.

6) Install the calibration apparatus and position the sphere at a range two- to three-fold the transducer far-field range, e.g. 15–25 m below the transducer, on or near its beam axis.

7) Measure the seawater temperature and salinity vs. depth. Use these data to estimate the water sound speed, c_w (m s^{-1}), values at the depth of the transducer and the sphere, and the harmonic-mean value between them. Also estimate the mean absorption coefficient, α_a (dB m^{-1}), over the same depth range for each frequency, f (Hz). Update these environmental settings in the GPT.

8) Calculate TS_{theory} using the c_w estimated for the depth of the sphere.

9) Launch Calibration.exe from the ER60 "Single Target Detection" dialogue box. Input TS_{theory}, the allowable TS deviation = 5 dB, and the upper and lower measurement ranges = sphere range ±3 m).

10) Record at least 100 sphere-TS measurements as it is moved throughout the beam to at least the edges of the nominal half-power beamwidth.

11) Record at least 10 sphere-TS measurements near the beam axis.

12) Stop recording and save the file. Examine the sphere-TS measurements overlaid on the beam-model fit, in both polar and planar views. Remove any outliers and re-save the file.

13) Confirm that the rms error for the beam-model is < ~0.4 (this value generally increases with frequency), and that the beam-model estimates of G_0 and $S_{a\,corr}$ are within ±0.5 dB of their expected values.

14) If desired, update the echosounder settings manually or, if using Calibration.exe, using "Update Beam Data".

4.2   Simrad ME70

4.2.1   Introduction

The Simrad ME70 multibeam echosounder transducer is composed of 800 elements configured in a 20 x 40 matrix. The interelement spacing is 15 mm alongships and 7.5 mm athwartships, forming a 30-cm^2 transducer surface. Operating in fishery mode (Cutter *et al.*, 2010), the ME70 can be configured to produce up to 45 steered, single- or split-beams (see Chapter 1), each spanning a portion of the total system bandwidth, 70–120 kHz (Trenkel *et al.*, 2008). This section presents some theory and then calibration

procedures for calibrating a vessel-mounted ME70 configured for operation with multiple split-beams operating at different centre frequencies. The procedure is based on the sphere method (see Section 4), applied to multiple beams (Ona *et al.*, 2009).

4.2.2 Theory

Relative to the other echosounders described in Section 4.1, the ME70 has some unique parameters and considerations. This section describes some features of the ME70 that are relevant to sphere calibration and data processing.

4.2.2.1 Adjust parameters

The ME70 software includes nominal values for on-axis gain, $G_{0\ nom}$ (dB re 1). The gain adjustment, ΔG_0 (dB re 1) is the difference between $G_{0\ nom}$ and the calibrated gain, G_0 (dB re 1):

$$G_0 = G_{0\ nom} + \Delta G_0 \ .$$

(4.10)

Similarly, the ME70 software includes nominal values for S_a correction, $S_{a\ corr\ nom}$ (dB re 1). The S_a correction adjustment, $\Delta S_{a\ corr}$ (dB re 1) is the difference between $S_{a\ corr\ nom}$ and the calibrated S_a correction, $S_{a\ corr}$ (dB re 1):

$$S_{a\ corr} = S_{a\ corr\ nom} + \Delta S_{a\ corr} \ .$$

(4.11)

4.2.2.2 Bearing angles

The ME70 provides target bearing angles in the alongships, α (°) and athwartships, β (°) planes for each echo sample within each beam. Using far-field beamforming, the electrical phase angle φ and target mechanical angle are related by:

$$\varphi = \frac{2\pi d_{eff}}{\lambda} [\sin(\theta_t) - \sin(\theta_s)] \ ,$$

(4.12)

where θ_t is the target mechanical angle (i.e. α or β), θ_s is the beam steering angle, and d_{eff} is the effective distance between the acoustic centres of the split-beam subarrays. In the case where θ_t is close to θ_s, Equation (4.12) can be approximated by:

$$\varphi = \frac{2\pi d_{eff}\cos(\theta_s)}{\lambda}(\theta_t - \theta_s) \ .$$

(4.13)

The error in the ME70 angle conversion factor, $\lambda/[2\pi d_{eff}\cos(\theta_s)]$, increases with increasing off-axis angle and beam steering angle (Figure 4.5).
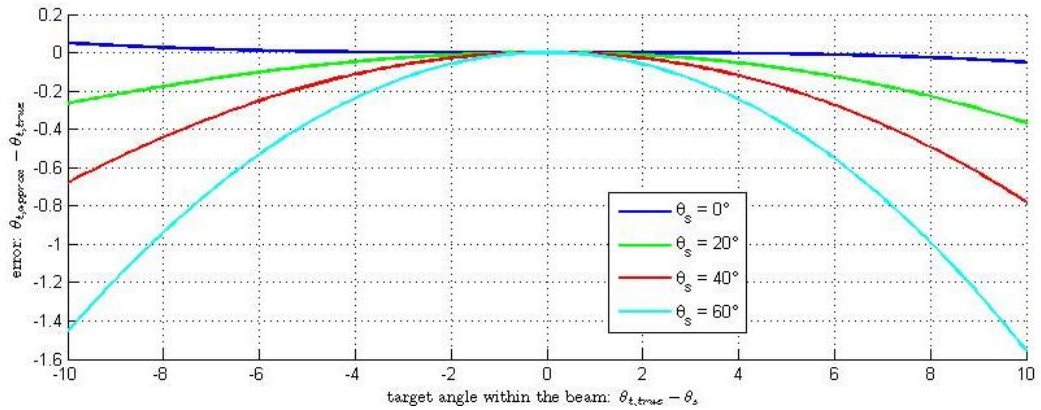
Figure 4.5. Differences between the target angles, θ_t, calculated from Equation (4.13) and the true target angles, relative to the beam axis.

The correct off-axis angle, $\theta_{t\ \mathrm{corr}}$, can be obtained using:

$$\theta_{t\ \mathrm{corr}} = \sin^{-1}[\cos(\theta_s)(\theta_t - \theta_s) + \sin(\theta_s)] .$$

(4.14)

To compute $\theta_{t\ \mathrm{corr}}$ from an electrical angle in units of phase steps, as from the ME70 .raw CON0 datagram, use:

$$\theta_{t\ \mathrm{corr}} = \sin^{-1}\left[\frac{\cos(\theta_s)}{\Lambda}\frac{\pi}{128}\varphi_{step} + \sin(\theta_s)\right],$$

(4.15)

where φ_{step} ranges from –127 to 128 phase steps, and the angle sensitivity, $\Lambda = 180/(0.75\theta_{-3\,\mathrm{dB}})$, is from the ME70 .raw file for each beam, in alongships or athwartships plane. In this case, $\theta_{-3\,\mathrm{dB}}$ is the –3 dB one-way beamwidth.

4.2.2.3 Beam axes

The ME70 beams are steered through classical beamforming. The signal phases for each of the transducer elements are aligned to transmit and receive coherently in the steered direction. For steered beams, the beam axis, the axis of maximum sensitivity, differs from the steering angle, the axis of zero phase.

The beam directivity pattern, $b(\alpha, \beta)$, results from the product of the single-element directivity pattern, $b_{\mathrm{el}}(\alpha, \beta)$, and the beamformed-array directivity pattern, $b_{\mathrm{array}}(\alpha, \beta)$:

$$b(\alpha, \beta) = b_{\mathrm{el}}(\alpha, \beta)\,b_{\mathrm{array}}(\alpha, \beta) .$$

(4.16)

For small steering angles, $b_{\mathrm{el}}(\alpha, \beta)$ is much broader than $b_{\mathrm{array}}(\alpha, \beta)$, and effectively constant within $b_{\mathrm{array}}(\alpha, \beta)$. Therefore, the shape of $b(\alpha, \beta)$ closely approximates $b_{\mathrm{array}}(\alpha, \beta)$, which is maximum for the steering angle. For large steering angles, however, $b_{\mathrm{el}}(\alpha, \beta)$ decreases rapidly enough to make the maximum $b(\alpha, \beta)$ shift towards the maximum $b_{\mathrm{el}}(\alpha, \beta)$. This effect is taken into account in the directivity-pattern models used in the ME70 *TS* computations and in the directivity-pattern models implemented in Calibration.exe V. 1.2.5.

4.2.2.4 Motion compensation

ME70 steering angles may be compensated for vessel pitch and roll angles to optimize the accuracies of the range and bearing measurements. However, this motion compensation reduces the accuracies of the calibrated measurements of target strength, TS (dB re 1 m²) and volume backscattering strength, S_v (dB re 1 m² m⁻³) (Figure 4.6). When the steering angles are compensated for motion, $b(\alpha, \beta)$ and, therefore, G_0 change. To a first-order approximation, the beamwidths change by:

$$\alpha_{-3\,\text{dB}} = \frac{\cos(\alpha + pitch)}{\cos(\alpha)}, \text{ and}$$

(4.17a)

$$\beta_{-3\,\text{dB}} = \frac{\cos(\beta + roll)}{\cos(\beta)},$$

(4.17b)

and both the on-axis directivity and the gain value change by the following factor:

$$\frac{b(\alpha + pitch, \beta + roll)}{b(\alpha, \beta)}.$$

(4.18)

Although these effects are negligible for small steering angles, motion compensation should not be used during calibration and for subsequent measures of TS and S_v. If motion compensation is used, then account should be made for the additional uncertainty in the measurements made in the most steered beams.
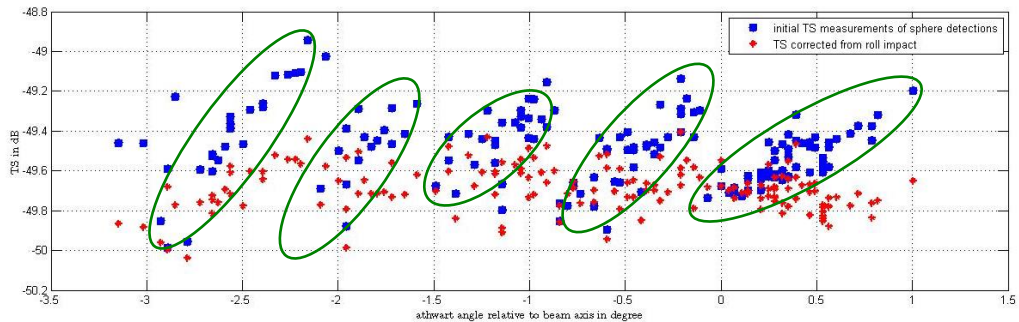

Figure 4.6. Example effect of roll correction (up to 1°) on the TS measurements of a sphere in a beam steered 57°. Biased detections are shown for five nominal sphere positions (blue). Overlaid are the measured TS with athwartships angles corrected using Equation (4.18) (red).

4.2.3   Calibration

The ME70 software includes a programme to calibrate configurations for measuring TS and S_v. The ME70 calibration utility is largely derived from the EK60 Calibration.exe utility. Therefore, it is assumed that readers of this section are familiar with EK60 calibration theory and procedures (see Chapters 1–3 and Section 4.1) and the ME70 manual (Simrad, 2012). The ME70 also includes some diagnostic utilities that should be run before a sphere calibration.

4.2.3.1 Diagnostics

In the ME70, 25 TRX32 cards control the signal transmission and reception on the 800 transducer elements (Figure 4.7). The ME70 software includes (i) BITE to test the function of each TRX32 card and each element and (ii) another utility to measure ambient acoustic noise within the bandwidths of the receivers.
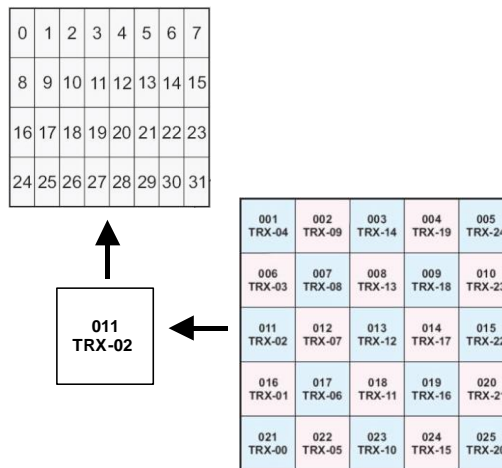
Figure 4.7. Each of 25 TRX32 cards, numbered 0–24 in the 5 x 5 matrix, control 32 of the 800 transducer elements.

4.2.3.1.1 BITE test

The BITE test identifies and disables any dysfunctional elements. The test should be run before a sphere calibration because disabled elements or other system malfunction may affect the calibration results.

1) In the "SetUp" menu, select "BITE".

The "B-Scan" tab presents the signal amplitude vs. time for the 800 transducer elements. Amplitudes during transmission are red and those during reception are blue.

2) To start the measurement, in the "Mode" field select "Element amplitude".
3) To freeze the display, toggle "None/Freeze".
4) To set the first and last samples to be displayed, fill the "Start Sample" and "Sample Range" fields. Using the 62.5 kHz sampling rate, the sample index can be interpreted as sample range (Table 4.8).

Table 4.8. Conversion of sample index to range.

Sample index	0	100	200	300	500	1 000	5 000
Range (m)	0	1.2	2.4	3.6	6	12	60

5) In the "Decimation Method" field, select "Single".
6) In the "Scale" field, select "Automatic". If necessary, in the "Sample pixel size" field, change the (default) "Width" (1) and "Height" (6) values.

   The "Matrix" tab presents the average amplitude of each element. If the averaging period includes a transmit pulse, the Matrix displays the beam-forming amplitudes applied to each element.

7) To start the measurement, in the "Mode" field select "Element amplitude".
8) To freeze the display, select "None/Freeze".
9) To set the first and last samples of the analysis period, fill the "Start Averaging" and "Averaging Range" fields. Values for analysing either the transmission or reception can be determined from the y-axis of the B-scan view.
10) In the "Scale" field, select "Manual" mode and set "Minimum" to 35 dB and "Maximum" to 45 dB.

11) In the "Element size in pixel" field, set the "Width" and "Height" to have a 1:2 proportion (e.g. 12 and 24, respectively) matching the aspect of the transducer (i.e. 7.5 mm athwartships and 15 mm alongships).

12) In the "Transmit pulse" field, select "Current".

Malfunctioning elements have weak, strong, or unstable levels during transmission, reception, or both (Figure 4.8). A large number of contiguous malfunctioning elements may be due to a faulty cable or power supply. However, element malfunctions are most often caused by a faulty TRX32 card. This does not necessarily mean that the card needs to be replaced. Malfunctioning elements can be disabled. This will affect the instrument performance and the calibration results, but the magnitude of the affect depends on the positions of the malfunctioning or disabled elements in the matrix. Elements near the centre of the array have a larger affect.
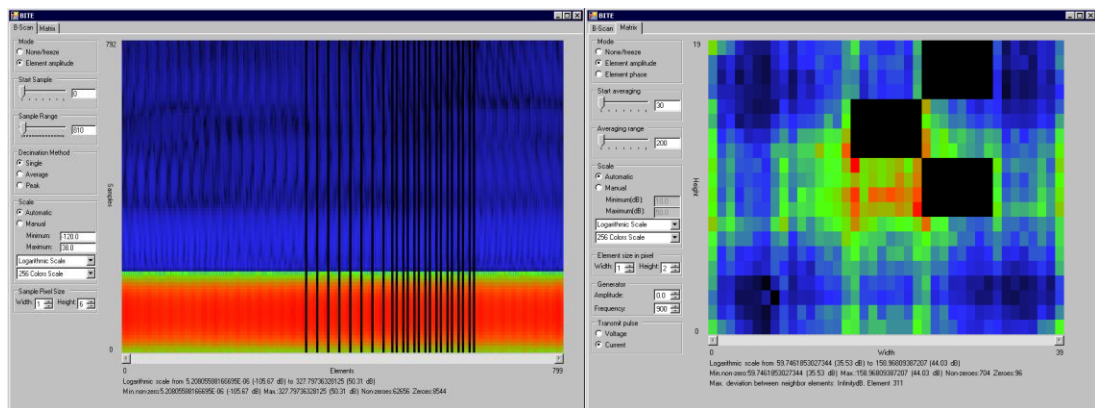

Figure. 4.8a. Matrix view during a reception period showing six disabled elements (black) and one defective, high-intensity element (red).

Figure. 4.8b. Matrix view during a transmission period showing three disabled elements (black) and one defective, high-intensity element (green amidst blue).
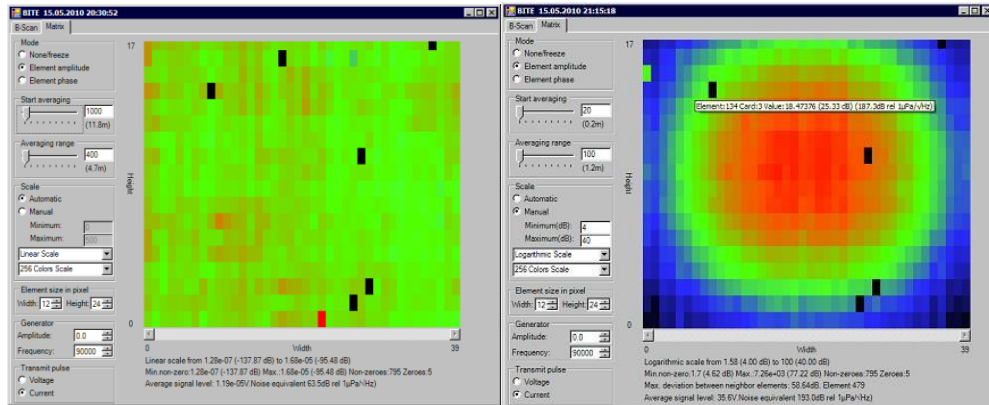
Figure. 4.8c. B-scan and Matrix views that are indicative of an unsynchronized or defective TRX32 card.

4.2.3.1.2 Noise test

The ME70 software includes a utility to measure noise. It tests that the electronic noise on the receiving boards conforms to the specification and helps to ensure that the system is running properly. Run the "Passive Test/Noise Level Determination" before calibrating the system.

1) Set "Range" to 300 m.
2) Set "Tx Mode" to Passive.
3) Position the cursor over the echogram for the most vertical beam and click the left mouse button to make this view active.
4) In the menu, open the "Extras" tab and read the noise value in dB ref 1W.

When the vessel is stopped and all other acoustic equipment is inactive, the noise estimate should be ≤ –145 dB re 1W.

4.2.3.2 Sphere

The ME70 should be calibrated using a 25-mm-diameter sphere made from tungsten carbide with 6% cobalt. A weight should be suspended at least two pulse lengths beneath the sphere to stabilize its position within the beam. Note that the apparent separation between the sphere and the weight decreases for measurements made in the most steered beams.

If fish or current are complicating the calibration, the calibration may be accomplished using both a 75- and an 84-mm diameter WC sphere. However, in that case, it is necessary to merge the results from the two calibrations. A Matlab script (concatenate_cal.m) is available that combines the measurements made with two spheres into one calibration data file.

4.2.3.3 Environment

The ME70 software has inputs for the water sound speed, c_w (m s^{-1}), at the transducer and throughout the sample range. The c_w at the transducer is used for beamforming. Measure the harmonic mean c_w for the sample range and input it to the ME70 software for estimating the range to each sample. If hydrographic conditions change significantly during the calibration procedure (e.g. indicated by a large tidal amplitude), the c_w measurements should be repeated during the calibration, and a revised harmonic mean c_w should again be input to the ME70 software.

The theoretical sphere target strength, TS_{theory} (dB re 1 m²) depends on c_w at the depth of the sphere. The TS_{theory}, specified in the ME70 calibration software, has been computed by Simrad for c_w = 1490 m s⁻¹. Generally, c_w will be a different value, and the calibration parameters must be adjusted accordingly. A Matlab script (compute_ME70_TS_Sphere_calibration.m) is [available] to generate TS_{theory} files for different values of c_w.

4.2.3.4 Sphere movement

When calibrating each beam, the sphere should always be in the transducer far-field. For vertical beams, the sphere range will equal the sphere depth minus the transducer depth. For steered beams, the sphere depth may be reduced while maintaining the far-field requirement.

Depending on the ease of obtaining sphere-echo detections in the most steered beams, either:

- Calibrate one of the most steered beams and then calibrate the others, moving sequentially from one side of the swath to the other; or

- Calibrate the most vertical beam and then calibrate the others on one side of the swath, moving sequentially to the most steered beam. Return the sphere to the most vertical beam and then calibrate the beams on the other side of the swath, moving sequentially to the most steered beam.

In either case, if the sphere range changes, adjust the minimum and maximum depth of the detection window.

4.2.3.5 Software

The ME70 software includes a calibration utility.

1) In the "C:\Program Files\Simrad\SMS\ME70\CalibrationReports" directory, create a subdirectory (e.g. named YYYYMMDD_SURVEY_CAL SITE) where the report will be saved.

2) In the "Setup\Install\Environment" tabs, input the water sound speed at the target depth in the "Water Column" tab; and input the water sound speed at the transducer face in the "Transducer Face" tab. Alternatively, input a sound speed profile.

3) In the "Operation\View Beam mode\Fan of Beams" tab, check that all of the beams are split beams.

4) In the "Operation\View Beam mode\Calibration" tab, check that calibration has been set to "Nominal Performance".

5) In the "Setup\Data output" menu, select "Record File". In the proposed data record directory, create a subdirectory with a descriptive name for the calibration raw data. These data may be used to later replay the calibration. Set an explicit "File Name Prefix" in the "Raw Data" tab, including, for example, the name of the configuration to be calibrated. Set the acquisition "Range".

6) Move the sphere in the central beam at the required depth and note the minimum and maximum depth of the desired detection window. This will be used later to set the "File/Setup" window parameters.

7) Start the calibration utility by selecting "Calibration" in the "Setup" menu.

8) In the "File/Setup" menu of the "Calibration" Display, set the following parameters:

- "Name" selects the calibration sphere used.
- "Max. Deviation" defines, for *TS* data collection, the maximum allowable difference between the measured and the theoretical *TS*. Default = "10 dB".
- "Target Depth Limits, Upper" sets the upper limit for *TS* data collection. All detections at smaller depths will be ignored.
- "Target Depth Limits, Lower" sets the lower limit for *TS* data collection. All detections at larger depths will be ignored.
- Click "OK".

The "Single Target Detection" window is available during calibration. To minimize erroneous targets (e.g. the weight beneath the sphere), the "Upper and Lower Target Depth Limits" should be frequently adjusted according to the sphere depth.

9) In the "File/Set-*TS* Detection" menu of the calibration display, set the following parameters:

- "Min. Threshold". The minimum *TS* detected. Typically set to the minimum theoretical sphere *TS* minus 8 dB. Lowering this parameter too much will decrease the detection performance.
- "Min. Echo Length". The minimum normalized echo length (duration of the echo pulse measured –3 dB relative to the peak divided by the duration of the transmitted pulse) to detect a target. Typically set to 0.8.
- "Max. Echo Length". The maximum normalized echo length to detect a target. Typically set to 1.8.
- "Max. phase deviation". The maximum standard deviation of split-beam phase sample in the echo pulse to detect a target. Typically set to 8.
- "Max. gain Comp". The maximum one-way beam-pattern compensation to detect a target. This parameter limits the maximum off-axis angle to which targets are detected. Typically set to 3 dB to allow target detections within the –3 dB one-way beamwidths. If the signal-to-noise ratio is high, then set to 6 dB to allow detections within the –6 dB one-way beamwidths.
- "Min. echo spacing". The minimum number of samples between echo pulses to detect a target. Typically set to 1.
- Click "OK".

Concurrently display both the sounder and calibration windows to observe the swath during the entire calibration procedure.

10) In the calibration display, select the "Result" tab.

11) In the calibration menu, begin the calibration by clicking "Start". Move the sphere to obtain approximately 100 measurements distributed throughout each beam, particularly in the athwartships plane.

To reduce variability in the sphere-*TS* measurements and post-processing time, stop the collection of calibration data during noisy periods (e.g. echoes from bubbles or animals).

13) In the display, locate and set the "Upper Depth" and "Lower Depth" ranges. Update these ranges when the sphere detections too closely approach these detection-range limits.

A Matlab script (clean_up_cal.m) is <u>available</u> to filter the sphere detections. To use this script, note the start and end times when the sphere is in each beam. The script will filter detections outside these periods and thereby save post-processing time.

14) When the data acquisition is complete, click the "Stop" button in the calibration menu and analyse the detection results for each beam.

In the "Result" tab, identify beam models with standard deviation values above 0.4 dB.

In the calibration "Fan View", select the beam to be analyzed.

Select the "TS-Data" tab to observe information about the target detections including detection "Number, Time, Depth" (= transducer depth + range from transducer to sphere), "TS-Comp" (target strength), "TS-UnComp" (target strength plus twice the directivity pattern), "Along[ships]" and "Athwart[ships]" beam angles (target position in the beam), and "s_a" (integrated volume backscattering coefficient for the target). Locate the invalid data through the sorting tools available for each column. For example, sort the data by "TS-Comp" or "Depth" values. The red and blue lines indicate the highest and lowest "TS-Comp" values, respectively.

Filter the invalid detections with the "Suspend" tool. The red and blue lines are refreshed.

15) In the "File" menu of the calibration display, select "Save as" to save the calibration data.

In the "C:\Program Files\Simrad\SMS\ME70\CalibrationReports" directory, select the directory in which to save the data. Click "OK".

Name the file with the current time. "Indicated name" will be automatically augmented to read "IndicatedName_ConfigurationName_Date."

In the "Description" field, indicate the calibration area and seabed depth; sphere material, size, and identification; weather conditions; post-processing detail; and any other relevant information. Click "OK".

16) If invalid detections have been removed (e.g. echoes from fish or the weight) answer "Yes" to "Do You want to save the calibration to the current beam configuration?" Otherwise, if more filtering is required, answer "No" and perhaps use the Matlab script (see Step 13) to filter invalid detections.

17) Answer "Yes" or "No" to the option for generating a calibration report (PDF format).

18) In the "File" menu, click "Exit" to quit the calibration utility.

19) In the "Operation/View Beam Configuration/Calibration" tab, check that the calibration gains have been updated.

4.2.3.6 Analysis

If there are additional invalid detections to be removed, post-process the calibration file. To do so, in the "File" menu of the calibration display, select "Replay XML" and select the recorded calibration report (Step 15). In the calibration display, click "Start" and follow the previously described procedure starting at Step 11. Pay attention to the target depth limits indicated in the "File/Setup" menu. It filters the target detections when clicking "Start".

If the target detection settings must be refined (e.g. *TS* values or depth limits), replay the raw data files and reprocess the entire calibration starting at Step 7.

4.2.3.7 Documentation

Save the calibration report (.xml format) that is located in the "C:\Program Files\Simrad\SMS\ME70\CalibrationReports" subdirectory. It allows filtering of the target detections off-line, if needed, and contains the following calibration information:

- sounder configuration parameters (e.g. number of beams, frequencies, powers, beamwidths, steering angles);
- sphere type(s);
- target detections for each beam, with their range, compensated and un-compensated TS, angles within the beam, and selected or suspended status; and
- calibration results (e.g. ΔG_0 and $\Delta S_{a\,corr}$ for each beam and measurement standard deviations)

Save the sample power and split-beam angle data (.raw format) acquired during calibration. These files may be replayed, e.g. with different target detection parameters, to redo the analysis, if necessary.

In addition to the acoustic data collected during calibration and the resulting values for G_0, and $S_{a\,corr}$, archive the following information:

- c_w values or profile(s);
- area name and geographic coordinates;
- weather conditions;
- configuration filename;
- sphere identification(s);
- TS_{theory} for each beam frequency;
- BITE test screenshots, particularly the Matrix view during transmission phase; and
- indices of disabled transducer elements.

Summarize the calibration results in spreadsheet (e.g. Table 4.9) to archive, compare with the results from previous calibrations, and evaluate any changes in the system performance. For example, plot ΔG_0 and $\Delta S_{a\,corr}$ vs. beam steering angle for successive calibrations of the same configuration.

Table 4.9. Example of calibration compilation results.

Date									
Vessel									
Configuration name									
Calibration area									
Weather condition									
Sphere type									
c_w at transducer									
c_w at sphere									
Disabled elements									
Comments:									
Beam number	1	2	3	4	5	6	7	8	9
f (Hz)									
Steering Angle									

TS_{theory}	
No. of detections	
TS std. dev.	
$G_{0\text{ nom}}$ (dB re 1)	
ΔG_0 (dB re 1)	
$G_{0\text{ nom}} + \Delta G_0$	
$\Delta S_{a\text{ corr}}$ (dB re 1)	
Previous ΔG_0	

5 Emerging protocols

5.1 Multibeam echosounders

A multibeam echosounder that is designed principally to collect bathymetry data is often called a "hydrographic" (Lurton, 2010) multibeam echosounder. Hydrographic multibeam echosounders inherently measure backscatter intensity while generating depth measurements, and most modern systems allow some or all of these echo intensities to be recorded. These backscatter intensities can coincide with the seabed or with objects in the water column. They can be used to estimate s_s, σ_{bs}, s_v, or s_a of fish, provided that some level of intensity calibration is ensured. The capability of hydrographic multibeams for recording backscatter intensity has improved as users increase demand for these data for a variety of purposes (see Brown and Blondel, 2009; Colbo *et al.*, 2014). Meanwhile, fishery multibeam echosounders have emerged that are designed principally to collect backscatter intensity data, but can also collect bathymetry data (see Section 4.2). Currently, both hydrographic and fishery multibeam echosounders are used to investigate fish and their seabed environments.

5.1.1 Requirements

The utility of data from either class of multibeam echosounder is increased if the instrument is calibrated to some level.

5.1.1.1 Level 1

Foremost, a multibeam echosounder must clearly image the surveyed seabed, with account for specular reflection at normal incidence and decreasing intensity with increasing grazing angle. The echo-intensity data should be compensated for the effects of transmit power and pulse duration, beam-directivity patterns, and gains. The first level of calibration uses nominal values based on the system design and specifications.

5.1.1.2 Level 2

A multibeam echosounder may also be used to measure variations in seabed reflectivities on various spatial scales. The second level of calibration must ensure that the system performance is stable vs. time (i.e. within and between survey periods) and the survey environment, e.g. water temperature and depth (Beamiss *et al.*, 2002). The stability of the multibeam echosounder performance must be systematically and periodically evaluated relative to the same reflector (e.g. a reference area of seabed; see Section 5.1.4).

5.1.1.3 Level 3

The highest level of system calibration ensures that the stability and accuracy of the backscatter intensity measurements is sufficient to compare data collected with other calibrated echosounders and to invert volume- or seabed-backscatter models to estimate physical properties. In this case, the performance stability of the multibeam echosounder must be systematically and periodically evaluated relative to a target chosen for its well characterized and stable backscatter, e.g. a sphere (see Chapter 2).

5.1.2 Measurements

Crude measurements of bathymetry (i.e. range from the transducer to the seabed) only require an estimate of the mean sound speed of water between the transducer and the seabed. This value is used to convert the two-way sound-propagation time to an estimate of the range to the seabed from the transducer. Measurements of bathymetry for

hydrography account for (i) the geographic position and time from a GPS receiver, (ii) sound speed vs. depth from a sound speed or conductivity-temperature-depth (CTD) probe, (iii) sound refraction (important if not projecting vertically), (iv) transducer movement (e.g. roll, pitch, yaw, and heave) from an attitude sensor, and (v) installation geometry of the transducer and ancillary sensors. The offset distances between the transducer and ancillary sensors, and the roll, pitch, and yaw biases, are estimated using a "patch test." This involves transects over flat areas and areas with a known feature, such as a slope or object on the seabed (e.g. pipeline or solid block). The accuracy of the bathymetric measurements is estimated from a model that combines the systematic error estimated for each measurement component.

Many multibeam echosounders also record backscatter intensity. Although measurements of bathymetry and uncalibrated measures of backscatter intensity are often used to classify seabed, those classifications are only comparable to measurements made at similar ranges with the same system and settings (e.g. beamwidth, gain, and transmit frequency, power, and pulse duration) (ICES, 2007). Therefore, it is important to calibrate multibeam echosounders to a high level if they will be used to measure surface backscattering coefficient, s_s (m^2 m^{-2}), or volume backscattering coefficient, s_v (m^2 m^{-3}), or both (Cutter et al., 2010), enabling comparisons of measurements with empirical or theoretical models for backscatter from fish (Foote, 1991b) or the seabed (Jackson and Richardson, 2007).

A high-level instrument calibration confirms that the multibeam echosounder is functioning properly and the data are accurate. Accurate seabed backscatter data may be used to estimate seabed slope, roughness, rock or sediment type, grain size, density, and porosity (Cutter and Demer, 2014) and improve statistical seabed classifications (ICES, 2007) that are comparable among sonars and over time. However, instrument calibration does not validate the seabed classifications.

5.1.3   System performance

With the receiver and transducer decoupled, reference voltages may be input to each receiver channel to check its response and sensitivity. Electrical impedance or admittance of each transducer element in both the transmit and receive arrays can also be measured vs. frequency. These tests may also measure the electrical impedance or admittance of transducer elements vs. frequency. The test results may identify failing receivers or transducer elements, and provide measures of gain and dynamic range. Some multibeam echosounders include utilities for these tests. Although this approach may be expanded to test all of the components involved in the transmit-and-receive process, it is more prone to cumulative error than reference-target methods for measuring the system response. Nevertheless, such tests should serve to monitor the performances of system components between periodic system calibrations with a standard target.

5.1.4   Seabed reference

Selected regions of the seabed have long been used as level-2 (see Section 5.1) calibration reference targets to check the general operation of single-beam echosounders, assess the effects of the environment (Dalen and Lovik, 1981), and compare their performances between ships (Hjellvik et al., 2008). Ideally, a reference seabed would have a constant, omni-directional backscatter. To approximate these requirements, the seabed reference should be comprised of objects that (i) scatter, vs. reflect, sound; (ii) have high volume attenuation and low bioturbation; and (iii) are virtually void of infauna and

epifauna. These characteristics will minimize fluctuations in the backscatter (ICES, 2007).

The expected seabed backscatter may be estimated from geophysical parameters (e.g. grain size, roughness) and a theoretical scattering model or by measurements made with an independent calibrated system. Assuming omni-directional backscattering from a flat, homogenous region of seabed, Hellequin *et al.* (2003) estimated the directivity pattern and gain of a hydrographic multibeam.

5.1.5 Sphere calibration

Multibeam echosounders typically measure split-beam angle data in one plane (e.g. athwartships) to detect the range to the seabed, but these data may not be recorded. Therefore, to use the sphere method (Foote *et al.*, 1987) commonly used to calibrate split-beam echosounders, the position of the sphere within the beam must be measured accurately and independently. Although this constraint is the same as for single-beam echosounders, multibeam echosounders have narrow beamwidths (e.g. 0.5–2°) that require the sphere position to be adjusted and known with higher accuracy (i.e. ≤0.1°). Despite these challenges, several protocols are emerging for calibrating multibeam echosounders.

The sphere method (see Chapter 2) has been used by Melvin *et al.* (2003) and Foote *et al.* (2005) to calibrate high-frequency multibeam echosounders in a sea well or test tank. They used a spherical target because its backscatter is the same for all acoustic incidence angles and, therefore, beam-steering angles. While adjusting the sphere depth, the multibeam transducer was accurately rotated to estimate the two-way beam directivities, alongships and athwartships beam angles, and the system gains (Figure 5.1).

Figure 5.1. Schematic diagram of the Woods Hole Oceanographic Institution sea well, as configured for calibrating a Simrad SM20. The receiving elements are in the horizontal plane, with $\theta = h = 0$. The rotational axis of the transducer is in the vertical plane.

5.1.5.1 Receiver linearity

The linearity of a multibeam echosounder receiver may be evaluated by changing the system gain while observing the sphere echo at different ranges (Foote *et al.*, 2005).

Alternatively, Greenaway and Weber (2010) used a seabed reference (see Section 5.1.4) and varied the source level and receiver gain settings throughout each of their respective ranges. The pulse duration could have also been modulated. Their results included the maximum linear receiver output at each gain in relative, system-specific units, and the relationship between the source level and gain settings and their actual values.

5.1.5.2 Transducer near-field

Generally, multibeam echosounders should be calibrated with the sphere in the transducer far-field. However, the near-field for a multibeam transducer may range from 10 m for high-frequency systems to several 10s–100s of metres (e.g. 500 m for an 8-m array at 12 kHz) for low-frequency systems. Also, some multibeam echosounders use dynamic focusing, i.e. beamforming of the received signals, to operate more effectively in the near-field. Near-field focusing can make the equivalent beam angles and the system gain dependent on range. Therefore, it may be necessary to calibrate some multibeam echosounders with the sphere in the transducer near-field.

In cases when the calibration can only be calibrated in the near-field or when the instrument is used to make measurements in the near-field, or both, the near-field response should be measured. This is done by positioning the sphere on the acoustic axis and measuring its echo at discrete positions. The beamformed results are plotted against the transducer target range. The measurements are used for comparison against computations based on the transducer geometry and transmit frequency. Account should be made for any beam focusing. Confirmation of the computational results provides support for the model, which can then be used to extrapolate to different ranges.

When calibrating a bistatic multibeam, it may be necessary or advantageous to orient the arrays so that their acoustic axes intersect at the target range. This is particularly important for reducing the effects of parallax in a near-field calibration. An easy method for adjusting the relative array orientations is to place shims between the bolts and mounting plate at the far end of one of the transducer arrays.

5.1.5.3 Directivity pattern

To measure the directivity pattern, suspend the sphere at a fixed distance from the transducer at the nominal depth of the transducer. Rotate the transducer to make measurements of the sphere until the echo amplitude steadily decreases and then rises, indicating that the measurements spanned the beam to the first null. Adjust the sphere depth by a distance corresponding to ~0.1-fold the nominal transducer beamwidth and repeat the measurements. Do this until the beam is mapped between nulls in the horizontal and vertical planes. Repeat for each beam.

From the data, for each beam, locate the beam axis and measure the beamwidth. Locate the centre of the swath by plotting the peak amplitudes of all of the beams. If needed, fit a quadratic or other nonlinear function to locate the centre. Repeat the measurement near this computed centre to precisely determine the acoustic centre and estimate any offset angles. If the acoustic centre is offset significantly from the geometric centre, the measurements should be repeated to ensure their precision.

5.1.5.4 Gain

With the sphere on the beam axis, measure the echo amplitude and compute the system gain (see Chapter 2). Repeat these measurements for each beam and gain and pulse duration setting. Periodic calibrations allow the system stability to be monitored. Note, however, that calibrations in a tank do not account for any effects of the transducer

platform used to conduct a survey (e.g. baffling by the hull, gondola or fairing, and diffraction from nearby objects (Lanzoni and Weber, 2010).

To apply the sphere method to hull-mounted multibeam echosounders, a more elaborate system is needed to accurately move the sphere under the vessel at large ranges. For example, Lanzoni and Weber (2011) explored the use of a split-beam echosounder mounted adjacent to a multibeam echosounder transducer to accurately position the target within the multibeam echosounder beams. In this case, the split-beam transducer must be (i) mounted rigidly and near the multibeam echosounder without affecting the multibeam echosounder's performance and (ii) moveable such that it can be used to position the sphere with each of the multibeam echosounder beams.

5.1.6 Simrad SM20

The Simrad SM20 (formerly the SM2000) is a multibeam imaging sonar that is available in two operating frequencies, 90 and 200 kHz. The system consists of a curved transmit-and-receive array (Figure 5.2). With an optional external linear transmit array, the two arrays form a Mills Cross. The radius of the curved array is 38.4 cm for the 90-kHz system and 20 cm for the 200-kHz system. It is comprised of 80 evenly spaced rectangular elements that create 128 beams spanning 94.2 and 88.2° for the 90 and 200 kHz systems, respectively. The external transmitter is 87 cm for the 90 kHz system and 42 cm for the 200-kHz system. When using the external transmitter, both systems have nominal azimuthal-beam resolutions of 1.5°.
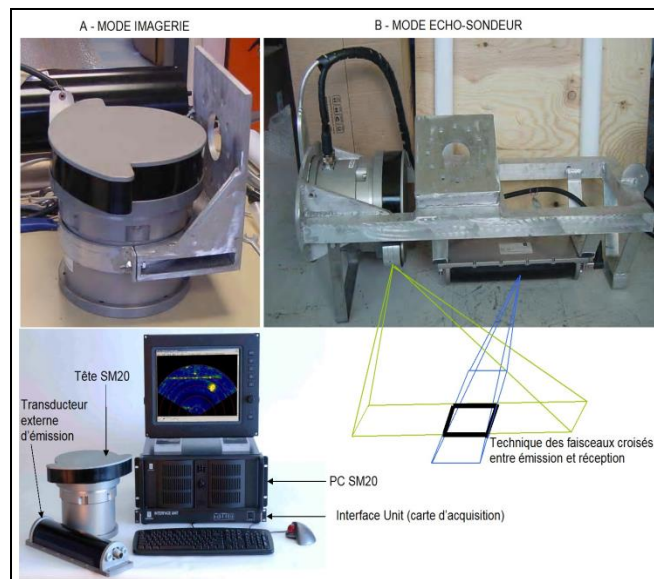
Figure 5.2. Photos of the SM20/200-kHz system. (A) Image mode (monostatic configuration). (B) Echosounder mode (bistatic configuration). (C) Sonar heads and desktop computer.

Below is a summary of the results from sphere calibrations of two SM20 systems. A 90-kHz system operating in profiling mode (bistatic) was calibrated in both the sea well on the Woods Hole Oceanographic Institution (WHOI) Iselin Dock and in a freshwater tank (Chu *et al.*, 2003). The targets were (i) 20- and 38.1-mm diameter spheres made from tungsten carbide with 6% cobalt, (ii) 23- and 60-mm diameter spheres made from copper, and (iii) a 60-mm diameter sphere made from aluminium. A 200-kHz system operating in imaging mode (monostatic) and profiling (bistatic) was calibrated by IRD

and Ifremer using a 20-mm diameter sphere made from tungsten carbide with 6% cobalt.

In the sea well, the 90-kHz SM20 system was mounted on the end of a shaft, aimed horizontally, and connected to a rotator. The rotator accuracy was ±0.1° and was controlled remotely either manually or using computer software (Matlab GUI script) (Figure 5.1). The calibration sphere, tied in a monofilament harness, was suspended from three monofilament lines controlled by motorized fishing reels in the far-field of the SM20 transducer (i.e. 23 m) at an initial depth of 3 m. During the calibration, the sphere remained in one position, and the transducer was rotated allowing all of the beams to scan the sphere. The sphere depth was then adjusted for successive scans to cover the entire width and length of the array.

The system directivity patterns are shown in the vertical plane at 23 and 11.7 m, respectively (Figure 5.3a and b), and in the horizontal plane (azimuth) at 11.7 m (Figure 5.4). The 1-D directivity patterns of the individual beams are shown in the equatorial-plane (horizontal) in Figure 5.5 and its 2-D directivity pattern (central region) is shown in Figure 5.6.
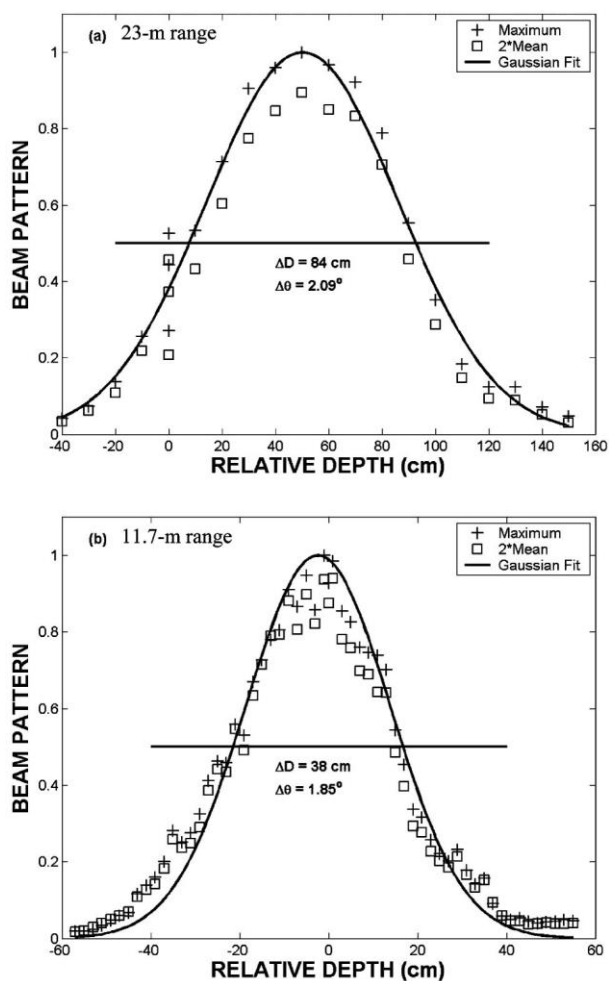
Figure 5.3. Directivity pattern of a 90-kHz SM20 multibeam transducer in the vertical plane, as determined by changing the depth of a rubber-walled focusing sphere (a) at 23-m range in 4-cm increments in a sea well; and (b) at 11.7-m range in 2-cm increments in a freshwater tank. The maximum intensity value is that observed in a spatial window consisting of five contiguous beams and five range cells centred on the respective beam and range of nominal greatest sensitivity. The mean is that of all echo values within the window. A Gaussian function is fitted to the maximum intensity values.
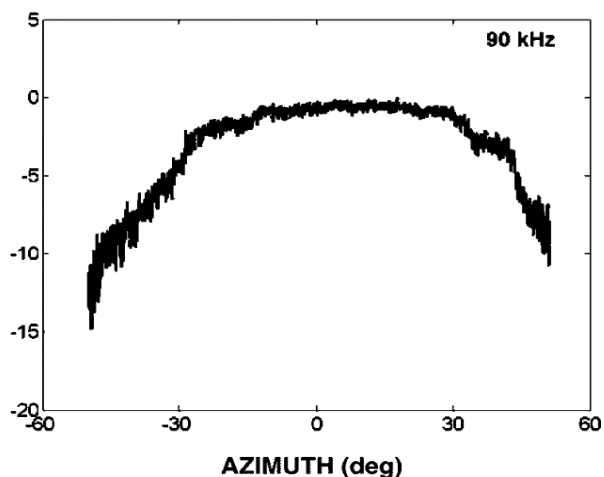
Figure 5.4. Measured equatorial-plane directivity pattern of a 90-kHz SM20 multibeam echo-sounder. The target range was 11.7 m.
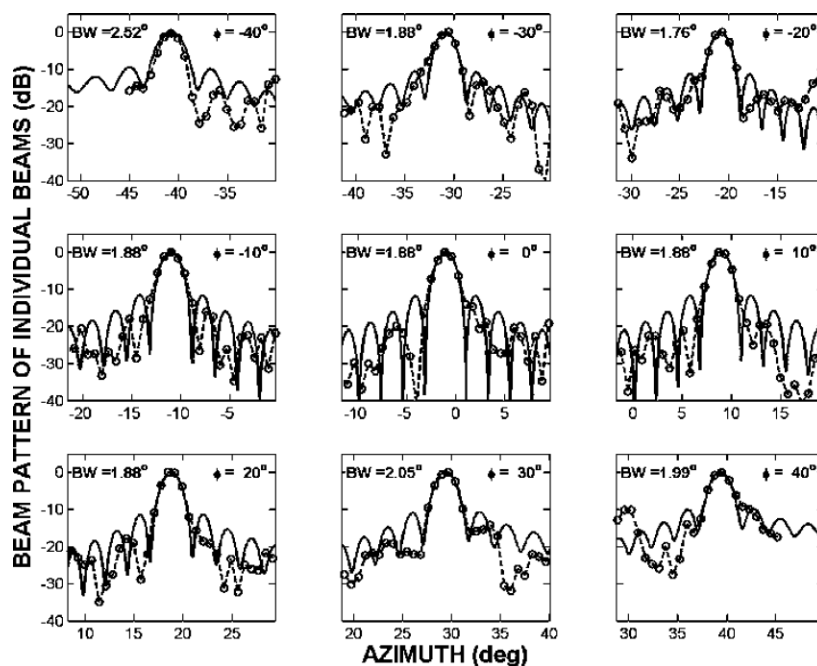
Figure 5.5. Equatorial-plane directivity patterns, measured and estimated, for a set of individual elements of a 90-kHz SM20 multibeam transducer. Measured values of the beamwidth (BW) are shown.
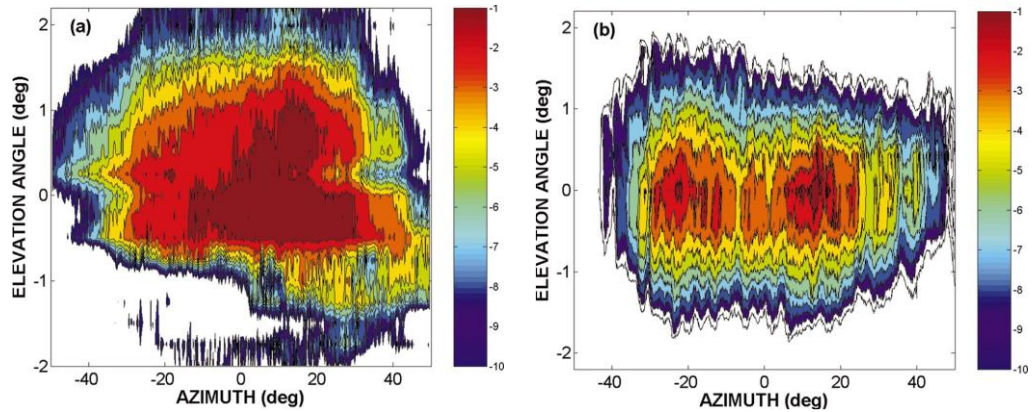
Figure 5.6. Measured 2-D directivity pattern in the central region of the beam for a 90-kHz SM20 multibeam transducer at: a) ~23-m range in the sea well; and b) ~11.7-m range in a freshwater tank. Echo levels spanning 21 to 0 dB are dark red.

The directivity patterns, horizontal (azimuth) and vertical (elevation) planes of the 200-kHz SM20 operating in imaging mode (monostatic), are shown in Figure 5.7.
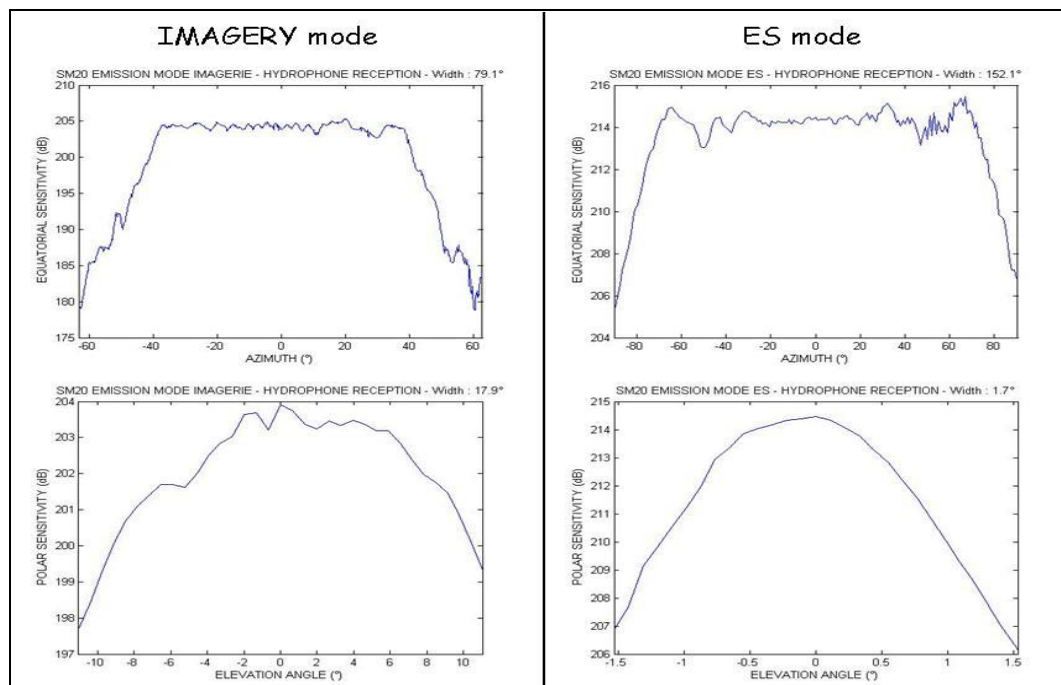
Figure 5.7. 200-kHz SM20 transmit directivity pattern and sensitivity (dB ref 1 μPa/V at 1m), measured with the hydrophone (pulse duration: 250 μs, power: high) in Imaging (left) and Echosounder modes (right).

5.2 Wide-bandwidth echosounders

Narrow-bandwidth echosounders transmit and receive finite-duration pulses of a continuous sinusoidal wave (CW) (Figure 5.8). A Fourier transform of the transmitted or

received signal indicates its frequency spectrum. Due to the pulse duration and system filters, the spectrum of a CW pulse is not entirely at the centre or carrier frequency, but is spread among the surrounding frequencies, the range of which is characterized as bandwidth (e.g. Section 2.4.4 in Simmonds and MacLennan, 2005).
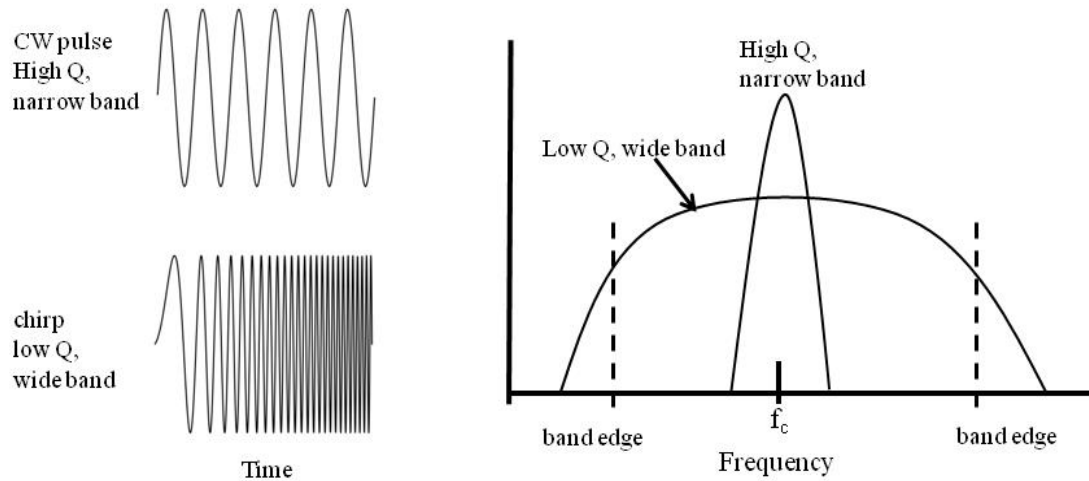
Figure 5.8. Schematic of a narrow band pulse (upper left), linear frequency modulated pulse (lower left), and the frequency responses of both (right panel). The centre frequency (f_c) and band edges are denoted.

The quality factor, Q, is defined as the ratio of the half-power bandwidth to the centre frequency. A higher Q indicates a narrower bandwidth and a lower Q indicates a broader or wider bandwidth (Figure 5.8). Referring to bandwidth, wide and broad are synonymous. Narrow and wide (or broad) refer to bandwidths that are a few percent and ≥10% of the centre frequency, respectively.

Wide-bandwidth echosounder transmit and receive finite-duration pulses of a wide-bandwidth signal. A linear frequency modulated chirp signal is commonly chosen as a transmit signal because it is simple and provides adequate resolution and bandwidth.

The wider the bandwidth, the more information is included in the backscatter spectra to potentially improve target classifications (e.g. Holliday, 1972b; Simmonds, 1990; Simmonds *et al.*, 1996; Zakharia *et al.*, 1996). A wide bandwidth also serves to improve estimations of fish sizes, speeds, and orientations (Holliday, 1974; Nero and Huster, 1996; Nero *et al.*, 1998; Stanton *et al.*, 2010). Despite their potential benefits, wide-bandwidth echosounders have not been used routinely in fishery surveys because they have not delivered sufficient power over the bandwidth to sample the requisite observation ranges. Explosives and arcers can produce high source levels with wide bandwidths, but they are dangerous and their signals are variable and unpredictable (Holliday, 1972b). Also, the receive sensitivity per frequency band is less in wide-bandwidth transducers compared to narrow-bandwidth transducers. Additionally, wide-bandwidth-system design is complicated. Nevertheless, as electronics get smaller, more powerful, and more reliable, commercial wide-bandwidth systems are being developed (Jones *et al.*, 2009). Consequently, the use of wide-bandwidth acoustic instrumentation is again receiving attention (Conti and Demer, 2003; Conti *et al.*, 2005b; Au and Benoit-Bird, 2008; Benoit-Bird *et al.*, 2008; Stanton *et al.*, 2012; Forland *et al.*, 2014).

Wide-bandwidth echosounders can be calibrated using the methods described in Chapters 2 and 4. As with narrow-band echosounders, the sphere method is recommended. Additional considerations for calibrations of wide-bandwidth echosounders

include the frequency dependence of many variables in the sonar (or radar) equations (see Chapter 1) and the sphere *TS*.

The received power, p_{er} (W), wavelength, λ (m), absorption coefficient, α_a (dB m^{-1} re 1), and equivalent two-way beam angle, ψ (sr), are all dependent on frequency. Additionally, due to the transmit signal and transducer response, the source level varies with frequency (Figure 5.9). The elements within a transducer have a natural resonance frequency, and a bandwidth over which electrical and acoustic energy can be efficiently converted. The quality factor Q of the transducer describes the shape of the frequency pass-band. Low Q transducers have wide bandwidths. Optimally, the transmitting and receiving responses are "flat" over the bandwidth such that the spectral shape of the received signal is only a function of the response of the target. Generally, however, the transducer transmitting and receiving responses are not flat and must be measured empirically and taken into account. The transducer transmitting and receiving response functions are usually measured once in controlled, high signal-to-noise ratio (*snr*) conditions (i.e., in a tank) before the transducer is mounted and then not measured again, at least not routinely, throughout the life of the transducer. For calibration and processing purposes, these response functions are input to the algorithms and used to derive the receive spectrum. Similar to narrow-band systems, the combined transmit and receive response function is often measured and used rather than using separate transmitting and receiving functions. The quality of the response functions is monitored over time by evaluating the received spectra of p_{er} from a calibration sphere. Changes in the spectral shape of p_{er} that cannot be explained by changes in the sphere, environmental factors, or other system components may be due to degradation of the transducer. In that case, the transducer should be independently evaluated.

The frequency dependence of the directivity pattern has substantial effects on off-axis measurements of σ_{bs} measurements and ψ (Lavery *et al.*, 2010a, 2010b). For a wide bandwidth transducer having a constant active area, its beamwidth is inversely proportional to frequency. For example, if the highest frequency equals twice the lowest frequency, then the beamwidth for the highest frequency will be half that for the lowest frequency.

The frequency-dependent beam patterns of split-beam transducers can be well approximated using split-beam estimates of off-axis angles, α, β (°). Using the sphere method (Chapters 2 and 4), the combined transmit-receive directivity pattern, $b(\alpha, \beta)^2$ (dimensionless), beam widths, $\alpha_{-3\,dB}$ and $\beta_{-3\,dB}$ (°), and axis offsets, α_o and β_o (°) can be estimated. To make these measurements of a single-beam transducer, it is necessary to have independent motion control of the transducer and sphere. It is possible to provide independent measures of sphere location from a concurrently operated multibeam, split beam, or lens system.

A major challenge to sphere calibrations of wide-bandwidth echosounders involves the consistency and prediction of $\sigma_{bs}(f)$ over the bandwidth of the system (Stanton and Chu, 2008). The $\sigma_{bs}(f)$ for even simple targets such as spheres have numerous resonances that are sensitive to the material properties of the target as well as the environmental conditions (see Chapters 2 and 3). These resonances are caused by the interference among the echoes from the front interface, internally refracted and reflected waves, and circumferential waves (Hickling, 1962; MacLennan, 1981).

For narrowband systems, resonances in $\sigma_{bs}(f)$ can be avoided by judicious choices of material and sizes of spheres. This may not be possible for wide-bandwidth systems. Although the sharp nulls provide well-defined features to compare the theoretical and measured spectra, their positions are sensitive to material properties of the sphere and

sound speed and density of the water. Therefore, the null positions may not be sufficiently well known to use for reliably calibrating $\sigma_{bs}(f)$ (Lavery *et al.*, 2010b; Hobaek and Forland, 2013). In addition to robust features in the sphere scattering spectra, it is advantageous to have flat or rising portions of the spectral response curve at the band edges. Such characteristics at the edges of the theoretical sphere backscattering spectra serve to better monitor the edges of the system bandwidth.

5.3   Partial-wave calibration

The sphere calibration described in Chapters 2 and 4 uses theoretical and measured values of sphere σ_{bs} derived from the entire backscattered wave. To calibrate wide-bandwidth echosounders, Stanton and Chu (2008) introduced a sphere calibration technique that uses only part of the wave backscattered from the sphere. This partial-wave σ_{bs} takes advantage of the fact that the echo from the front interface is relatively insensitive to frequency (Dragonette *et al.*, 1981) and that this component can be separated from the total echo using pulse-compression techniques (Figure 5.9) (Chu and Stanton, 1998). In practice, this calibration technique is robust and reliable, even when spheres on the order of 10s of cm in diameter are used to calibrate systems in the 1-10 kHz range (Stanton *et al.*, 2010).
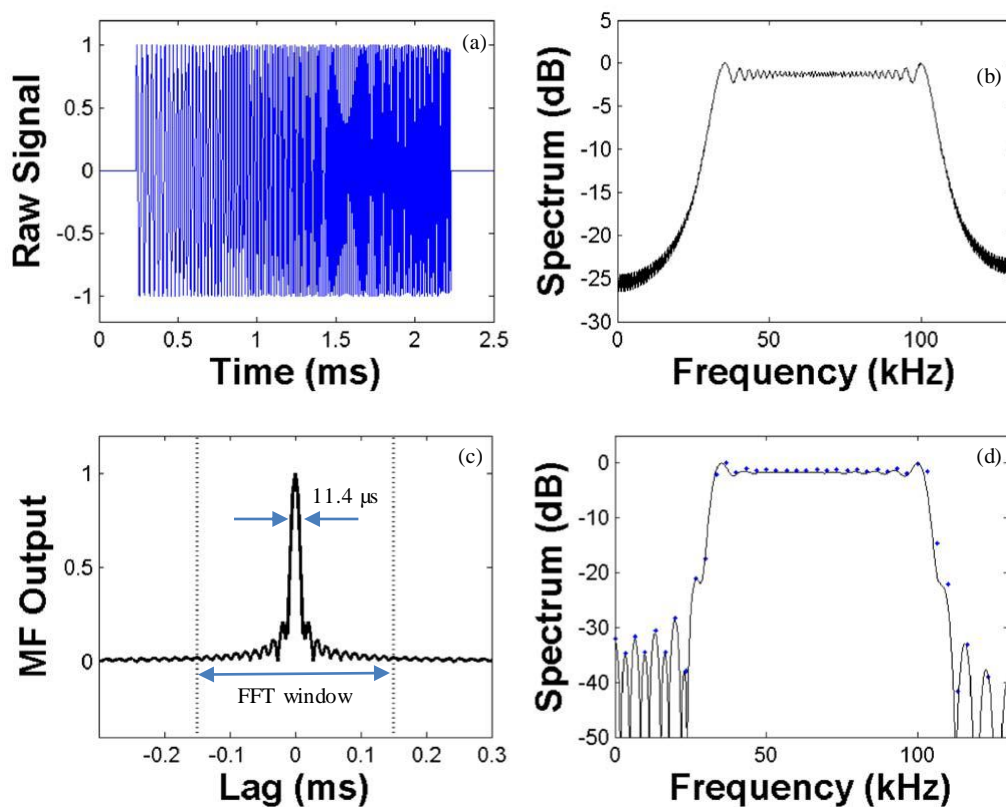
Figure 5.9. Effects of pulse-compression processing of a wide-bandwidth signal. (a) A 2-ms chirp transmit signal (raw); (b) its frequency spectrum; (c) the envelope of its pulse-compressed signal, achieved by autocorrelation or matched filtering (MF); and (d) the frequency spectrum of its pulse-compressed signal. The blue dots indicate the frequency spectrum calculated using a 300-µs-long window.

The range resolution of a narrow-band echosounder is dependent on the pulse duration, and targets must be separated by greater than half the pulse length ($c_w\tau/2$) to be resolved. For wide-bandwidth systems, range resolution is inversely proportional to bandwidth (Ehrenberg and Torkelson, 2000). With increased bandwidth, finer range

resolution is achieved through pulse compression techniques (Chu and Stanton, 1998), a form of matched filtering. For example, as a result of pulse-compression processing, a 2-ms chirp, which corresponds to a narrow-bandwidth range resolution of 1.5 m, can be compressed to a signal with a duration of about 11.4 μs (Figure 5.9) and a range resolution of about 8.6 mm. This fine range resolution can facilitate a partial-wave calibration (Stanton and Chu, 2008; Stanton *et al.*, 2010) by resolving the echoes from the front of a sphere and the latent circumferential waves. Thus, pulse-compression techniques can be used to differentiate full wave and partial wave contributions to the spectrum of backscattering as shown in Figure 5.10.
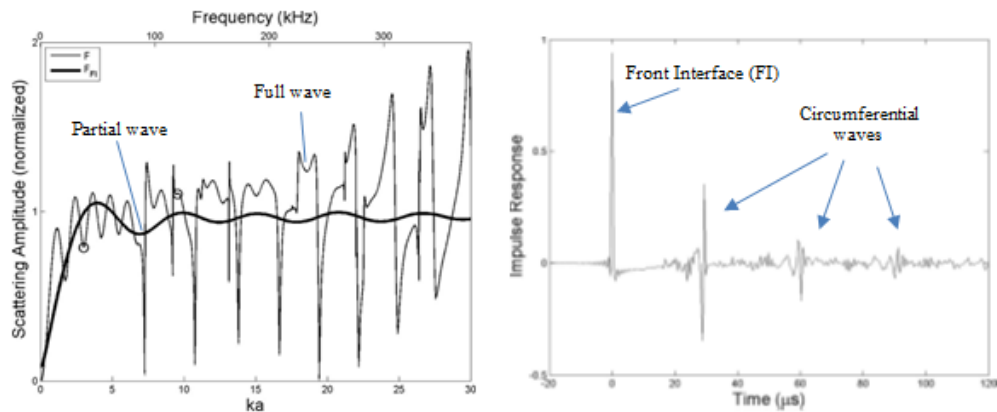
Figure 5.10. Acoustic backscatter from a 38.1-mm diameter tungsten carbide sphere. (a) The full-wave sphere-scattering amplitude (thin curve) and the partial-wave sphere-scattering amplitude for the echo from the front interface of the sphere (bold curve), each normalized by half the sphere radius. The circles indicate values at 38 and 120 kHz. (b) The impulse response of backscattering from the sphere. The impulse response of the echo from the front interface was used to define the partial wave scattering amplitude.

5.3.1.1 Example partial-wave calibration

A wide-bandwidth echosounder system housed in a towed body was calibrated in 2006 (Stanton *et al.*, 2010). During the calibration, the system, normally towed in surveys with its acoustic beams aimed downward, was suspended 10 m directly below the vessel, which was anchored. The system was tethered so that the acoustic beams were aimed in the downward direction. Several calibration spheres were used, one at a time, suspended 30 m below the towed body with a weight positioned ~10 m below the sphere. The wide-bandwidth systems did not have split-beam transducers, so single-beam calibration methods were used.

The towed body, sphere, and weight were all free to move, which fortuitously moved the sphere in the beam. Account was taken for the pitch and roll of the tow body, which caused significant variability in the echo level. The acoustic data were indexed with values of heave, pitch, and roll from a motion sensor. Echoes with pitch and roll values near 0° were assumed to be "on-axis" and were used for analysis.
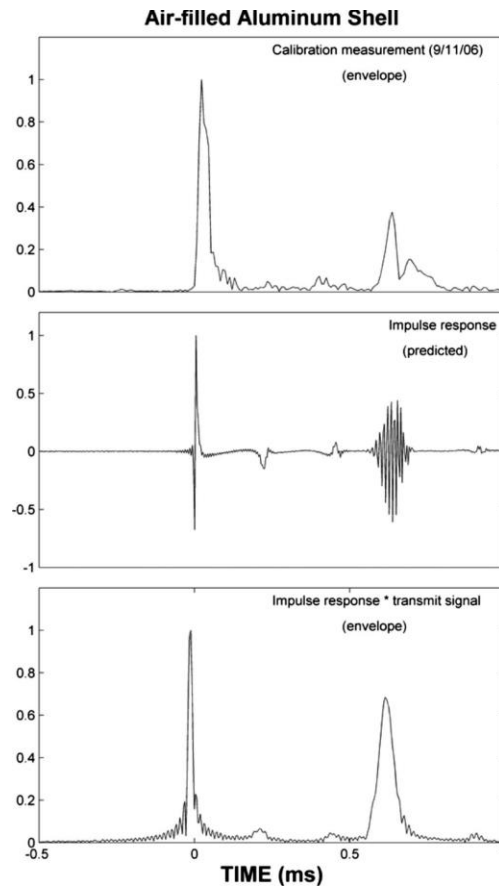
Figure 5.11. Time-domain analysis of an echo from a 41.5-cm-diameter air-filled aluminum sphere suspended 30 m below the towed-body. (Top) Envelope of the pulse-compressed echo. The echo at 0 ms is from the front interface and the smaller echo at ~0.6 ms is an echo from a circumferential wave (Lamb wave). (Middle) Fourier transform (impulse response) of the exact modal series solution for the sphere echo. (Bottom) Envelope of the impulse response convolved with the transmit signal. Each plot is normalized to unity.

The transmit signal used in the pulse-compression processing was measured from the reflection off an air–water interface. The compressed pulse resolved various features in the backscatter from the sphere (Figure 5.11). The partial-wave and full-wave backscatter signals were extracted by gating the signal in time such that the echo from the front interface (300-μs gate) and the entire sphere (3-ms gate) were resolved both temporally and spectrally. Each period was zero padded to form 4-ms time-series. For each series, the backscatter signals were obtained using an inverse Fourier transform over the appropriate bandwidth. An amplitude-weighting function was used to suppress side lobes.

The results from the two time-gates were compared (Figure 5.12a). The spectrum of the echo from the front interface is smoothly varying over the entire bandwidth. The spectrum of the entire echo (i.e., front interface and circumferential waves), is rapidly oscillating over the bandwidth. This observation is consistent with the theoretical predictions shown in Figure 5.9.

The system response of this wide-bandwidth echosounder was then determined from an analysis of the partial-wave backscatter spectra (Figure 5.12). This example shows that the partial-wave technique is less sensitive to uncertainties in sphere material properties and dimensions and may, therefore, significantly reduce the error in sphere calibration of a wide-bandwidth echosounder. Furthermore, due to the high

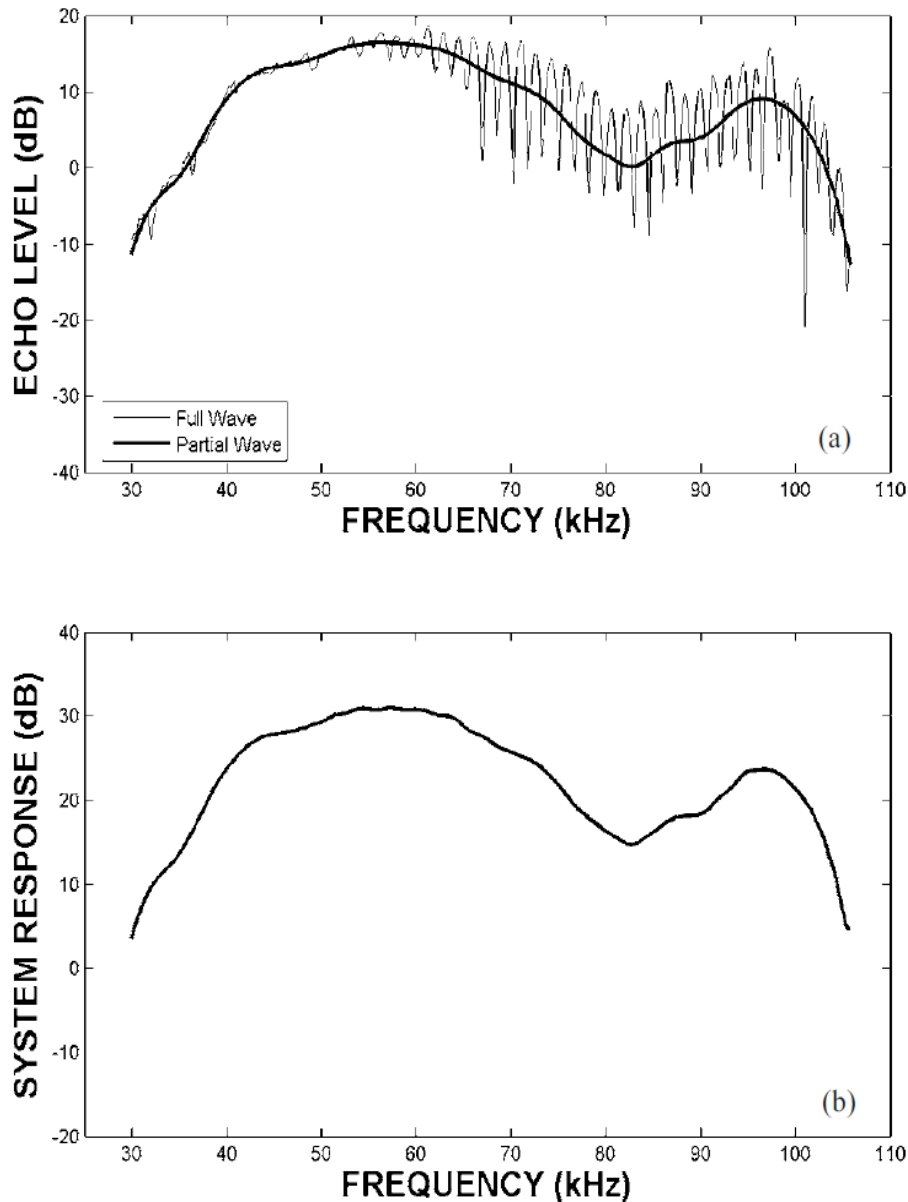range resolution provided by pulse compression, the diameter of the calibration sphere may be minimized.

Figure 5.12. Spectra of signals and system response associated with a calibration performed with an air-filled spherical shell. (Upper) Spectra of the full-wave backscatter (thin line), and the partial-wave backscatter from the front interface (thick line). The spectra were calculated using the pulse-compressed signal illustrated in the bottom panel of Figure 5.11. (Lower) System response of the wide-bandwidth transducer as derived through the partial-wave analysis.

5.4   Acoustic Doppler current profilers

Since the mid-1980s, acoustic Doppler current profilers (ADCPs) have been fitted to many research vessels (Brierley *et al.*, 1998b) and other platforms, and ADCP measurements have become an integral component of physical oceanographic studies (Woodward and Appell, 1986). Concurrently, ocean observatories have become key tools to monitor global climate change and its effects, as well as to provide indicators

of ecosystem status and trend. Therefore, it is worth considering how calibrated ADCP data may be used to complement echosounder data. Relative to data from scientific echosounders, ADCP data are generally limited by:

- larger vertical resolution;

- larger blind zones near the sea surface and seabed;

- lower receiver dynamic range;

- temperature sensitive system performance;

- multiple, non-vertical single beams; and

- difficult sphere calibrations (due to non-vertical single-beams).

Notwithstanding these limitations, ADCPs can provide measures of current velocity, and fish and zooplankton velocity (Demer *et al.*, 2000; Zedel *et al.*, 2003, 2005; Zedel and Cyr-Racine, 2009) and volume backscattering coefficient, s_v (m² m⁻³) (Brierley *et al.*, 1998a). The calibration protocol in this section is relevant to the measurements of s_v.

ADCP measurements of s_v may be validated using one of three methods:

1) Estimate the sonar-equation parameters (see Chapter 1, component calibration);
2) Compare the measurements with those from a calibrated echosounder (see Chapter 1, comparison method); or
3) Compare the measurements with biomass metrics from net samples or the output of backscatter models parameterized with animal species, sizes, and abundance estimated from net samples.

5.4.1   Component calibration

In commonly used ADCPs (e.g. Teledyne RD Instruments or RDI), volume backscattering strength, S_v (dB re 1 m² $(4\pi\,\mathrm{m}^3)^{-1}$), is calculated for data from each of four acoustic beams using the following sonar equation:

$$S_v = 10 \, \log_{10} \left(\frac{4.47 \times 10^{-20} K_2 K_s (t_w + 273) \left(10^{K_c(E-E_r)/10} - 1 \right) r^2}{c_w P K_1 10^{-\alpha_a r/5}} \right),$$

(5.1)

where t_w (°C) is the water temperature at the transducer, r (m) is the range along the beam to the scatterers, α_a (dB m⁻¹) is the absorption coefficient of water, P (m) is the transmit pulse length, c_w (m s⁻¹) is the mean sound speed between the transducer and the scatterers, K_1 (W) is the beam specific transmitted power in the water (i.e. p_{at}), E (counts) is the received acoustic intensity, E_r (counts) is the reference acoustic intensity, K_c (dB count⁻¹) is the beam specific count conversion factor (aka RSSI), K_2 (dimensionless) is the system noise constant, and K_s (dimensionless) is the frequency-specific system constant. Note that the units and terminology in Equation (5.1) are different from those in the other sections of this document. Also note that the expression for K_1 in Zhou *et al.* (1994) and Heywood (1996) was corrected in Wade and Heywood (2001) as used in Fiedler *et al.* (1998), Plimpton *et al.* (2004), Lee *et al.* (2004), and Radenac *et al.* (2010). Some of the parameters in Equation (5.1) are nominal values from the manufacturer; the others must be measured. For mobile ADCPs, the parameters in Equation (5.1) may be measured in a test tank using a calibrated transducer (Tessier, 2006; Tessier *et al.*, 2008).

To measure backscatter intensity using either a broad- (BB-ADCP) or a narrow-bandwidth ADCP (NB-ADCP), Deines (1999) proposed a "working version" of Equation (5.1),

$$S_v = C + 10 \log_{10}\big((T_x + 273.16)R^2\big) - L_{DBM} - P_{DBW} + 2\alpha_a R + K_c(E - E_r)\,,$$
$$(5.2)$$

where C accounts for the transducer efficiency, noise bandwidth, noise factor, transducer diameter, and transducer beam angle, $L_{DBM} = 10\log_{10}(P)$; and $P_{DBW} = 10\log_{10}(K_1)$. Note that (Gostiaux and van Haren, 2010) identified a typographical error in Equation A-5 in Deines (1999) and proposed a new formulation that may be less biased for measurements with low signal-to-noise ratios (snr). Table 1 in Deines (1999) provides values for C (accurate to ±3 dB), P_{DBW}, and Rayleigh distance, R_0, for multiple RDI ADCPs. A BB-ADCP provides more precise measures, 1 dB vs. 5.6 dB for both current velocity and backscatter intensity, respectively, and their performances are less sensitive to temperature than to an NB-ADCP (Deines, 1999). Irrespective of the type of ADCP used, measurements should be made in the transducer far-field (Chapter 4). The α_a values should be estimated from CTD profiles in the survey environment. The E_r value can be estimated as the counts measured at the largest recorded range, when noise dominates any remaining signal. If there is no effect of ship speed on E_r, its value may be estimated while the vessel is stationary (Brierley *et al.*, 1998b).

ADCP measurement of S_v may be more precise if the data span large spatial scales (Postel *et al.*, 2007). Variation in measured S_v may be caused by the random positions and orientations of scatterers within the insonified volume, and noise. The S_v measured with each of the four ADCP beams may be averaged to improve measurement precision of randomly oriented organisms and to reduce measurement bias for polarized targets, e.g. schooling animals (Zedel *et al.*, 2005).

5.4.2   Echosounder comparison

ADCP measurements of S_v may be compared to S_v measurements made with a calibrated echosounder and adjusted for observed differences. For example, Brierley *et al.* (1998a) recorded t_w throughout a survey and compared S_v measurements of krill made concurrently with a multifrequency (38-, 120-, and 200-kHz) scientific echosounder (Simrad EK500). They compared measurements from two krill layers, one shallow and homogeneously distributed, and the other deep and heterogeneously distributed (Figure 5.13).
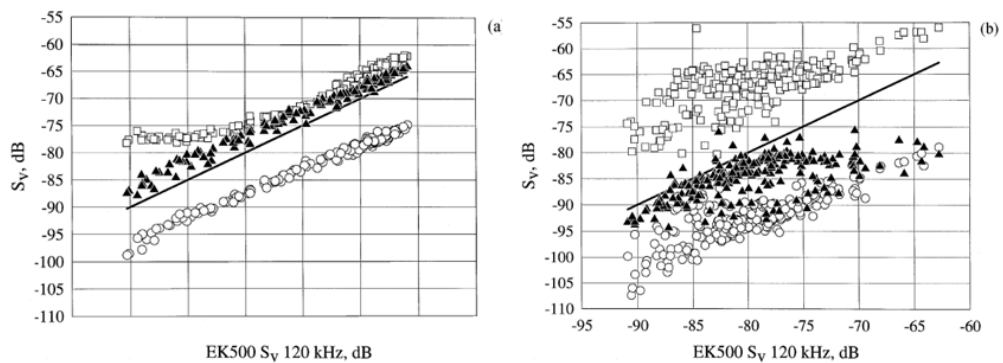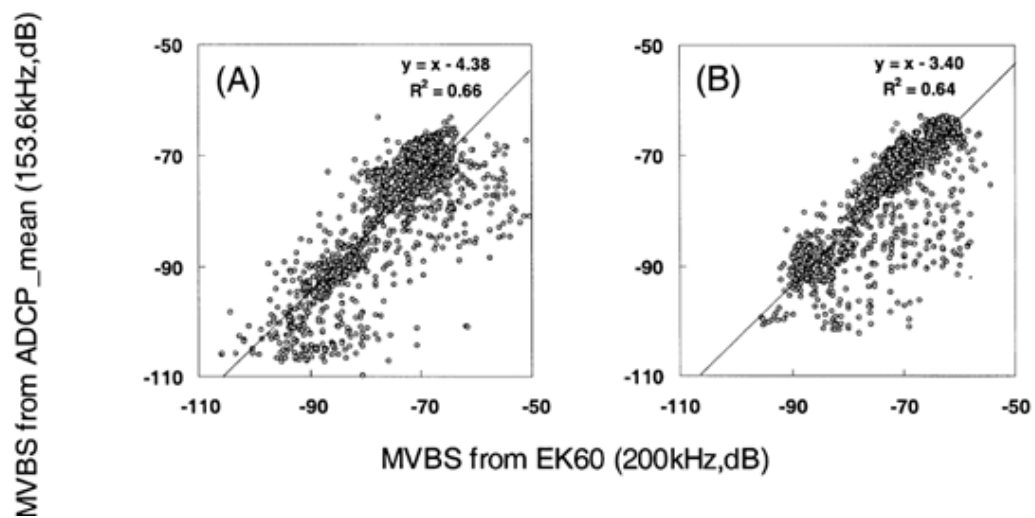

Figure 5.13. Volume backscattering strength (S_v) measurements of krill made concurrently with a 153.6-kHz narrow-bandwidth ADCP and a calibrated multi-frequency (38-, 120-, and 200-kHz) scientific echosounder (Simrad EK500). The krill were aggregated (a) shallow and homogenously distributed during night-time; and (b) deep and heterogeneously distributed during daytime. The *x*-axis labels are the same for both plots. The symbols indicate measurement at 120 kHz (solid line), ADCP (triangles), 200 kHz (squares), and 38 kHz (circles).

For the shallow layer, the measures from the two instruments were well correlated, except for S_v at 200 kHz < ~–80 dB, where the echosounder measurement were dominated by noise. For the deep layer, the correlation was degraded, perhaps due to the patchiness of the scatterers, but mostly due to saturation of the ADCP receivers at S_v > ~–77 dB. Similarly, Fiedler *et al.* (1998) compared measurement from a 150-kHz ADCP with those from a 38-kHz scientific echosounder (Simrad EK400) and found that the correlation decreased with increasing depth (i.e. r^2 = 0.83 at 25 m and 0.53 at 185 m), likely due to the decreasing snr. Lee *et al.* (2004) compared measurements of krill aggregations at various depths made concurrently with a 153.6-kHz BB-ADCP and a 200-kHz scientific echosounder (Simrad EK60) (Figure 5.14).

Figure 5.14. Mean volume backscattering strength (MVBS) measurements of krill made concurrently with a 153.6-kHz broad-bandwidth ADCP (four-beam average) and a calibrated multi-frequency (200-kHz) scientific echosounder (Simrad EK60). The measurements were made while cruising (A) away from shore during day; and (B) towards shore during night. The lines indicate least-squares fits to the data.

5.4.3   Net catch comparison

ADCP measurements of S_v have been compared to (i) metrics of plankton biomass (e.g. displacement volume, dry weight, ash free dry mass) sampled in nets or (ii) S_v estimated from models parameterized with data from net samples. For these comparisons, account must be made of the volumes sampled by the ADCP and the net.

Wade and Heywood (2001) compared S_v measured with a 153-kHz ADCP (RDI) to catches in a 200-μm mesh net and estimates of dry-weight by size fractions. The correlations were highest (r^2 = 0.76) for the largest (500–2000 μm) size fraction (Figure 5.15). Lynn (2003) compared S_v measured with a 150-kHz ADCP (RDI) to displacement volume (after removal of large gelatinous plankton) in samples from an oblique 0.505-mm-mesh bongo net (Figure 5.16).
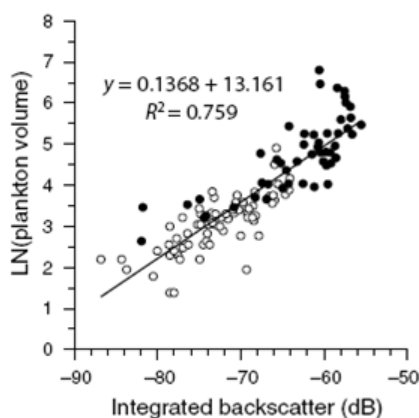
Figure 5.15. log_e (**plankton volume**) (**cm³ 1000m⁻³**) **vs. mean volume backscattering strength (MVBS; dB) measured concurrently during two cruises (filled and open circles). The least-squares-fit line is for the combined data.**
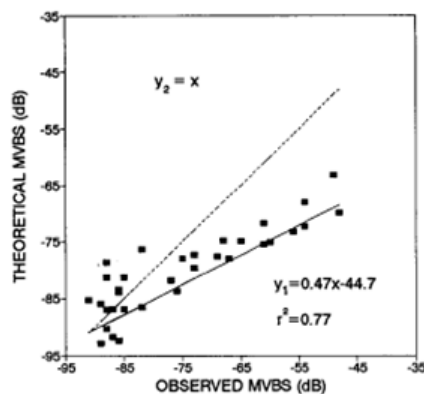

Figure 5.16. Theoretical mean volume-backscattering strength (MVBS; dB), calculated with a straight cylinder model with data on MOCNESS catches of euphausiids, and MVBS measured with an ADCP. Also shown are the ideal 1:1 relationship (dashed line) and the regression (solid line).

Postel *et al*. (2007) compared S_v measured at short ranges with two 300-kHz BB-ADCPs to ash-free dry mass measure with 55- and 200-μm plankton nets. Generally, the correlations increased with size fraction (except the largest size class with a diverse species composition) and layer density, i.e. for the highest snr (e.g. Wade and Heywood, 2001).

Takikawa *et al.* (2008) compared S_v measured with a 38-kHz BB-ADCP (RDI) dry-weight samples from a 0.33-mm-mesh net. Although nearly 90% of the dry weight was comprised of euphausiids, copepods, and appendicularians that are weak scatterers at 38 kHz, the correlation was highly significant.

Zhou *et al.* (1994) compared S_v measurements made with a 153-kHz ADCP (RDI) to S_v estimated from a straight-cylinder model parameterized using data from MOCNESS-net samples of euphausiids. They found large differences when the abundance is high (Figure 5.17), perhaps due to undersampling by the net.
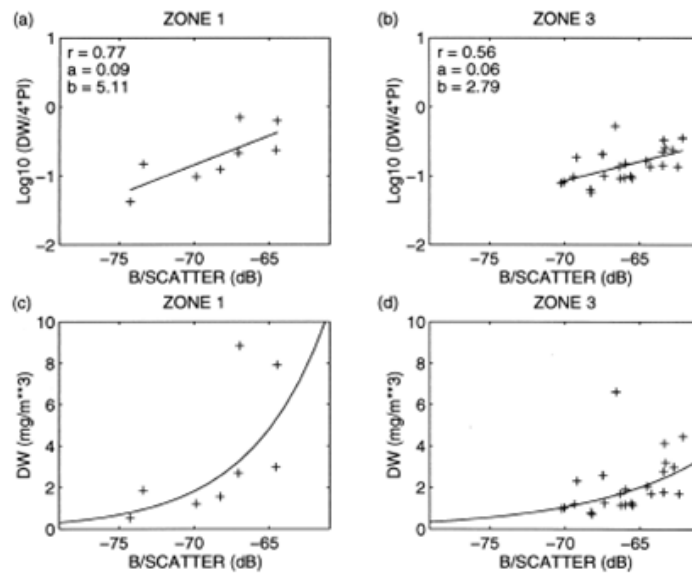
Figure 5.17. Regression fits using estimated dry-weight biomasses for two geographic zones.

Ressler (2002) compared S_v measurements made with a 153-kHz NB-ADCP to S_v estimated from scattering models for several species groups parameterized using data from MOCNESS-net samples of a variety of animals. The correlation was high for crustaceans, small fish, and fragments of non-gas-bearing siphonophores, but insignificant for gelatinous zooplankton, pteropods, atlantid molluscs, and gas-filled siphonophore floats.

Fielding *et al.* (2004), following (Flagg and Smith, 1989), compared S_v measurements made with a 153-kHz NB-ADCP to S_v estimated from scattering models for several species groups using data from 280-µm-mesh Longhurst-Hardy plankton recorder samples including amphipods, chaetognaths, copepods, euphausiids, fish, and pteropods. The correlations were better when only the most significant acoustic scatterers (amphipods, chaetognaths, copepods, euphausiids, fish, and pteropods) were considered. The species in the mixed assemblage did not contribute proportionately to the S_v, highlighting the need to account for species-specific backscatter when interpreting ADCP data (Figure 5.18).
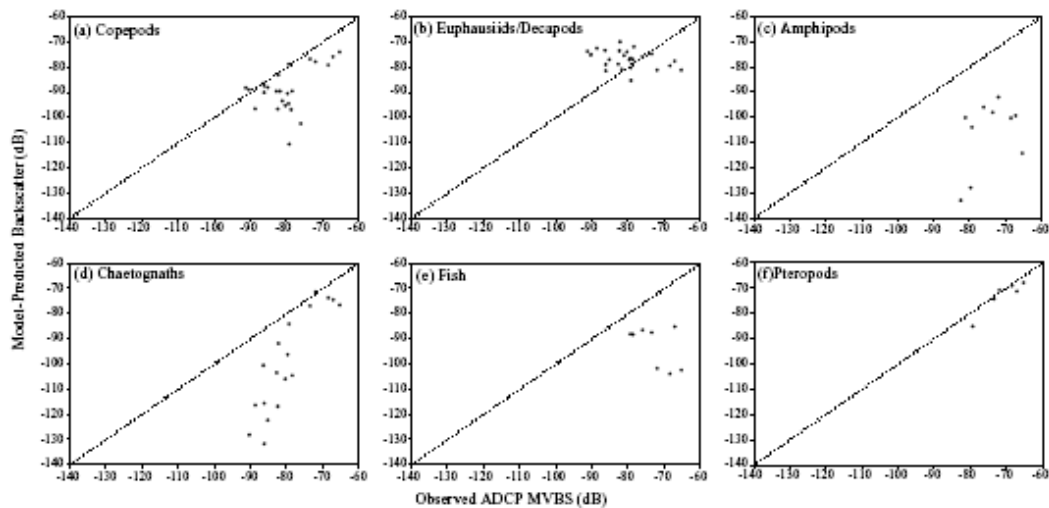
Figure 5.18. Model-predicted backscatter mean volume backscattering strength (MVBS) vs. observed MVBS for (a) copepods, (b) euphausiids and decapods, (c) amphipods, (d) chaetognaths, (e) fish, and (f) pteropods.

S_v measured with a single-frequency ADCP cannot be used for quantitative abundance estimates of mixed-species aggregations, but they may indicate the general zooplankton distribution (Flagg and Smith, 1989; Heywood *et al.*, 1991; Fielding *et al.*, 2004).

5.5 Imaging sonars

Acoustic cameras are high-frequency multibeam imaging sonars with linear transducer arrays with narrow beamwidths. During the past decade, advances in beamforming technology and miniaturization of hardware components have yielded several acoustic cameras (e.g. DIDSON, ARIS, BlueView, and Kongsberg M3) that may be used for fishery research. This section details some efforts to calibrate a Dual-frequency IDentification SONar (DIDSON).

5.5.1 DIDSON

DIDSON is a high-definition acoustic camera originally developed by the University of Washington's Applied Physics Laboratory for application to military surveillance missions. The sonar and transducer array are well described by Belcher *et al.* (2001).

The DIDSON can collect multibeam data at two frequencies, depending on the desired target range and resolution. The high frequency (1.8 MHz) mode has high azimuthal (i.e. lateral, athwartships) resolution at small ranges (<15 m). The low frequency (1.1 MHz) mode has low azimuthal resolution at large ranges (15–40 m). The high frequency mode uses 96 beams, each $\phi = 0.3°, \theta = 14°$, where ϕ is the azimuthal beamwidth and θ is the elevation beamwidth. The total field-of-view is, therefore, 29 x 14°, respectively. In low-frequency mode, each beam is $\phi = 0.4°, \theta = 14°$.

Depending on the mode and total range, data can be collected at 4–21 frames s⁻¹. Each frame is comprised of data from eight pulse sequences, each comprising 12 of the 96 beams. The data are stored as 8-bit (counts 0–255), N_{beam} x 512-pixel images, where N_{beam} is the number of beams. The total range equals the initial offset, the range from the active transducer elements to the first observation values, plus the observation "window" length. The range resolution equals the total range divided by 512 m pixel⁻¹. The value of N_{beam} defines the swath width, the lateral extent of the data.

Rather than using digital beamforming, DIDSON uses acoustic lenses to form beams. The combination of a lens array and high operating frequency offer target resolutions that approach conventional optical methods (Simmonds and MacLennan, 2005). DIDSON images have been used for remote identification of targets based on morphology, behavior, and energetics (Moursund *et al.*, 2003; Holmes *et al.*, 2006; Mueller *et al.*, 2006, 2010; Handegard *et al.*, 2009). DIDSON also outputs estimates of target length and range, but these values are known to be biased (Burwen *et al.*, 2010). Therefore, despite the many benefits of acoustic sensing in water and the high resolution two-dimensional (2-D) images it provides, DIDSON must be calibrated to provide more quantitative measures.

5.5.2   Backscatter calibration

A DIDSON can be calibrated for measurements of backscatter amplitude vs. range using methods similar to those used to calibrate single-beam echosounders (see Chapter 2). It is, however, very helpful to pair the DIDSON with a split-beam echosounder to monitor the sphere position. The DIDSON measurements of backscatter intensity, coupled with the split-beam measurements of target position, provide more accurate measures of backscattering cross section vs. off-axis angles. As described by Jech *et al*. (2012), the sphere positions identified by the split-beam were generally accurate to within 1–2 cm and precise to within a few millimetres.

Because the DIDSON beams are narrow, the sphere diameter must be much smaller than the beam cross section at the calibration range (see Chapter 4). This is so that the measurements of the sphere echo are made outside of the near-field range of the sphere, and the directivity pattern is approximately constant for the solid angle spanning the sphere. For example, if a 0.0381-m-diameter sphere was positioned in a 0.3° beam at 7.3 m range, the sphere would span the entire beam cross section. Moreover, the sphere echo would be sensed by multiple adjacent beams, causing spatial ambiguity.

The directivity patterns should be mapped for each lens configuration used. These maps can be used to correct image distortions caused by lens-specific imperfections (Negahdaripour, 2005). A nonlinear cubic distortion model may be applied to the horizontal field of view, but the model parameters are specific to each DIDSON and lens configuration (Negahdaripour, 2005; Negahdaripour *et al.*, 2009).

5.5.3   Position calibration

To translate the positions of objects detected in 2-D DIDSON images to 3-D space, data are needed from two DIDSON having overlapping sample volumes. For example, (Negahdaripour *et al.*, 2005) applied stereo-optical and machine-vision techniques to calibrate two DIDSONs in a stereo-pair configuration. Jech *et al.* (2012) mounted two DIDSON in a test tank such that the two arrays were rotated 90° relative to each other (Figure 7.19). They used two 38.1-mm-diameter spheres made from tungsten carbide with 6% cobalt to map the directivity patterns and a 120-kHz split-beam echosounder transducer (Simrad ES120-7) to provide independent estimates of the target positions.
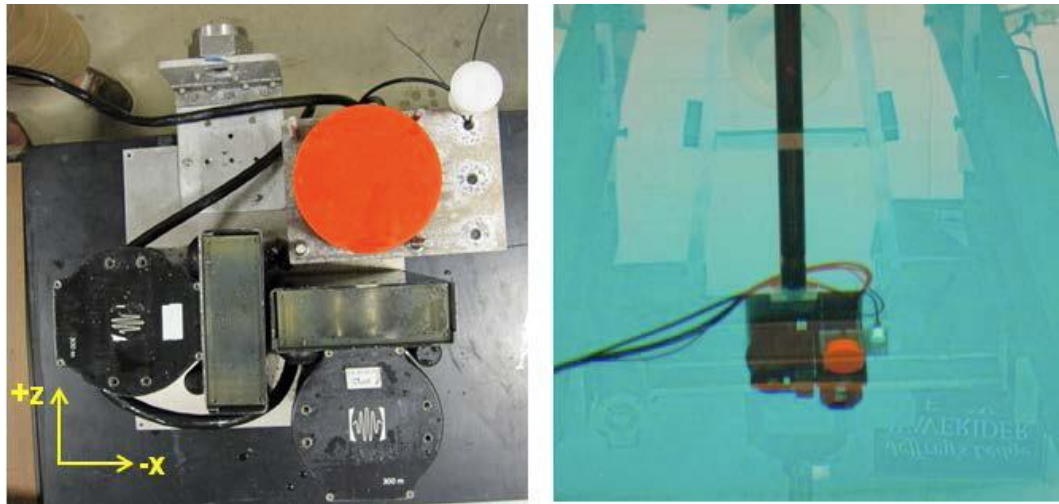
Figure 5.19. (left) Two DIDSON mounted orthogonally, and a 120-kHz split-beam transducer (Simrad ES120-7). Within the volume sampled by both DIDSON, the units on the left and right provide information about the vertical (azimuth) and horizontal dimensions, respectively. (right) The array in a test tank at the University of New Hampshire.

The array was rotated, controlled by computer, while the spheres remained stationary. One sphere remained on the geometric centers of the DIDSON swaths, while the relative positions of the two spheres were measured by the DIDSON and split-beam systems. The 3-D positions of the spheres were estimated by merging the 2-D positions measured from the two DIDSON. The backscatter strength values were also recorded from each DIDSON.

Backscatter strength values (1–126; 93% between 50 and 105) were measured vs. location within the beams (Figure 5.20). For the horizontal and vertical DIDSON, the backscatter strength values measured near the edges of the beams were approximately 37 and 23% less than those measured near the beam axis, respectively. The overlapping field-of-view was approximately 14 x 14°, so the measured directivity patterns (Figure 5.20) do not represent the complete 14 x 28° swaths for each DIDSON.
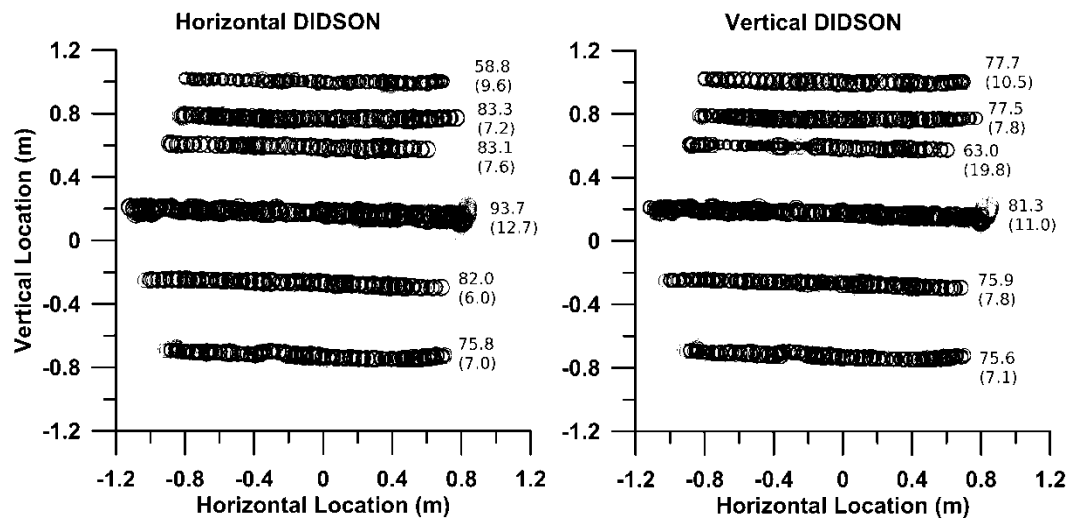

Figure 5.20. Echo strength as a function of the sphere position measured by the horizontal (left) and vertical (right) DIDSON. The size of the circular symbol is proportional to the echo strength (values ranged from 1 to 126). Echo strength values, and their standard deviations in parentheses, are shown to the right of each measurement series.

5.6 Scanning sonar

Vertical echosounders sample beneath the ship, but do not detect marine life located close to the sea surface (Axenrot *et al*., 2004; Scalabrin *et al.,* 2009; Totland *et al*., 2009). Scanning sonars, in comparison, sample a much larger volume, including the region near the sea surface. Scanning sonars may sample using multiple frequencies and provide a 360° radar-like scan from a moving ship. For example, the Simrad SH80 sonar operates at frequencies between 110 and 122 kHz (1 kHz step) and has 64 beams (Figure 5.21).
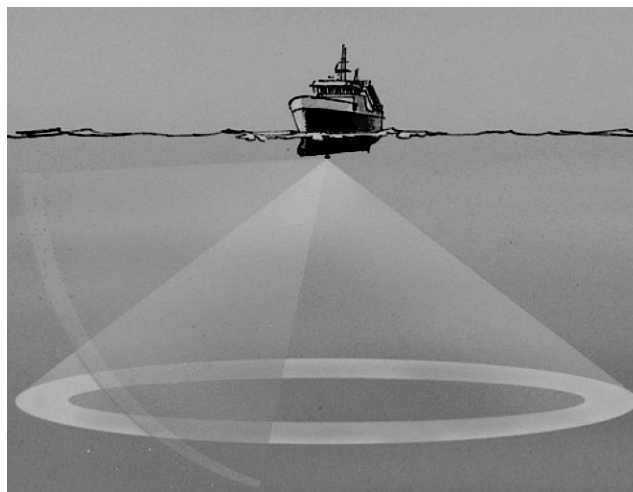

Figure 5.21. Illustration of the combined vertical detection capabilities of the Simrad SH80. In this example, the beams are set to look down 30° from the horizontal plane, while the vertical slice is sounding ahead in line with the ship course (Image from Simrad, Kongsberg Maritime AS).

Despite these attributes, scanning sonars have rarely been used quantitatively (Hewitt *et al*., 1976; Misund *et al*., 1995; Brehmer *et al*., 2006; Bernasconi *et al*., 2009; Nishimori *et al*., 2009). Nishimori *et al.* (2009) developed a quantitative echo-integration method for estimating fish school abundance from scanning sonars, which showed their clear potential to sample fish in much larger volumes than vertical sounders. Some of the important technical specifications of this class of sonar are listed in Table 5.2.

Table 5.1. Specifications of three Simrad scanning sonars.

Specification	SH80	SX90	SH90
Frequency (kHz)	110–122 (1-kHz step)	20–30 (1-kHz step)	111.5–116.5 (0.5-kHz step)
Tilt	+10 to –60° (0.5° step)	+10 to –60° (0.5° step)	+10 to –60° (0.5° step)
Signal Type	CW/FM	CW/FM	CW/Chirp
Number of elements	480	256	480
Transmission mode	Horizontal/vertical (360/180°)	Horizontal/vertical (360/180°)	Horizontal/vertical (360/180°)
Horizontal beam	8 or 360°		
Vertical beam	9 or 60°		
Horizontal transmission		360°	360°
Vertical transmission		7–10.5°	7.5°

Specification	SH80	SX90	SH90
Horizontal reception		8.3–13°	8°
Vertical reception		7.4–11.4°	7.5°
Vertical resolution (Transmit+Receive)			5.5°
Range (m)	50–2 000 (10 steps)	150–4 500 (11 steps)	50–2 000

5.6.1 Simrad SH80

This section provides an example of a sphere calibration (Chapter 2) of a Simrad SH80 so the data may be used to quantify backscatter from fish schools (Nottestad *et al.*, 2007) and large whales (Nottestad *et al.*, 2002; Bernasconi *et al.*, 2009, 2011). The SH80 transducer was installed on the ship's centreline under the bow (Figure 5.22). The sonar samples 64 sectors, each 5.62°, totalling 360°. The axis of each 8°-beamwidth is in the centre of each sector.

Before the calibration, profiles of the environmental conditions were made using a CTD probe. These measurements indicated that the water temperature, $t_w = 15.6$℃, sound speed, $c_w = 1502.8$ m s^{-1}, and absorption coefficient, $\alpha_a = 35$ dB m^{-1} were stable at the depth of the transducer, $d_w = 6.2$ m.

A 75-mm-diameter sphere made from tungsten carbide with 6% cobalt was used to measure the system response for eight 110-kHz beams and pulse durations ranging from 0.8 to 3.8 ms. The sphere weighs 3.3 kg, so is stable when suspended in the water. It has target strength, TS, of approximately –34.4 dB re 1 m² at 110 kHz. (A 65-mm-diameter sphere made from tungsten carbide with 6% cobalt may have a more stable TS over the SH80's range of frequencies).

Consulting the ship's engineering plans, the approximate positions of each beam axis were marked with tape on the ship's bow rail. Using these marks as reference, the calibration sphere was lowered to depths coinciding with the beam axis which, with the sonar tilt angle set at 0° (horizontally), was equivalent to the transducer depth (Figure 5.22).
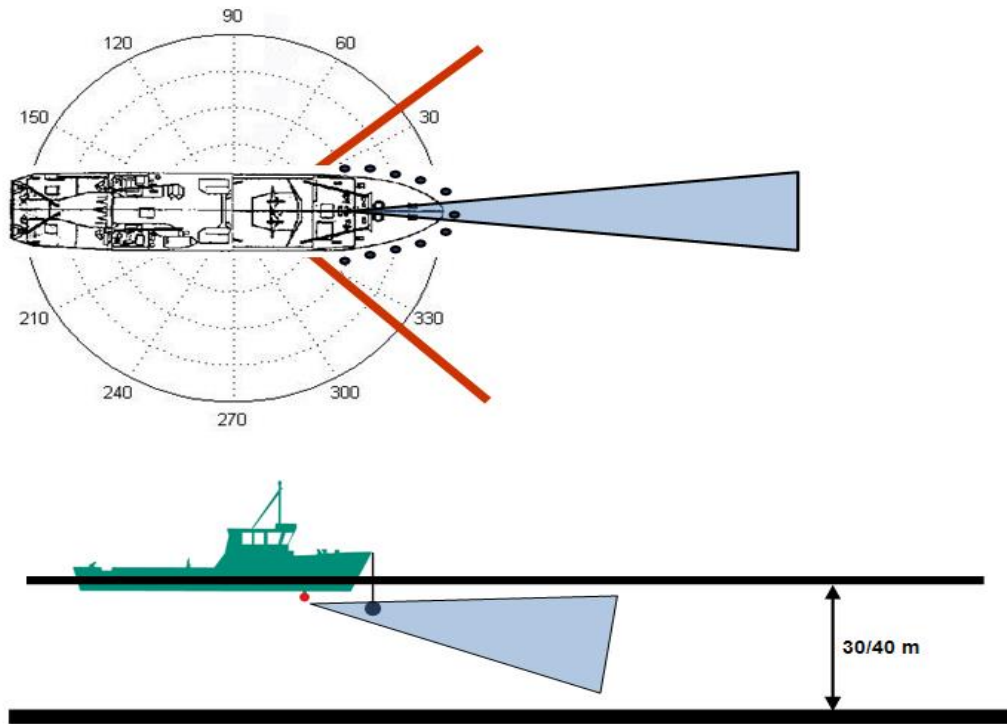
Figure 5.22. The calibration configuration aboard FV "M-60 Eros HØ".

For each of the eight selected beams and pulse duration values, an average of 476 sphere-TS measurements was recorded. The received voltages, u_{er} (V) corresponding to backscatter from the sphere, measured at different ranges, were converted from binary to ASCII format (Sonar Data Converter V9.04, Simrad) and echo level, EL (dB re 1 µPa) using,

$$EL = 20\log_{10}(u_{er}) - M_u$$

(5.3)

where M_u is the frequency-dependent sonar receiving sensitivity (M_u = −204.8 dB re 1 V µPa^{-1} at 110 kHz; Simrad; Horten, Norway). The EL between 5.5 and 7.2 m varied by ~8.5 dB for each beam (average of ~375 pings), similar to variations observed (Ona *et al.*, 2009).

The on-axis gain, G_0 (dB re 1), was then estimated by solving the sonar equation with values for EL; source level, SL (dB re 1 µPa at 1m), the theoretical sphere TS (dB re 1 m^2) (MacLennan, 1981), the range between the transducer and the sphere, r (m), and the absorption coefficient, α_a (dB m^{-1}) (Francois and Garrison, 1982a). The results confirm that G_0 should be calibrated for each pulse duration used.

The method described above is time consuming and should be refined to expedite the calibration process and more accurately position the sphere on the axis of each beam.

6   Acknowledgements

We are very appreciative of Randy Cutter, Roger Hewitt, Richard O'Driscoll, Josiah Renfree, and Kevin Stierhoff for reviewing drafts of this report. We thank Lars Nonboe Andersen and David MacLennan for their reviews and technical guidance. We thank Emory Anderson, Claire Welling, Katie Rice Eriksen, Simon Cooper, and Søren Lund for their editorial and administrative contributions.

7   References

Ainslie, M. A., and McColm, J. G. 1998. A simplified formula for viscous and chemical absorption in sea water. Journal of the Acoustical Society of America, 103: 1671–1672.

Andersen, L. N. 2006. Combining the two worlds. Simrad-Kongsberg. 5 pp.

Anon. 2014. A metadata convention for processed acoustic data from active acoustic systems. SISP 4 TG-AcMeta, ICES WGFAST Topic Group, TG-ACMeta. 40 pp.

Au, W. W. L., and Benoit-Bird, K. J. 2008. Broadband backscatter from individual Hawaiian mesopelagic boundary community animals with implications for spinner dolphin foraging. Journal of the Acoustical Society of America, 123: 2884–2894.

Axenrot, T., Didrikas, T., Danielsson, C., and Hansson, S. 2004. Diel patterns in pelagic fish behaviour and distribution observed from a stationary, bottom-mounted, and upward-facing transducer. ICES Journal of Marine Science, 61: 1100–1104.

Barange, M., Hampton, I., and Soule, M. 1996. Empirical determination of *in situ* target strengths of three loosely aggregated pelagic fish species. ICES Journal of Marine Science, 53: 225–232.

Beamiss, G. A., Robinson, S. P., Hayman, G., and Esward, T. J. 2002. Determination of the variation in free-field hydrophone response with temperature and depth. Acta Acustica United with Acustica, 88: 799–802.

Belcher, E., Matsuyama, B., and Trimble, G. 2001. Object identification with acoustic lenses. Oceans 2001 Mts/IEEE: An Ocean Odyssey, Vols. 1–4, Conference Proceedings: 6-11.

Benoit-Bird, K. J., Gilly, W. F., Au, W. W. L., and Mate, B. 2008. Controlled and in situ target strengths of the jumbo squid *Dosidicus gigas* and identification of potential acoustic scattering sources. Journal of the Acoustical Society of America, 123: 1318–1328.

Berger, L., Poncelet, C., and Trenkel, V. M. 2009. A method for reducing uncertainty in estimates of fish-school frequency response using data from multifrequency and multibeam echosounders. ICES Journal of Marine Science, 66: 1155–1161.

Bernasconi, M., Nottestad, L., Axelsen, B. E., and Krakstad, J. O. 2011. Acoustic observations of dusky dolphins *Lagenorhynchus obscurus* hunting Cape horse mackerel *Trachurus capensis* off Namibia. Marine Ecology Progress Series, 429: 209–218.

Bernasconi, M., Patel, R., Nøttestad, L., Knudsen, F. R., and Brierley, A. S. 2009. Use of active sonar for cetacean conservation and behavioral-ecology studies: a paradox? *In* Proceedings of the Institute of Acoustics, pp. 112–118. Loughborough, UK.

Blue, J. E. 1984. Physical calibration. Rapports et Procès-Verbaux des Réunions du Conseil International pour l'Exploration de la Mer, 184: 19–24.

Bobber, R. J. 1988. Underwater Electroacoustic Measurements, Peninsula Publishing, Los Altos, California, USA.

Bodholt, H. 2002. The effect of water temperature and salinity on echosounder measurements. ICES Symposium on Acoustics in Fisheries. Montpellier June 2002, presentation 123.

Brehmer, P., Lafont, T., Georgakarakos, S., Josse, E., Gerlotto, F., and Collet, C. 2006. Omnidirectional multibeam sonar monitoring: applications in fisheries science. Fish and Fisheries, 7: 165–179.

Brierley, A. S., Brandon, M. A., and Watkins, J. L. 1998b. An assessment of the utility of an acoustic Doppler current profiler for biomass estimation. Deep-Sea Research Part I-Oceanographic Research Papers, 45: 1555–1573.

Brierley, A. S., Goss, C., Watkins, J. L., and Woodroffe, P. 1998a. Variations in echosounder calibration with temperature, and some possible implications for acoustic surveys of krill biomass. CCAMLR Science, 5: 276–281.

Brierley, A. S., Saunders, R. A., Bone, D. G., Murphy, E. J., Enderlein, P., Conti, S. G., and Demer, D. A. 2006. Use of moored acoustic instruments to measure short-term variability in abundance of Antarctic krill. Limnology and Oceanography-Methods, 4: 18–29.

Brown, C. J., and Blondel, P. 2009. Developments in the application of multibeam sonar backscatter for seafloor habitat mapping. Applied Acoustics, 70: 1242–1247.

Burdic, W. S. 1991. Underwater Acoustics System Analysis, Peninsula Publishing.

Burwen, D. L., Fleischman, S. J., and Miller, J. D. 2010. Accuracy and precision of salmon length estimates taken from DIDSON sonar images. Transactions of the American Fisheries Society, 139: 1306–1314.

Carstensen, E. L. 1947. Self‐reciprocity calibration of electroacoustic transducers. Journal of the Acoustical Society of America, 19: 961–965.

Chen, C. T., and Millero, F. J. 1977. Speed of sound in seawater at high-pressures. Journal of the Acoustical Society of America, 62: 1129–1135.

Chu, D. Z., Foote, K. G., Hufnagle, L. C., Hammar, T. R., Liberatore, S. P., Baldwin, K. C., Mayer, L. A., et al. 2003. Calibrating a 90-kHz multibeam sonar. Oceans 2003 Mts/IEEE: Celebrating the Past...Teaming toward the Future: 1633–1636.

Chu, D. Z., and Stanton, T. K. 1998. Application of pulse compression techniques to broadband acoustic scattering by live individual zooplankton. Journal of the Acoustical Society of America, 104: 39–55.

Clay, C. S., and Medwin, H. 1977. Acoustical Oceanography, John Wiley & Sons, Inc. 544 pp.

Colbo, K., Ross, T., Brown, C., and Weber, T. 2014. A review of oceanographic applications of water column data from multibeam echosounders. Estuarine, Coastal and Shelf Science, 145: 41–56.

Conti, S. G., and Demer, D. A. 2003. Wide-bandwidth acoustical characterization of anchovy and sardine from reverberation measurements in an echoic tank. ICES Journal of Marine Science, 60: 617–624.

Conti, S. G., Demer, D. A., and Brierley, A. S. 2005b. Broad-bandwidth, sound scattering, and absorption from krill (*Meganyctiphanes norvegica*), mysids (*Praunus flexuosus* and *Neomysis integer*), and shrimp (*Crangon crangon*). ICES Journal of Marine Science, 62: 956–965.

Conti, S. G., Demer, D. A., Soule, M. A., and Conti, J. H. E. 2005a. An improved multiple-frequency method for measuring *in situ* target strengths. ICES Journal of Marine Science, 62: 1636–1646.

Cutter, G. R., Berger, L., and Demer, D. A. 2010. A comparison of bathymetry mapped with the Simrad ME70 multibeam echosounder operated in bathymetric and fisheries modes. ICES Journal of Marine Science, 67: 1301–1309.

Cutter, G. R., and Demer, D. A. 2007. Accounting for scattering directivity and fish behaviour in multibeam-echosounder surveys. ICES Journal of Marine Science, 64: 1664–1674.

Cutter, G. R., and Demer, D. A. 2014. Seabed classification using surface backscattering strength versus acoustic frequency and incidence angle measured with vertical, split-beam echosounders. ICES Journal of Marine Science, 71: 882–894.

Dalen, J., and Lovik, A. 1981. The influence of wind‐induced bubbles on echo integration surveys. Journal of the Acoustical Society of America, 69: 1653–1659.

Dalen, J., Nedreaas, K., and Pedersen, R. 2003. A comparative acoustic-abundance estimation of pelagic redfish (*Sebastes mentella*) from hull-mounted and deep-towed acoustic systems. ICES Journal of Marine Science, 60: 472–479.

Davis, R. W., Ortega-Ortiz, J. G., Ribic, C. A., Evans, W. E., Biggs, D. C., Ressler, P. H., Cady, R. B., *et al*. 2002. Cetacean habitat in the northern oceanic Gulf of Mexico. Deep-Sea Research Part I-Oceanographic Research Papers, 49: 121–142.

De Moustier, C. 2001. Lecture 16: Sound refraction in the water column. Seafloor surveying with swath bathymetry sonars. 41 pp.

De Robertis, A., Hjellvik, V., Williamson, N. J., and Wilson, C. D. 2008. Silent ships do not always encounter more fish: comparison of acoustic backscatter recorded by a noise-reduced and a conventional research vessel. ICES Journal of Marine Science, 65: 623–635.

De Robertis, A., and Wilson, C. D. 2006. Walleye pollock respond to trawling vessels. ICES Journal of Marine Science, 63: 514–522.

Deines, K. L. 1999. Backscatter estimation using broadband acoustic Doppler current profilers. Proceedings of the IEEE Sixth Working Conference on Current Measurement: 249–253.

Del Grosso, V. A. 1974. New equation for the speed of sound in natural waters (with comparisons to other equations). Journal of the Acoustical Society of America, 56: 1084–1091.

Demer, D. A. 1994. Accuracy and precision of echo integration surveys of Antarctic krill. PhD thesis. University of California, San Diego / Scripps Institution of Oceanography. 144 pp.

Demer, D. A. 2004. An estimate of error for the CCAMLR 2000 survey estimate of krill biomass. Deep-Sea Research Part II-Topical Studies in Oceanography, 51: 1237–1251.

Demer, D. A., Barange, M., and Boyd, A. J. 2000. Measurements of three-dimensional fish school velocities with an acoustic Doppler current profiler. Fisheries Research, 47: 201–214.

Demer, D. A., Cutter, G. R., Renfree, J. S., and Butler, J. L. 2009b. A statistical-spectral method for echo classification. ICES Journal of Marine Science, 66: 1081–1090.

Demer, D. A., and Hewitt, R. P. 1993. Calibration of an acoustic echo-integration system in a deep tank, with gain comparisons over standard sphere material, water temperature and time. SC-CAMLR Selected Scientific Papers, 9: 127–144.

Demer, D. A., Kloser, R. J., MacLennan, D. N., and Ona, E. 2009a. An introduction to the proceedings and a synthesis of the 2008 ICES Symposium on the Ecosystem Approach with Fisheries Acoustics and Complementary Technologies (SEA-FACTS). ICES Journal of Marine Science, 66: 961–965.

Demer, D. A., and Renfree, J. S. 2008. Variations in echosounder–transducer performance with water temperature. ICES Journal of Marine Science, 65: 1021–1035.

Demer, D. A., Soule, M. A., and Hewitt, R. P. 1999. A multiple-frequency method for potentially improving the accuracy and precision of *in situ* target strength measurements. Journal of the Acoustical Society of America, 105: 2359–2376.

Demer, D. A., Zwolinski, J. P., Byers, K. A., Cutter, G. R., Renfree, J. S., Sessions, T. S., and Macewicz, B. J. 2012. Prediction and confirmation of seasonal migration of Pacific sardine (*Sardinops sagax*) in the California Current Ecosystem. Fishery Bulletin, 110: 52–70.

Doonan, I. J., Coombs, R. F., and McClatchie, S. 2003. The absorption of sound in seawater in relation to the estimation of deep-water fish biomass. ICES Journal of Marine Science, 60: 1047–1055.

Dragesund, O., and Olson, S. 1965. On the possibility of estimating year-class strength by measuring echo-abundance of 0-group fish. Fiskeridirektoratets Skrifter. Serie Havundersøkelser, 13(8): 47–75.

Dragonette, L. R., Numrich, S. K., and Frank, L. J. 1981. Calibration technique for acoustic scattering measurements. Journal of the Acoustical Society of America, 69: 1186–1189.

Ehrenberg, J. E., and Lytle, D. W. 1972. Acoustic techniques for estimating fish abundance. IEEE Transactions on Geoscience Electronics, GE-10: 138–145.

Ehrenberg, J. E., and Torkelson, T. C. 2000. FM slide (chirp) signals: a technique for significantly improving the signal-to-noise performance in hydroacoustic assessment systems. Fisheries Research, 47: 193–199.

Eriksen, C. C., Osse, T. J., Light, R. D., Wen, T., Lehman, T. W., Sabin, P. L., Ballard, J. W., *et al.* 2001. Seaglider: a long-range autonomous underwater vehicle for oceanographic research. IEEE Journal of Oceanic Engineering, 26: 424–436.

Faran, J. J. 1951. Sound scattering by solid cylinders and spheres. Journal of the Acoustical Society of America, 23: 405–418.

Fernandes, P. G., Brierley, A. S., Simmonds, E. J., Millard, N. W., McPhail, S. D., Armstrong, F., Stevenson, P., *et al.* 2000. Oceanography: Fish do not avoid survey vessels. Nature, 404: 35–36.

Fernandes, P. G., and Simmonds, E. J. 1996. Practical approaches to account for receiver delay and the TVG start time in the calibration of the Simrad EK500. ICES Document CM 1996/B: 17. 12 pp.

Fernandes, P. G., Stevenson, P., Brierley, A. S., Armstrong, F., and Simmonds, E. J. 2003. Autonomous underwater vehicles: future platforms for fisheries acoustics. ICES Journal of Marine Science, 60: 684–691.

Fiedler, P. C., Barlow, J., and Gerrodette, T. 1998. Dolphin prey abundance determined from acoustic backscatter data in eastern Pacific surveys. Fishery Bulletin, 96: 237–247.

Fielding, S., Griffiths, G., and Roe, H. S. J. 2004. The biological validation of ADCP acoustic backscatter through direct comparison with net samples and model predictions based on acoustic-scattering models. ICES Journal of Marine Science, 61: 184–200.

Fisher, F. H., and Simmons, V. P. 1977. Sound absorption in seawater. Journal of the Acoustical Society of America, 62(3): 558–564.

Flagg, C. N., and Smith, S. L. 1989. On the use of the acoustic Doppler current profiler to measure zooplankton abundance. Deep-Sea Research Part a-Oceanographic Research Papers, 36: 455–474.

Fofonoff, P., and Millard, R. 1983. Algorithms for computation of fundamental properties of seawater. UNESCO Technical Papers in Marine Science. 53 pp.

Foldy, L. L., and Primakoff, H. 1945. A general theory of passive linear electroacoustic transducers and the electroacoustic reciprocity theorem. I., Journal of the Acoustical Society of America, 17: 109–120.

Foote, K. G. 1980. Importance of the swimbladder in acoustic scattering by fish - a comparison of gadoid and mackerel target strengths. Journal of the Acoustical Society of America, 67: 2084–2089.

Foote, K. G. 1982. Optimizing copper spheres for precision calibration of hydroacoustic equipment. Journal of the Acoustical Society of America, 71: 742–747.

Foote, K. G. 1983a. Linearity of fisheries acoustics, with addition theorems. Journal of the Acoustical Society of America, 73: 1932–1940.

Foote, K. G. 1983b. Maintaining precision calibrations with optimal copper spheres. Journal of the Acoustical Society of America, 73: 1054–1063.

Foote, K. G. 1987. Dependence of equivalent beam angle on sound speed. ICES Document CM 1987/B: 2.

Foote, K. G. 1990. Spheres for calibrating an eleven-frequency acoustic measurement system. Journal du Conseil, 46: 284–286.

Foote, K. G. 1991a. Acoustic sampling volume. Journal of the Acoustical Society of America, 90: 959–964.

Foote, K. G. 1991b. Summary of methods for determining fish target strength at ultrasonic frequencies. ICES Journal of Marine Science, 48: 211–217.

Foote, K. G. 1996. Coincidence echo statistics. Journal of the Acoustical Society of America, 99: 266–271.

Foote, K. G. 2007. Acoustic robustness of two standard spheres for calibrating a broadband multibeam sonar. Oceans 2007 - Europe, Vols 1–3: 885–888.

Foote, K. G., Chu, D. Z., Hammar, T. R., Baldwin, K. C., Mayer, L. A., Hufnagle, L. C., and Jech, J. M. 2005. Protocols for calibrating multibeam sonar. Journal of the Acoustical Society of America, 117: 2013–2027.

Foote, K. G., Knudsen, H. P., Vestnes, G., MacLennan, D. N., and Simmonds, E. J. 1987. Calibration of acoustic instruments for fish density estimation: a practical guide. ICES Cooperative Research Report No. 144. 69 pp.

Foote, K. G., and MacLennan, D. N. 1984. Comparison of copper and tungsten carbide calibration spheres. Journal of the Acoustical Society of America, 75: 612–616.

Forland, T. N., Hobæk, H., Ona, E., and Korneliussen, R. J. 2014. Broad bandwidth acoustic backscattering from sandeel—measurements and finite element simulations. ICES Journal of Marine Science, doi.10.1093/icesjms/fsu010.

Francois, R. E., and Garrison, G. R. 1982a. Sound absorption based on ocean measurements. Part II: Boric acid contribution and equation for total absorption. Journal of the Acoustical Society of America, 72: 1879–1890.

Francois, R. E., and Garrison, G. R. 1982b. Sound absorption based on ocean measurements: Part I: Pure water and magnesium sulfate contributions. Journal of the Acoustical Society of America, 72: 896–907.

Furusawa, M. 1991. Designing quantitative echo sounders. Journal of the Acoustical Society of America, 90: 26–36.

Gangl, R. S., and Whaley, R. A. 2004. Comparison of fish density estimates from repeated hydroacoustic surveys on two Wyoming waters. North American Journal of Fisheries Management, 24: 1279–1287.

Gerlotto, F., Soria, M., and Freon, P. 1999. From two dimensions to three: the use of multibeam sonar for a new approach in fisheries acoustics. Canadian Journal of Fisheries and Aquatic Sciences, 56: 6–12.

Gostiaux, L., and van Haren, H. 2010. Extracting meaningful information from uncalibrated backscattered echo intensity data. Journal of Atmospheric and Oceanic Technology, 27: 943–949.

Greenaway, S. F., and Weber, T. C. 2010. Test methodology for evaluation of linearity of multibeam echosounder backscatter performance. Oceans 2010: 1–7.

Handegard, N. O., Pedersen, G., and Brix, O. 2009. Estimating tail-beat frequency using split-beam echosounders. ICES Journal of Marine Science, 66: 1252–1258.

Hellequin, L., Boucher, J. M., and Lurton, X. 2003. Processing of high-frequency multibeam echo sounder data for seafloor characterization. IEEE Journal of Oceanic Engineering, 28: 78–89.

Hersey, J. B., Backus, R. H., and Hellwig, J. 1962. Sound-scattering spectra of deep scattering layers in the western North Atlantic Ocean. Deep Sea Research, 8: 196–210.

Hewitt, R. P., and Demer, D. A. 1991. Krill abundance. Nature, 353: 310–310.

Hewitt, R. P., and Demer, D. A. 1993. Dispersion and abundance of Antarctic krill in the vicinity of Elephant Island in the 1992 austral summer. Marine Ecology Progress Series, 99: 29–39.

Hewitt, R. P., and Demer, D. A. 2000. The use of acoustic sampling to estimate the dispersion and abundance of euphausiids, with an emphasis on Antarctic krill, *Euphausia superba*. Fisheries Research, 47: 215–229.

Hewitt, R. P., Smith, P. E., and Brown, J. C. 1976. Development and use of sonar mapping for pelagic stock assessment in California Current area. Fishery Bulletin, 74: 281–300.

Heywood, K. J. 1996. Diet vertical migration of zooplankton in the Northeast Atlantic. Journal of Plankton Research, 18: 163–184.

Heywood, K. J., Scropehowe, S., and Barton, E. D. 1991. Estimation of zooplankton abundance from ship-borne ADCP backscatter. Deep-Sea Research Part A - Oceanographic Research Papers, 38: 677–691.

Hickling, R. 1962. Analysis of echoes from a solid elastic sphere in water. Journal of the Acoustical Society of America, 34: 1582–1592.

Hjellvik, V., Handegard, N. O., and Ona, E. 2008. Correcting for vessel avoidance in acoustic-abundance estimates for herring. ICES Journal of Marine Science, 65: 1036–1045.

Hobaek, H., and Forland, T. N. 2013. Characterization of target spheres for broad-band calibration of acoustic systems. Acta Acustica United with Acustica, 99: 465–476.

Holliday, D. V. 1972a. Resonance structure in echoes from schooled pelagic fish. Journal of the Acoustical Society of America, 51: 1322–1332.

Holliday, D. V. 1972b. Resonant structure in echoes from schooled marine fish. Journal of the Acoustical Society of America, 51: doi: 10.1121/1.1981727.

Holliday, D. V. 1974. Doppler structure in echoes from schools of pelagic fish. Journal of the Acoustical Society of America, 55: 1313–1322.

Holmes, J. A., Cronkite, G. M. W., Enzenhofer, H. J., and Mulligan, T. J. 2006. Accuracy and precision of fish-count data from a "dual-frequency identification sonar" (DIDSON) imaging system. ICES Journal of Marine Science, 63: 543–555.

Humborstad, O. B., Nottestad, L., Lokkeborg, S., and Rapp, H. T. 2004. RoxAnn bottom classification system, sidescan sonar and video-sledge: spatial resolution and their use in assessing trawling impacts. ICES Journal of Marine Science, 61: 53–63.

Hwang, B-K., Furusawa, M., and Ogata, M. 2007. Validation of multi-frequency inversion method by using dummy scatterers of zooplankton. Fisheries Science, 73: 250–262.

ICES. 1994. Report from the ICES Workshop on Hydroacoustic Instrumentation. ICES Document CM 1994/B: 9. 9 pp.

ICES. 2007. Acoustic seabed classification of marine physical and biological landscapes. ICES Cooperative Research Report No. 286. 183 pp.

Imaizumi, T., Furusawa, M., Akamatsu, T., and Nishimori, Y. 2008. Measuring the target strength spectra of fish using dolphin-like short broadband sonar signals. Journal of the Acoustical Society of America, 124: 3440–3449.

Islas-Cital, A., Atkins, P. R., and Foo, K. Y. 2010. Standard target calibration of broadband active sonar systems in a laboratory tank. Oceans 2010 - MTS/IEEE Sydney: 144–146.

Jackson, D., and Richardson, M. 2007. High-Frequency Seafloor Acoustics. Springer Science+Business Media. 618 pp.

Jech, J. M., Boswell, K. M., Barao, T., Condiotty, J., Melvin, G. D., Taylor, J. C., Wakefield, W. W., *et al*. 2012. Calibration of two orthogonal dual-frequency identification sonars (DIDSONs). *In* 11th European Conference on Underwater Acoustics 2012. Edinburgh, Scotland.

Jech, J. M., Foote, K. G., Chu, D. Z., and Hufnagle, L. C. 2005. Comparing two 38-kHz scientific echosounders. ICES Journal of Marine Science, 62: 1168–1179.

Jin, G., and Tang, D. 1996. Uncertainties of differential phase estimations associated with interferometric sonars. IEEE Journal of Oceanic Engineering, 21: 53–63.

Johnsen, E., Pedersen, R., and Ona, E. 2009. Size-dependent frequency response of sandeel schools. ICES Journal of Marine Science, 66: 1100–1105.

Jones, B. A., Lavery, A. C., and Stanton, T. K. 2009. Use of the distorted wave Born approximation to predict scattering by inhomogeneous objects: Application to squid. Journal of the Acoustical Society of America, 125: 73–88.

Kerr, D. E. 1988. Propagation of Short Radio Waves, 2nd edn. Peninsula Publishing, Los Altos, CA, USA.

Kimura, K. 1929. On the detection of fish-groups by an acoustic method. Journal of the Imperial Fisheries Institute, Tokyo, 24: 41–45.

Knudsen, H. P. 2009. Long-term evaluation of scientific-echosounder performance. ICES Journal of Marine Science, 66: 1335–1340.

Korneliussen, R. J., Diner, N., Ona, E., Berger, L., and Fernandes, P. G. 2008. Proposals for the collection of multifrequency acoustic data. ICES Journal of Marine Science, 65: 982–994.

Korneliussen, R. J., Heggelund, Y., Eliassen, I. K., Oye, O. K., Knutsen, T., and Dalen, J. 2009. Combining multibeam-sonar and multifrequency-echosounder data: examples of the analysis and imaging of large euphausiid schools. ICES Journal of Marine Science, 66: 991–997.

Lanzoni, J. C., and Weber, T. C. 2010. High-resolution calibration of a multibeam echo sounder. IEEE Oceans 2010, doi: 10.1109/OCEANS.2010.5664519.

Lanzoni, J. C., and Weber, T. C. 2011. A method for field calibration of a multibeam echo sounder. IEEE Oceans 2011: 1–7.

Lavery, A. C., Chu, D. Z., and Moum, J. N. 2010a. Observations of broadband acoustic backscattering from nonlinear iInternal waves: assessing the contribution from microstructure. IEEE Journal of Oceanic Engineering, 35: 695–709.

Lavery, A. C., Chu, D., and Moum, J. N. 2010b. Measurements of acoustic scattering from zooplankton and oceanic microstructure using a broadband echosounder. ICES Journal of Marine Science, 67: 379–394.

Lee, K., Mukai, T., Kang, D. H., and Iida, K. 2004. Application of acoustic Doppler current profiler combined with a scientific echo sounder for krill *Euphausia pacifica* density estimation. Fisheries Science, 70: 1051–1060.

Leroy, C. C. 1969. Development of simple equations for accurate and more realistic calculation of speed of sound in seawater. Journal of the Acoustical Society of America, 46: 216–226.

Leroy, C. C., and Parthiot, F. 1998. Depth-pressure relationships in the oceans and seas. Journal of the Acoustical Society of America, 103: 1346–1352.

Leroy, C. C., Robinson, S. P., and Goldsmith, M. J. 2008. A new equation for the accurate calculation of sound speed in all oceans. Journal of the Acoustical Society of America, 124: 2774–2782.

Loland, A., Aldrin, M., Ona, E., Hjellvik, V., and Holst, J. C. 2007. Estimating and decomposing total uncertainty for survey-based abundance estimates of Norwegian spring-spawning herring. ICES Journal of Marine Science, 64: 1302–1312.

Lurton, X. 2000. Swath bathymetry using phase difference: theoretical analysis of acoustic measurement. IEEE Journal of Oceanic Engineering, 25: 351–363.

Lurton, X. 2010. An Introduction to Underwater Acoustics: Principles and Applications, 2nd edn. Springer Praxis Books / Geophysical Sciences. 724 pp.

Lynn, R. J. 2003. Variability in the spawning habitat of Pacific sardine (*Sardinops sagax*) off southern and central California. Fisheries Oceanography, 12: 541–553.

Mackenzie, K. V. 1981. Nine-term equation for sound speed in the oceans. Journal of the Acoustical Society of America, 70: 807–812.

MacLean, W. R. 1940. Absolute measurement of sound without a primary standard. Journal of the Acoustical Society of America, 12: 140–146.

MacLennan, D. N. 1981. The theory of solid spheres as sonar calibration targets. Scottish Fisheries Research, 22. 17 pp.

MacLennan, D. N. 1982. Target strength measurements on metal spheres. Department of Agriculture and Fisheries for Scotland, Aberdeen (UK) Marine Lab. 11 pp.

MacLennan, D. N. 2011. Real-time calibration of *in situ* measurements of target strength. ICES Journal of Marine Science, 68: 626–631.

MacLennan, D. N., and Dunn, J. R. 1984. Estimation of sound velocities from resonance measurements on tungsten carbide calibration spheres. Journal of Sound and Vibration, 97: 321–331.

MacLennan, D. N., Fernandes, P. G., and Dalen, J. 2002. A consistent approach to definitions and symbols in fisheries acoustics. ICES Journal of Marine Science, 59: 365–369.

MacLennan, D., and Simmonds, J. 1992. Fisheries Acoustics. Chapman and Hall, London. 325 pp.

Medwin, H., and Clay, C. S. 1998. Fundamentals of Acoustical Oceanography. Academic Press, Boston. 712 pp.

Melvin, G. D., Cochrane, N. A., and Li, Y. 2003. Extraction and comparison of acoustic backscatter from a calibrated multi- and single-beam sonar. ICES Journal of Marine Science, 60: 669–677.

Millero, F. J., and Li, X. 1994. On equations for the speed of sound in seawater - comment. Journal of the Acoustical Society of America, 95: 2757–2759.

Misund, O. A., Aglen, A., and Fronaes, E. 1995. Mapping the shape, size, and density of fish schools by echo integration and a high-resolution sonar. ICES Journal of Marine Science, 52: 11–20.

Mitson, R. B., and Knudsen, H. P. 2003. Causes and effects of underwater noise on fish abundance estimation. Aquatic Living Resources, 16: 255–263.

Miyanohana, Y., Ishii, K., and Furusawa, M. 1993. Spheres to calibrate echo sounders at any frequency. Nippon Suisan Gakkaishi, 59: 933–942.

Moursund, R. A., Carlson, T. J., and Peters, R. D. 2003. A fisheries application of a dual-frequency identification sonar acoustic camera. ICES Journal of Marine Science, 60: 678–683.

Mueller, A. M., Burwen, D. L., Boswell, K. M., and Mulligan, T. 2010. Tail-beat patterns in dual-frequency identification sonar echograms and their potential use for species identification and bioenergetics Studies. Transactions of the American Fisheries Society, 139: 900–910.

Mueller, R. P., Brown, R. S., Hop, H., and Moulton, L. 2006. Video and acoustic camera techniques for studying fish under ice: a review and comparison. Reviews in Fish Biology and Fisheries, 16: 213–226.

Myriax. 2014. Echoview software, version 6.0.89. Myriax Software Pty. Ltd., GPO Box 1387, Hobart, Tasmania, Australia.

Nam, G. H., Cox, M. G., Harris, P. M., Robinson, S. P., Hayman, G., Beamiss, G. A., Esward, T. J., *et al.* 2007. A model for characterizing the frequency-dependent variation in sensitivity with temperature of underwater acoustic transducers from historical calibration data. Measurement Science and Technology, 18: 1553 doi:10.1088/0957-0233/18/5/047.

Negahdaripour, S. 2005. Calibration of DIDSON forward-scan acoustic video camera. Oceans 2005, Vols 1-3: 1287–1294.

Negahdaripour, S., Firoozfam, P., and Sabzmeydani, P. 2005. On processing and registration of forward-scan acoustic video imagery. 2nd Canadian Conference on Computer and Robot Vision, Proceedings: 452–459.

Negahdaripour, S., Sekkati, H., and Pirsiavash, H. 2009. Opti-acoustic stereo imaging: On system calibration and 3-D target reconstruction. IEEE Transactions on Image Processing, 18: 1203–1224.

Nero, R. W., and Huster, M. E. 1996. Low-frequency acoustic imaging of Pacific salmon on the high seas. Canadian Journal of Fisheries and Aquatic Sciences, 53: 2513–2523.

Nero, R. W., Thompson, C. H., and Love, R. H. 1998. Low-frequency acoustic measurements of Pacific hake, *Merluccius productus*, off the west coast of the United States. Fishery Bulletin, 96: 329–343.

Nielson, R. L., Hampton, I., and Everson, I. 1980. Calibration of Hydro-acoustic Instruments. NOAA, Washington, DC. 52 pp.

Nishimori, Y., Iida, K., Furusawa, M., Tang, Y., Tokuyama, K., Nagai, S., and Nishiyama, Y. 2009. The development and evaluation of a three-dimensional, echo-integration method for estimating fish-school abundance. ICES Journal of Marine Science, 66: 1037–1042.

Nottestad, L., Ferno, A., Mackinson, S., Pitcher, T., and Misund, O. A. 2002. How whales influence herring school dynamics in a cold-front area of the Norwegian Sea. ICES Journal of Marine Science, 59: 393–400.

Nottestad, L., Misund, O. A., Melle, W., Ulvestad, B. K. H., and Orvik, K. A. 2007. Herring at the Arctic front: influence of temperature and prey on their spatio-temporal distribution and migration. Marine Ecology, 28: 123–133.

O'Driscoll, R. L. 2004. Estimating uncertainty associated with acoustic surveys of spawning hoki (*Macruronus novaezelandiae*) in Cook Strait, New Zealand. ICES Journal of Marine Science, 61: 84–97.

Ona, E. (Ed). 1999. Methodology for target strength measurements (with special reference to *in situ* techniques for fish and mikro-nekton. ICES Cooperative Research Report No. 235. 59 pp.

Ona, E., Mazauric, V., and Andersen, L. N. 2009. Calibration methods for two scientific multibeam systems. ICES Journal of Marine Science, 66: 1326–1334.

Ona, E., and Mitson, R. B. 1996. Acoustic sampling and signal processing near the seabed: The deadzone revisited. ICES Journal of Marine Science, 53: 677–690.

Ona, E., Zhao, X., Svellingen, I., and Foote, K. G. 1996. Some pitfalls of short-range standard-target calibration. ICES Document CM 1996/B: 36. 19 pp.

Patel, R., and Ona, E. 2009. Measuring herring densities with one real and several phantom research vessels. ICES Journal of Marine Science, 66: 1264–1269.

Patterson, R. 1967. Using ocean surface as a reflector for a self-reciprocity calibration of a transducer. Journal of the Acoustical Society of America, 42: 653–655.

Pedersen, G. 2007. Methodology for *in situ* target strength measurement of fish. PhD thesis. University of Bergen, Norway.

Pike, J. M., and Beiboer, F. L. 1993. A comparison between algorithms for the speed of sound in seawater. The Hydrographic Society, Special Publication No. 34.

Plimpton, P. E., Freitag, H. P., and McPhaden, M. J. 2004. Processing of subsurface ADCP data in the Equatorial Pacific. NOAA Technical Memorandum, OAR-PMEL-125.

Postel, L., da Silva, A. J., Mohrholz, V., and Lass, H. U. 2007. Zooplankton biomass variability off Angola and Namibia investigated by a lowered ADCP and net sampling. Journal of Marine Systems, 68: 143–166.

Primakoff, H., and Foldy, L. L. 1947. A general theory of passive linear electroacoustic transducers and the electroacoustic reciprocity theorem. II., Journal of the Acoustical Society of America, 19: 50–58.

Radenac, M. H., Plimpton, P. E., Lebourges-Dhaussy, A., Commien, L., and McPhaden, M. J. 2010. Impact of environmental forcing on the acoustic backscattering strength in the equatorial Pacific: Diurnal, lunar, intraseasonal, and interannual variability. Deep-Sea Research Part I-Oceanographic Research Papers, 57: 1314–1328.

Ressler, P. H. 2002. Acoustic backscatter measurements with a 153 kHz ADCP in the northeastern Gulf of Mexico: determination of dominant zooplankton and micronekton scatterers. Deep-Sea Research Part I-Oceanographic Research Papers, 49: 2035–2051.

Reynisson, P. 1990. A geometric method for measuring the directivity of hull-mounted transducers. Rapports et Procès-Verbaux des Réunions du Conseil International pour l'Exploration de la Mer, 189: 176–182.

Reynisson, P. 1998. Monitoring of equivalent beam angles of hull-mounted acoustic survey transducers in the period 1983–1995. ICES Journal of Marine Science, 55: 1125–1132.

Rihaczek, A. W. 1969. Principles of High-Resolution Radar. McGraw-Hill, New York, NY.

Rogers, P. H., and Van Buren, A. L. 1978. New approach to a constant beamwidth transducer. Journal of the Acoustical Society of America, 64: 38–43.

Rose, G. A. 2003. Monitoring coastal northern cod: towards an optimal survey of Smith Sound, Newfoundland. ICES Journal of Marine Science, 60: 453–462.

Rudnick, D. L., Davis, R. E., Eriksen, C. C., Fratantoni, D. M., and Perry, M. J. 2004. Underwater gliders for ocean research. Journal of the Marine Technology Society, 38: 73–84.

Ryan, T. E., and Kloser, R. J. 2004. Quantification and correction of a systematic error in Simrad ES60 echosounders. *In* ICES FAST, Gdanck. Copy available from CSIRO Marine and Atmospheric Research, GPO Box 1538, Hobart, Australia.

Sabin, G. A. 1956. Transducer calibration by impedance measurements. Journal of the Acoustical Society of America, 28: 705–710.

Sawada, K., and Furusawa, M. 1993. Precision calibration of echosounder by integration of standard sphere echoes. Journal of the Acoustical Society of Japan, 14: 243–249.

Scalabrin, C., Marfia, C., and Boucher, J. 2009. How much fish is hidden in the surface and bottom acoustic blind zones? ICES Journal of Marine Science, 66: 1355–1363.

Schottky, W. 1926. Das Gesetz des Tiefempfangs in der Akustik und Electroakustik. Zeits. F. Physik, 36: 689–736.

Seabird. 2013. Seasoft V2 - SBE Data Processing Manual revision 7.22.4. p. 174. Sea-Bird Electronics, Washington, USA.

Shabangu, F. W., Ona, E., and Yemane, D. 2014. Measurements of acoustic attenuation at 38 kHz by wind-induced air bubbles with suggested correction factors for hull-mounted transducers. Fisheries Research, 151: 47–56.

Sherman, C., and Butler, J. L. 2007. Transducers and Arrays for Underwater Sound. Springer, New York. 612 pp.

Simmonds, E. J. 1984a. A comparison between measured and theoretical equivalent beam angles for seven similar transducers. Journal of Sound and Vibration, 97: 117–128.

Simmonds, E. J. 1984b. The effect of mounting on the equivalent beam angle of acoustic survey transducers. ICES Document CM 1984/B: 32. 5 pp.

Simmonds, E. J. 1990. Very accurate calibration of a vertical echosounder: a five-year assessment of performance and accuracy. Rapport et Procès-Verbaux des Réunions du Conseil International pour l'Exploration de la Mer, 189: 183–191.

Simmonds, E. J., Armstrong, F., and Copland, P. J. 1996. Species identification using wideband backscatter with neural network and discriminant analysis. ICES Journal of Marine Science, 53: 189–195.

Simmonds, J., Gerlotto, F., Fernandes, P., and MacLennan, D. 1999. Observation and extraction of three‐dimensional information on fish schools. Journal of the Acoustical Society of America, 105: 996–996.

Simmonds, E. J., and MacLennan, D. N. 2005. Fisheries Acoustics: Theory and Practice. Blackwell Publishing, Oxford. 437 pp.

Simrad. 1993. Simrad EK500 Scientific echosounder instruction manual, Simrad Subsea A/S, Horten, Norway.

Simrad. 1997. EK500 Scientific echo sounder operator manual, Simrad Subsea A/S, Horten, Norway.

Simrad 2001. EK60 Scientific echo sounder instruction manual, Simrad Subsea A/S, Horten, Norway. 246 pp.

Simrad. 2004. ES60 Fishery echo sounder manual, Simrad Subsea A/S, Horten, Norway. 213 pp.

Simrad. 2008. ER60 Scientific echo sounder software reference manual, Simrad Subsea A/S, Horten, Norway. 221 pp.

Simrad. 2010. ES70 fish finding echo sounder operator manual, Simrad Subsea A/S, Horten, Norway. 93 pp.

Simrad. 2012. Simrad ME70 Scientific multibeam echo sounder operator manual, Release 1.2.5. Kongsberg Maritime AS, Norway. 109 pp.

Soule, M., Hampton, I., and Barange, M. 1996. Potential improvements to current methods of recognizing single targets with a split-beam echo-sounder. ICES Journal of Marine Science, 53: 237–243.

Speisberger, J. L., and Metzger, K. 1991. New estimates of sound speed in water. Journal of the Acoustical Society of America, 89: 1697–1700.

Stanton, T. K., and Chu, D. 2008. Calibration of broadband active acoustic systems using a single standard spherical target. Journal of the Acoustical Society of America, 124: 128–136.

Stanton, T. K., Chu, D. Z., Jech, J. M., and Irish, J. D. 2010. New broadband methods for resonance classification and high-resolution imagery of fish with swimbladders using a modified commercial broadband echosounder. ICES Journal of Marine Science, 67: 365–378.

Stanton, T. K., Sellers, C. J., and Jech, J. M. 2012. Resonance classification of mixed assemblages of fish with swimbladders using a modified commercial broadband acoustic echosounder at 1-6 kHz. Canadian Journal of Fisheries and Aquatic Sciences, 69: 854–868.

Stanton, T. K., Wiebe, P. H., Chu, D. Z., and Goodman, L. 1994. Acoustic characterization and discrimination of marine zooplankton and turbulence. ICES Journal of Marine Science, 51: 469–479.

Stewart, W. K., Chu, D. Z., Malik, S., Lerner, S., and Singh, H. 1994. Quantitative seafloor characterization using a bathymetric sidescan sonar. IEEE Journal of Oceanic Engineering, 19: 599–610.

Stockwell, J. D., Weber, T. C., Baukus, A. J., and Jech, J. M. 2013. On the use of omnidirectional sonars and downwards-looking echosounders to assess pelagic fish distributions during and after midwater trawling. ICES Journal of Marine Science, 70: 196–203.

Sun, Z. G., Gimenez, G., Vray, D., and Denis, F. 1991. Calculation of the impulse-response of a rigid sphere using the physical optic method and modal method jointly. Journal of the Acoustical Society of America, 89: 10–18.

Sund, O. 1935. Echo sounding in fishery research. Nature, 135: 953.

Takikawa, T., Kitamura, M., and Horimoto, N. 2008. Horizontal current field, ADCP backscatter, and plankton distribution in Sagami Bay, Japan. Fisheries Oceanography, 17: 254–262.

Tessier, C. 2006. Caractérisation et dynamique des turbidités en zone côtière: l'exemple de la région marine Bretagne Sud. PhD thesis, Université de Bordeaux.

Tessier, C., Le Hir, P., Lurton, X., and Castaing, P. 2008. Estimation of suspended sediment concentration from backscatter intensity of acoustic Doppler current profiler. Comptes Rendus Geoscience, 340: 57–67.

Thorp, W. H. 1967. Analytic description of the low‐frequency attenuation coefficient. Journal of the Acoustical Society of America, 42: 270–270.

Tichy, F. E., Solli, H., and Klaveness, H. 2003. Non-linear effects in a 200-kHz sound beam and the consequences for target-strength measurement. ICES Journal of Marine Science, 60: 571–574.

Totland, A., Johansen, G. O., Godo, O. R., Ona, E., and Torkelsen, T. 2009. Quantifying and reducing the surface blind zone and the seabed dead zone using new technology. ICES Journal of Marine Science, 66: 1370–1376.

Trenkel, V. M., Mazauric, V., and Berger, L. 2008. The new fisheries multibeam echosounder ME70: description and expected contribution to fisheries research. ICES Journal of Marine Science, 65: 645–655.

Urick, R. J. 1983. Principles of Underwater Sound, 3rd edn. McGraw-Hill, New York.

Vagle, S., Foote, K. G., Trevorrow, M. V., and Farmer, D. M. 1996. A technique for calibration of monostatic echosounder systems. IEEE Journal of Oceanic Engineering, 21: 298–305.

Van Buren, A. L., Drake, R. M., and Paolero, A. E. 1999. Temperature dependence of the sensitivity of hydrophone standards used in international comparisons. Metrologia, 36: 281–285.

Wade, I. P., and Heywood, K. J. 2001. Acoustic backscatter observations of zooplankton abundance and behaviour and the influence of oceanic fronts in the northeast Atlantic. Deep-Sea Research Part II-Topical Studies in Oceanography, 48: 899–924.

Warren, J. D., and Demer, D. A. 2010. Abundance and distribution of Antarctic krill (*Euphausia superba*) nearshore of Cape Shirreff, Livingston Island, Antarctica, during six austral summers between 2000 and 2007. Canadian Journal of Fisheries and Aquatic Sciences, 67: 1159–1170.

Weinberg, N. L. 1971. Ray tracing with non-linear sound velocity profiles. Journal of the Acoustical Society of America, 50: 101. doi.org/10.1121/1.1977431.

Wenz, G. M. 1962. Acoustic ambient noise in the ocean: spectra and sources. Journal of the Acoustical Society of America, 34: 1936–1956.

Widener, M. W. 1980a. Correction. Journal of the Acoustical Society of America, 68: 706.

Widener, M. W. 1980b. Measurement of transducer efficiency using self-reciprocity techniques. Journal of the Acoustical Society of America, 67: 1058–1060.

Wilson, O. B. 1988. Introduction to Theory and Design of Sonar Transducers. Peninsula Publishing, Los Altos, CA. 191 pp.

Wilson, W. D. 1960. Speed of sound in sea water as a function of temperature, pressure, and salinity. Journal of the Acoustical Society of America, 32: 641–644.

Woillez, M., Rivoirard, J., and Fernandes, P. G. 2009. Evaluating the uncertainty of abundance estimates from acoustic surveys using geostatistical simulations. ICES Journal of Marine Science, 66: 1377–1383.

Woodd-Walker, R. S., Watkins, J. L., and Brierley, A. S. 2003. Identification of Southern Ocean acoustic targets using aggregation backscatter and shape characteristics. ICES Journal of Marine Science, 60: 641–649.

Woodward, W. E., and Appell, G. F. 1986. Current velocity-measurements using acoustic Doppler backscatter - a review. IEEE Journal of Oceanic Engineering, 11: 3–6.

Zakharia, M. E., Chevret, P., and Magand, F. 1996. Estimation of shell characteristics using time-frequency patterns and neural network. *In* Proceedings of the IEEE Ultrasonics Symposium: 713–716.

Zedel, L., and Cyr-Racine, F-Y. 2009. Extracting fish and water velocity from Doppler profiler data. ICES Journal of Marine Science, 66: 1846–1852.

Zedel, L., Knutsen, T., and Patro, R. 2003. Acoustic Doppler current profiler observations of herring movement. ICES Journal of Marine Science, 60: 846–859.

Zedel, L., Patro, R., and Knutsen, T. 2005. Fish behaviour and orientation-dependent backscatter in acoustic Doppler profiler data. ICES Journal of Marine Science, 62: 1191–1201.

Zhou, M., Nordhausen, W., and Huntley, M. 1994. ADCP measurements of the distribution and abundance of euphausiids near the Antarctic peninsula in winter. Deep-Sea Research Part I-Oceanographic Research Papers, 41: 1425–1445.

Author contact information

Laurent Berger
Ifremer, Centre de Bretagne
ZI de la Pointe du Diable
29280, Plouzané, France
Laurent.Berger@ifremer.fr

Matteo Bernasconi
Institute of Marine Research
Nordnesgaten 50
5005 Bergen, Norway
matteo.bernasconi@imr.no

Eckhard Bethke
Thuenen Institute of Sea Fisheries
Bundesallee 50
38116 Braunschweig, Germany
eckhard.bethke@ti.bund.de

Kevin Boswell
Florida International University
3000 NE 151st St.
MSB355
North Miami, Florida 33181, USA
kmboswel@fiu.edu

Dezhang Chu
NOAA Fisheries
Northwest Fisheries Science Center
2725 Montlake Boulevard East
Seattle, Washington 98112, USA
Dezhang.Chu@noaa.gov

David Demer
NOAA Fisheries
Southwest Fisheries Science Center
8901 La Jolla Shores Drive
La Jolla, California 92037, USA
David.Demer@noaa.gov

Réka Domokos
NOAA Fisheries
Pacific Islands Fisheries Science Center
1845 Wasp Boulevard, Building 176
Honolulu, Hawaii 96818, USA
Reka.Domokos@noaa.gov

Adam Dunford

301 Evans Bay Parade

Hataitai

Private Bag 14901

Wellington 6021, New Zealand

a.dunford@niwa.co.nz

Sascha Fässler

IMARES Wageningen UR

Haringkade 1

1976 CP

IJmuiden, The Netherlands

sascha.fassler@wur.nl

Stéphane Gauthier

Fisheries and Oceans Canada

Institute of Ocean Sciences

9860 West Saanich Road

P.O Box 6000

Sidney, British Columbia, V8L 4B2, Canada

Stephane.Gauthier@dfo-mpo.gc.ca

Lawrence Hufnagle

NOAA Fisheries

Northwest Fisheries Science Center

2725 Montlake Boulevard East

Seattle, Washington 98112, USA

Lawrence.C.Hufnagle@noaa.gov

Mike Jech

NOAA Fisheries

Northeast Fisheries Science Center

166 Water Street

Woods Hole, Massachusetts 02543, USA

Michael.Jech@noaa.gov

Naig Le Bouffant

French Research Institute for Exploitation of the Sea

Ifremer, Centre de Bretagne

ZI de la Pointe du Diable

29280 Plouzané, France

Naig.Le.Bouffant@ifremer.fr

Anne Lebourges-Dhaussy

Research Institute for Development

IRD Bretagne

ZI de la Pointe du Diable

29280 Plouzané, France

Anne.Lebourges.Dhaussy@ird.fr

Xavier Lurton
French Reserach Institute for Exploitation of the Sea
Ifremer, Centre de Bretagne
ZI de la Pointe du Diable
29280 Plouzané, France
Xavier.Lurton@ifremer.fr

Gavin Macaulay
Institute of Marine Research
Nordnesgaten 50
5005 Bergen, Norway
gavin.macaulay@imr.no

Sandra Parker-Stetter
NOAA Fisheries
Northwest Fisheries Science Center
2725 Montlake Boulevard East
Seattle, Washington 98112, USA
sandy.parker-stetter@noaa.gov

Yannick Perrot
Research Institute for Development
IRD Bretagne,
ZI de la Pointe du Diable
29280 Plouzané, France
Yannick.Perrot@ird.fr

Tim Ryan
Commonwealth Scientific and Industrial Research Organisation
Oceans and Atmosphere Flagship
GPO Box 1538
Hobart, TAS, 7001 Australia
Tim.Ryan@csiro.au

Sarah Stienessen
NOAA Fisheries
Alaska Fisheries Science Center
7600 Sand Point Way N.E., Building 4
Seattle, Washington 98115, USA
Sarah.Stienessen@noaa.gov

Thomas Weber
Center for Coastal and Ocean Mapping
University of New Hampshire
24 Colovos Road
Durham, NH 03824, USA
weber@ccom.unh.edu

Neal Williamson

NOAA Fisheries - retired
Alaska Fisheries Science Center
7600 Sand Point Way N.E., Building 4
Seattle, Washington 98115, USA
NealW4@comcast.net